To the Graduate Council:

I am submitting herewith a dissertation written by Suichu Luo entitled "Study of electron-specimen interactions". I have examined the final copy of this dissertation for form and content and recommend that it be accepted in partial fulfillment of the requirements for the degree of Doctor of Philosophy, with a major in Solid State Physics.

David C Joy

David C. Joy, Major Professor

We have read this dissertation
and recommend its acceptance :

John J Turner

Peter B Hirsch

R. H. Ritchie

Accepted for the Council:

Lewis Winkel

Associate Vice Chancellor
and Dean of The Graduate School

STUDY OF ELECTRON-SPECIMEN INTERACTIONS

A Dissertation

Presented for the

Doctor of Philosophy

Degree

The University of Tennessee, Knoxville

Suichu Luo

May 1994

This dissertation is dedicated to my parents, my husband, and my son

ACKOWLEDGMENT

I would like to express my sincere gratitude to my major professor, Dr. David C. Joy, who was instrumental in all aspects of this research, for his concern, guidance, patience, encouragement, and all his support throughout this research. Appreciation is also expressed for the help of my committee members: Dr. R.H. Ritchie, Dr. J. J. Quinn and Dr. P. Liaw. Dr. Ritchie reviewed our papers and his encouragement was a great support for me; Dr. Quinn was always available to answer my questions, I have learned a lot from his classes; and Dr. Liaw supplied the SiC sample.

The author is indebted to a number of individuals who have participated in the research presented in this dissertation. I would like to thank Dr. John Dunlap for his help, discussions and training on the TEM; Mr. Richard Williams for his help and training on the sample preparation; and Dr. Neal Evans for his training on the TEM at the Oak Ridge National Labratory. I would also like to thank Dr. Carolyn Joy for her help and training on the SEM, and to Mrs. Jennifer Trollinger for all her kind help and support.

Appreciation is also extended to all the professors and my fellow graduate students in the Department of Physics and the Department of Materials Science and Engineering for their generous support and encouragement, specifically Y. Sun, S. Zhu, I. Huang, G. Chen, M. Zhang, X. Wang, X. Zhang, S. Cao, M. Schmidt, and A. Mohan.

ABSTRACT

In the last four decades a variety of microscopes have been developed. Now the electron microscopes have well been established and become one of the most important tools to investigate the fundamental properties of electron-specimen interactions. When an electron beam irradiates a specimen, the resulting elastic scattering process canbe used to form images and diffraction patterns in the TEM, while the inelastic scattering induces secondary emissions, such as secondary electrons, Auger electrons and X-rays, which are the signals in the SEM, TEM, and STEM. EELS, an important analytical technique, which can be carried out only in the TEM or STEM, provides a direct access to the full information resulted from elastic and inelastic mixed scattering processes in the electron-specimen interactions.

This thesis is concentrated on understanding the physical processes for signal generation in microanalysis. For SEM we have developed a detailed quantitative model to describe the production and escape of SE. For Monte Carlo simulation, a modified Rutherford formula has been proposed in order to obtain a satisfactory accuracy and more convenient computer procedure. For EELS, a new method to remove plural scattering and determine the local thickness of a specimen has been developed. This thesis also develops and applies an experimental method for the determination of stopping power in the low and medium energy range .

The ionization of atoms by electrons is an important process in microanalysis. In this thesis we present the calculations of ionization cross sections of K , L and M shells covering the entire periodic table and spanning the energy range from the critical ionization energy up to 100 keV using Hartree-Slater self- consistent field model. In order to provide convenient access to this data some empirical formulae are derived, providing good quality fits to the computed results.

TABLE OF CONTENTS

CHAPTER PAGE

1.INTRODUCTION.....1

2.BASIC THEORY OF EELS.....4

2.1 History of EELS.....4

2.2 Transmitted electrons in TEM and STEM.....6

2.3 The basic principles of electron energy loss spectroscopy.....9

3.ADVANCED ELECTRON ENERGY LOSS SPECTROSCOPY --NEW WORK ON MIXED SCATTERING.....18

3.1 Electron scattering theory.....18

3.1.1 Elastic scattering.....18

3.1.2 Inelastic scattering.....25

3.2 Plural scattering in EELS and it's correlations.....31

3.3 New approach on mixed scattering.....36

3.4 Local thickness determination by EELS.....42

4.MONTE CARLO CALCULATIONS OF SECONDARY ELECTRON EMISSION.....45

4.1 Introduction.....45

4.2 Model for secondary electron production.....50

4.3 Results and discussion.....63

4.4 Conclusions.....85

5. STOPPING POWER DETERMINATION.....88

5.1 Introduction.....88

5.2 An empirical stopping power relationship for low energy electrons.....99

5.3 Experimental determinations of electron stopping power at low energies.....100
5.3.1 Outline of method.....101
5.3.2 Experimental procedure.....103
5.3.3 Practical applications.....105
6. CALCULATIONS OF X-RAY IONIZATION CROSS SECTIONS.....127
6.1 Introduction.....128
6.2 Calculation procedure.....131
6.3 Results and discussions.....133
6.3.1 General characteristics of the results.....133
6.3.2 Comparison with other models.....137
6.3.3 Comparison with experiment.....143
6.3.4 The Fano plot.....146
6.4 Conclusions.....152
BIBLIOGRAPHY.....154
APPENDICES.....176
VITA.....203

LIST OF TABLES

TABLE **PAGE**

4.1 Calculated data for Au..... 67

4.2 Calculated data for Ag..... 67

4.3 Calculated data for Cu..... 68

4.4 Calculated data for Al..... 68

4.5 The yield of SE for Cu, Au and Al.....72

4.6 The β-factor for Au and Al.....73

5.1 k values for C, Al, Si, Cu, Ni, Ag, and Au.....96

LIST OF FIGURES

FIGURE PAGE

2.1 Scattering kinematics for an incident electron.....7

2.2 The electron ray paths through the magnetic prism spectrometer.....10

2.3 The angular distribution of (a) the incident beam,
(b) elastically scattered electrons, (c) plasmon excitations and
(d)inner shell losses.....15

3.1 Comparison of backscattering coefficients for Au.....23

3.2 Comparison of energy deposition of depth for Al at 3 keV.....24

3.3 Comparison of calculated and experimental EELS for Al at 100 keV
with semi-collection angle 5 mrad.....41

3.4 Comparison of single scattering distributions with and without
mixed angular correction.....41

3.5 Comparison of experimental and calculated spectra for Al
1 and 2 are EELS for two different thickness samples.....44

3.6 Comparison of experimental data-3 (Egerton,1986) and the
calculated spectra-3 for Al in this work.....44

4.1 The variations of the yield of SE and SE1 with beam energy for Au..65

4.2 The variations of the yield of SE and SE1 with beam energy for Ag..65

4.3 The variations of the yield of SE and SE1 with beam energy for Cu..66

4.4 The variations of the yield of SE and SE1 with beam energy for Al...66

4.5 Normalized secondary electron energy distribution curves for Au
at 1 keV.....70

4.6 Normalized secondary electron energy distribution curves for Cu
at 1 keV.....70

4.7 Comparison of theoretical and experimental normalized distributions of SE for Al at 1 keV.....71
4.8 The variation of the β-factor with beam energy for Au.....75
4.9 The variation of the β-factor with beam energy for Ag.....75
4.10 The variation of the β-factor with beam energy for Cu.....76
4.11 The variation of the β-factor with beam energy for Al.....76
4.12 The variation of SE yield with thickness.
The experimental data for Cu is from Joy (1970).....78
4.13 The variation of SE yield with thickness.
The experimental data for Al is from Reimer and Drescher (1977)...78
4.14 The variation of SE yield with thickness.
The experimental data for Au is from Reimer and Drescher(1977) ...79
4.15 The variation of layer thickness with escape angle θ.....80
4.16 Comparison of our angular distribution calculated by isotropic distribution model of internal SE and the cosine law for Al at 2 keV.
1: our calculation 2: Cosine Law.....82
4.17 Comparison of our angular distribution calculated by isotropic distribution model of internal SE with energy 50 eV and the cosine law for Au .
1:Angular distribution of SE with energy 50 eV 2:Cosine Law.....82
4.18 Comparison of curves of inelastic and elastic mean free path varying with energy of SE for Al.....84
4.19 The discrepancy in the angular distribution caused by inelastic scattering.
1. Cosine Law distribution
2. The distribution as influenced by inelastic scattering.....86
5.1 Stopping power of aluminum calculated from Eq.5.8a (Joy and

Luo,1988), Bethe (1930), Tung et al. (1979) and Rao-Sahib and Wittry(1974).....95

5.2 Variation of electron range with incident energy for Al, Cu, and Au as computed from the original Bethe model extended by the Rao-Sahib Wittry extrapolation (BRSW) and from the modified Bethe (MB) equation.....98

5.3 Experimentally determined variation of N_{eff} with energy for vitreous ice (open squares, our experiment). The optical data (La Verne and Mozumder,1983) for liquid water is shown for comparison(closed squares).....107

5.4 Variation of I_{eff} with energy for vitreous ice (open squares, our experiment). The optical data (La Verne and Mozumder, 1983) for liquid water is shown for comparison (closed squares).....107

5.5 Comparison of our experimentally determined stopping power for vitreous ice with Bethe equation data.....109

5.6 Experimentally determined variation of N_{eff} and I_{eff} for GaAs (dielectric function from Daniels et al.,1970).....109

5.7 Comparison of our computed stopping power for GaAs from dielectric function (Daniels et al.,1970)and the Bethe equation's...110

5.8 Comparison of our computed stopping power for SiO_2 from dielectric function (Daniels et al., 1970) and the standard Bethe equation's.....111

5.9 Comparison of our stopping power data calculated from dielectric function (Ashley,1982) and the standard Bethe equation's for Al_2O_3.....111

5.10 Experimentally determined stopping power using this method for InSb. O: form optical data; E: from EELS, B: from standard Bethe equation for InSb. The dielectric function is from Daniels et al.(1970).....112
5.11 Experimentally determined stopping power using this method for GaSb. The dielectric function is from Daniels et al.(1970).....112
5.12 Stopping power for MoS_2 (data from our experiment).....113
5.13 Stopping power for MgO calculated from dielectric function (Ashley, 1982).....113
5.14 Stopping power for Si (data from our experiment).....114
5.15 Stopping power for Ti , calculated from dielectric function (Tougaard,1988).....114
5.16 Stopping power for V, calculated from dielectric function (Tougaard,1988).....115
5.17 Stopping power for Cr (data from our experiment).....115
5.18 Stopping power for Mn, calculated from dielectric function (Tougaard,1988).....116
5.19 Stopping power for Fe, calculated from dielectric function (Tougaard,1988) 116
5.20 Stopping power for Co, calculated from dielectric function (Tougaard, 1988).....117
5.21 Stopping power for Ni, calculated from dielectric function (Tougaard, 1988).....117
5.22 Stopping power for Cu (our experiment data). The curves are our stopping powers and the calculated from Bethe equation, respectively.....118

5.23 Stopping power for Ge. The curves are stopping power for a crystalline specimen, the stopping power computed from optical data (Daniels et al. 1970); and calculated from the Bethe equation, respectively.....118

5.24 Stopping power for Pd(our experiment data). The curves are our stopping power and the calculated from Bethe equation, respectively 119

5.25 Stopping power for Ag (dielectric function from Daniels et al., 1970).The curves are our calculated stopping power, and the calculated from Bethe equation.....119

5.26 Stopping power for Pt (data from our experiment).....120

5.27 Stopping power for Au (data from our experiment).....120

5.28 Stopping power for Superconductor: $Bi_{1.8}Pb_{0.3}Sr_2Ca_2Cu_3O_{10}$ (data from our experiment).....121

5.29 Stopping powers computed from this method for Guanine. E: from EELS data, Opt: from optical data (Ashley,1982); B: from standard Bethe equation 121

5.30 Stopping power for Pb (data from our experiment)..... 122

5.31 Stopping power for DNA. 1: calculated from dielectic function (Ashley, 1982) ; 2: calculated from Bethe equation.....122

5.32 Experimentally determined stopping power for carbon including K shell contribution (data from our experiment).....123

5.33 Stopping power for ZnSe (the dielectric function from Daniels et al.,1970).....124

5.34 Comparison of electron energy loss functions for Si,C and their compound SiC (data from our experiments).....125

5.35 Comparison of the effective electron number N_{eff} for Si,C and their compound SiC (data from our experiments).....125
5.36 Comparison of the electron stopping powers for Si, C, and their compound SiC below 10 keV (data from our experiments).....126
5.37 Comparison of the electron stopping powers for Al (data from our experiment)..... 126
6.1 Comparison of the optimal and non-optimal steps data.....134
6.2a Calculated K shell cross section for carbon.....134
6.2b Calculated K shell cross section for silicon.....135
6.2c Calculated K shell cross section for copper.....136
6.2d Calculated K shell cross section for silver.....136
6.3 The overvoltage of cross section peak position.....137
6.4a The calculated L_{23} cross sections for carbon.....138
6.4b The calculated L_{23} cross sections for aluminum.....139
6.4c The calculated L_{23} cross sections for copper.....139
6.4d The calculated L_{23} cross sections for silver.....140
6.5a The calculated M_{45} cross sections for silver.....141
6.5b The calculated M_{45} cross sections for ytterbium.....141
6.5c The calculated M_{45} cross sections for gold.....142
6.6 Comparison of our data with other calculated data for Al K shell...142
6.7 Comparison of our data with other calculated data for Al L_{23} shell.143
6.8 Comparison of our data with other calculated data for Al M_1 shell.144
6.9 Comparison of our data with experimental data for Al K shell.....144
6.10 Comparison of our data with computed and measured data for carbon K shell.....145
6.11 Fano plot of K shell data for selected elements.....147

6.12a Fano plot of L shell data for selected elements.....147
6.12b Fano plot of M shell data for selected elements.....148
6.13 The parameters for empirical formula of K shells.....150
6.14 The parameters for empirical formula of L shells.....152
A1 Schematic representation of angular distribution of two successive scattering events.....179
C1 K-shell ionization cross sections for Al.....186
C2 K-shell ionization cross sections for Ca.....187
C3 K-shell ionization cross sections for Mn.....188
C4 K-shell ionization cross sections for Br.....189
C5 K-shell ionization cross sections for Zr.....190
C6 L-shell ionization cross sections for Ca.....191
C7 L-shell ionization cross sections for Mn.....192
C8 L-shell ionization cross sections for Br.....193
C9 L-shell ionization cross sections for Zr.....194
C10 L-shell ionization cross sections for Ag.....195
C11 L-shell ionization cross sections for Cs.....196
C12 M-shell ionization cross sections for Ag.....197
C13 M-shell ionization cross sections for Cs.....198
C14 M-shell ionization cross sections for Nd.....199
C15 M-shell ionization cross sections for Yb.....200
C16 M-shell ionization cross sections for Hg.....201
C17 M-shell ionization cross sections for U.....202

CHAPTER 1

INTRODUCTION

Scientific advances often follow improvements of the measuring instruments. Electron microscopes have yielded steady increases in spatial resolution and, consequently, improvements in our fundamental knowledge of matter. The electron microscope is now a well-established research tool in the Physics, Chemistry, Materials science and Biology (Hirsch et al., 1977; Joy, 1979; Egerton,1986; Buseck et al., 1992). In Physics, many of the fundamental electronic properties of the solid states, such as elastic mean free path, inelastic mean free path and dielectric function, can be successfully determined by electron microscopy. In Materials Science electron microscopy is particularly known for the study of physical properties of many materials at atomic scale and employed to determine structure, defects, interfaces, surfaces and spatially resolved elemental composition. In the Life Sciences, the electron microscope is routinely used for the study of both tissue, individual cells , and macromolecules.

In the last four decades different types of microscopes have been developed depending on different types of interactions between electrons and specimens. Methods for the microscopic examination of matter continue to expand in both their variety and their complexity. The electron beam can be used to irradiate thin films and the resulting elastic scattering process is used in the Transmission Electron Microscope (TEM) to form images and electron diffraction patterns. Inelastic scattering of the incident electron beam can induce secondary emissions , for example, secondary electrons, Auger electrons and X-rays or visible light. Instruments employed for the analysis of these secondary signals

are the Scanning Electron Microscope (SEM) and the Scanning Transmission Electron Microscope (STEM). Electron Energy Loss Spectroscopy (EELS) is an important analytical technique, which can be carried out only in the TEM and STEM .

In recent years the new technique of high-resolution transmission electron microscopy (HRTEM) has become available and can provide information on an atomic scale at high resolution in space, energy or time. It is now a powerful and common technique of material characterization. The highest possible resolution of HRTEM is 1 to 2 Å, during normal every day use, a resolution of the order 10 Å is obtained. However, since many experimental variables are involved, there are severe problems in particular electron-optical aberrations. To overcome this problem and so improve resolution, a new technique, electron holography which directly provides quantitative information on both the amplitude and the phase, has been developed rapidly in the last decade(Tonomura,1986; Lichte,1986; Joy et al.,1993a).

The research described in this thesis is concentrated on understanding the physical processes important for signal generation in electron microscopy and microanalysis. The macroscopic measure of the interaction of an electron with a solid is the stopping power. This dissertation develops and applies an experimental method for the determination of stopping power in the low and medium energy range for which little or no other experimental data is available.

The stopping power determines the scale and magnitude (lateral and depth distribution) of all electron solid interactions, in particular the production of Secondary Electrons(SE) and the generation of fluorescent X-rays. In this thesis we develop a detailed quantitative theory for the production and escape of SE. For the corresponding

computation of X-ray yields a complete set of X-ray ionization cross section is calculated paying special attention to the behavior at low overvoltage ratios.The key experimental technique for the study of these processes is EELS since it gives direct access to the angular and energy distributions resulting from scattering.A detailed analysis of EELS is carried out to permit accurate quantitative analysis to be performed.

CHAPTER 2

BASIC THEORY OF EELS

In the last ten years electron energy loss spectroscopy (EELS) has become one of the most popular microanalytical techniques due to the development of commercial, high performance, spectrometers and computerized data handling. In addition to revealing the composition of the sample, EELS can provide fundamental insights into the atomic , and band , structure of the sample through analysis of the momentum transfer and the energy transfer suffered by an electron interacting with the solid. It is therefore the most powerful and important tool for experimental studies of electron scattering and the electron interaction with the solid.

2.1 HISTORY OF EELS

The first measurement of the EEL spectrum of transmitted electrons was reported by Ruthemann in 1941. He used incident energy from 2 to 10 keV and recorded the ELS for aluminum. In 1942 he reported the observation of inner shell losses of collodion in a form of nitrocellulose. Further pioneer work was carried out by Hiller and Baker (1944) who also showed good inner shell edges. In 1949 Mollenstedt published a design of an electrostatic energy analyzer, and his analyzer was subsequently added to conventional electron microscopes in several laboratories. A combination of electric and magnetic fields (Wien filter) was first employed for transmission energy loss measurements by Boersch et al.(1962) in Berlin. In the sixties great advances were made in the development of instruments combining the facilities of transmission electron microscopy with energy analysis of the transmitted electrons (Watenabe and Uyeda, 1962; Castaing and Henry,

1964; Castaing, Hili and Henry, 1965; Cundy, Metherell and Whelan, 1966; Wittry, Ferrier and Cosslett,1969. A general review is given by Daniels et al., 1970). Since the seventies the main experimental and theoretical principles and techniques have been established and there have been a lot of studies and applications carried out (Johnson and Spence, 1974; Egerton, 1975; Joy and Maher, 1977; Batson, 1978; Colliex and Trebbia, 1978; Joy and Maher,1980). In the last decade considerable advances have been made in the development of more powerful microscopes with field emission guns combining the parallel energy loss spectrometry (PEELS). The field emission gun with a resolution about 0.3 eV together with the parallel collection system (a detection system can record all energy losses simultaneously) are much more efficient and considerably improve the sensitivity of EELS.

Applications of this technique to various problems are briefly as follows:

(a) Contrast effects: Watenabe and Uyeda (1962); Castaing et al. (1967); Cundy et al. (1969).

(b) Microanalysis of plasmon energy losses : Cundy and Grundy (1966), Cundy et al.(1968); Spalding et al.(1969); Hibbert et al.(1972); Batson and Silcox(1983); Yuan et al.(1988); Dunlap et al.(1989); Luo et al. (1991, 1993); Joy et al. (1990,1993b).

(c) Microanalysis of inner shell ionization: Wittry et al.(1969); Ferrier and Hills (1974); Egerton(1974); Egerton et al.(1975); Joy and Maher(1977); Maher et al. (1979); Leapman et al.(1980) and Skiff et al.(1988).

(d) Extended electron-loss fine structure(EXELFS): the use of EELS for extended X-ray-absorption fine structure(EXAFS) was first suggested by Ritsko et al.(1974) and Leapman and Cosslett (1976) and was applied to nanometer sized areas by Batson and Craven (1979); Lindner et al. (1985); Spence (1985); Neuman and Spence (1987). A comprehensive review is given by Teo and Joy (1981).

(e) Thickness measurement: Leapman et al. (1984); Egerton and Cheng(1987); Crozier and Egerton(1989); Egerton and Wang (1990); Rez et al.(1992); Zhao et al. (1993), Ho et al. (1993) and Blackson et al.(1993).

(f) A method for the determination of electron stopping power by EELS has been developed and will be discussed later in this thesis.

Now the EELS is well established and widely used. In the near future it is expected that the fundamental understanding and instrumental developments in this field will progress continually.

2.2 TRANSMITTED ELECTRONS IN TEM AND STEM

In the transmission electron microscope, incident electrons are accelerated from 10 keV to 10 MeV to ensure that they are transmitted through a thin specimen. When an electron passes through a thin film , it can interact both with the positive charge on the nucleus of atoms, and with the bound or free electrons surrounding atomic nucleus. Typically these interactions can be divided into two categories: elastic and inelastic . In an elastic scattering event the direction of the electron trajectory is changed but the energy remains unchanged. In an inelastic scattering event both the direction of travel and the energy of the incident electron are changed. Such a process is schematically presented in Figure 2.1. Before and after a collision the incident electron is in the initial state energy E_0 with the wave vector $\mathbf{K_i}$ and in the final state energy $E_0 - E$ with the wave vector $\mathbf{K_f}$, where E is the energy transfer, and $\mathbf{q} = \mathbf{K_i} - \mathbf{K_f}$ is the momentum transfer. In an inelastic scattering event there are two kinds of excitations: single electron excitation or collective excitation. An interaction of a fast incident electron with an inner shell or outer shell electron can cause a single electron excitation. If the excited electron absorbs an

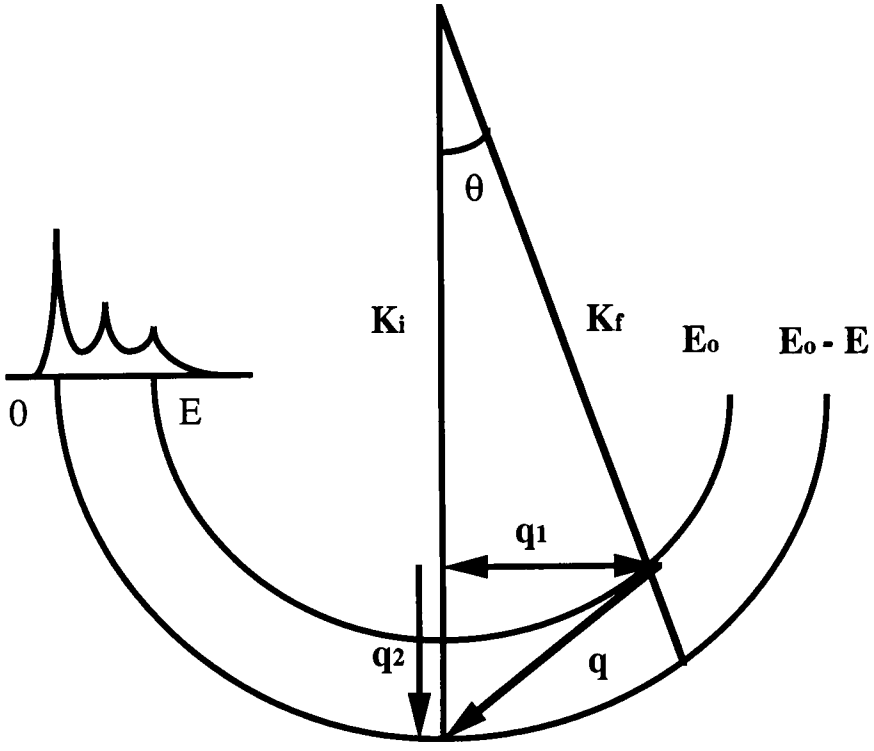


Figure 2.1. Scattering kinematics for an incident electron. The EEL spectrum is schematically indicated at the left.

amount of energy E which is greater than the inner shell binding energy or the energy for outer shell electron transition, it will make an upward transition from its ground state into an unoccupied electron state. Because of the conservation of the total energy the fast electron loses the same amount of energy E. For light elements the inner shell binding energy is several hundreds or thousands eV below the fermi level of the solid. For a 100keV incident electron after an inelastic collision with an inner shell electron the typical inelastic scattering angle θ is of the order of 10 mrad.

Another important process is the collective excitation of valence electrons. The approach to derive electric properties of the solid state starts with the plasma concept. In some materials, for example metals, the free electrons can be treated as an electron liquid of high density of about 10^{23} electrons/cm^{-3}. The longitudinal density fluctuations, i.e. plasma oscillations , propagate through the whole sample. The quanta of these "bulk plasmons" have an energy

$$E_p = (ne^2h^2/\pi m_0)^{1/2} = h\omega_p/2\pi \qquad (2.1)$$

of the order 10eV, where n is the valence electron density, m_0 the electron rest mass and ω_p is the plasmon frequency. For many metals the plasmon resonance is predominant. On the other hand for rare gas solids there is no plasmon existent. Most materials lies between these two extremes.

An important extension of the bulk plasmon is the concept of 'surface plasmons'. Ritchie (1957) first indicated the existent of surface plasmon at each exterior surface. Maxwell's theory shows that electromagnetic surface waves can be propagate along the surfaces with the bulk plasmon frequency. The surface plasmons play an very important

role in Surface Physics . However, in TEM or STEM when the sample is thick the surface plasmon does not have a strong intensity compared with bulk plasmon and can be ignored .

2.3 THE BASIC PRINCIPLES OF ELECTRON ENERGY LOSS SPECTROSCOPY

In a TEM or STEM the beam of transmitted electrons is directed into a electron energy spectrometer which separates the electrons according to their kinetic energy as shown in Figure 2.2 and produces a energy loss spectrum . All the information that can be obtained about the sample is contained in the angular and energy distribution of the electrons that passed through the specimen. Usually, however, it is sufficient to collect all the transmitted electrons lying within a cone of semiangle β about the incident beam direction. The result that we obtain from such an experiment is then an electron energy loss spectrum in which we plot the transmitted signal intensity as a function of the energy loss E for all the electrons scattering within the angular cone β accepted by the spectrometer. This destroys the information about the momentum transfer , since the spectrometer is integrating information from the whole angular range which it is accepting. But because it allows us to use simpler designs of spectrometers , and as the information produced is related to the important properties of the specimen after a mathematical convolution procedure (The procedure we developed as explained in this thesis can also be used to remove the plural scattering due to the thickness of the specimen and improve the spectrometer resolution as well) , this approach is the one most generally used.

A recorded EEL spectrum can be used for microanalysis purposes. In EELS experiment the intensity $I(E,\theta)$, which is the intensity of the transmitted signal at the

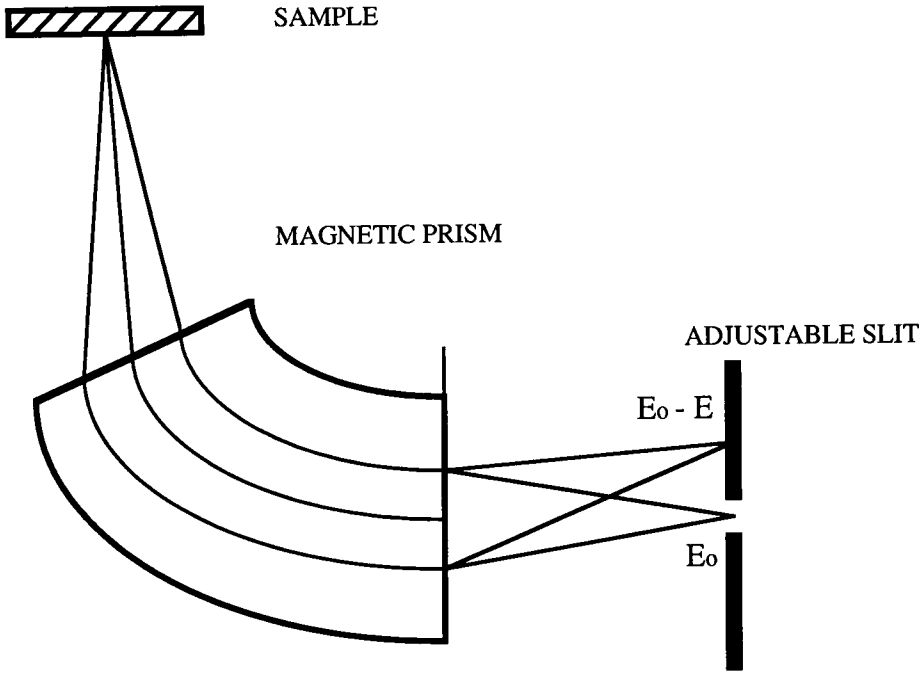


Figure 2. 2.The electron ray paths through the magnetic prism spectrometer.

energy loss E for a measurement made over a solid angle $d\Omega$ about the angle θ from the original direction, is proportional to the double differential cross section $d^2\sigma(E, \theta)/dEd\Omega$:

$$\frac{I(E,\theta)}{I} \approx n_s \cdot \frac{d^2\sigma(E,\theta)}{dE \cdot d\Omega} \qquad (2.2)$$

where I is the incident beam intensity, n_s is the number of atoms per unit area in the volume examined. This cross section, which is measured from EEL experiment, can be related to the properties of our specimen in two different but equivalent ways (Joy, 1979). The first of these is the "Macroscopic" approach. In this approach all the microscopic details of the specimen such as its chemistry and crystallography are ignored and described only in terms of its dielectric constant ε, which is the physical parameter of measuring the response of the material to an electromagnetic wave (such as electrons or light). The relationship between $d^2\sigma(E, \theta)/dEd\Omega$ and ε can be shown to be (Ritchie,1957):

$$\frac{d^2\sigma}{dE \cdot d\Omega} = \frac{[\mathrm{Im}(-1/\varepsilon)]}{2\pi^2 a_0 n E_0} \cdot \frac{1}{\theta^2 + \theta_E^2} \qquad (2.3)$$

where a_0 is the Bohr atomic radius; E_0 is the incident electron energy and n is the density (atoms/ cm^3); θ_E is the " Characteristic inelastic scattering angle", defined as

$$\theta_E = \frac{E}{2E_0} \qquad (2.4)$$

Using this model our EELS experiment thus actually measures $\mathrm{Im}(-1/\varepsilon)$. Once it has been obtained the real part $\mathrm{Re}(1/\varepsilon)$ can also be determined using the Kramers-Kronig

transform (Daniels et al., 1970) and hence the complete complex dielectric constant of the specimen can be obtained, and from that all the optical properties , the inelastic mean free path , and the stopping power can be calculated. An advantage of this technique for determining ε is that it can be done for any value of **q** whereas an optical measurement can only be done at **q**=0.

The second description is the " Microscopic approach". In this approach the cross-section is related to specific types of interactions between the specimen and the incident electron using a mathematical and physical model involving quantities which are of micro-analytical interest. A typical electron energy loss spectrum is over a range of about 1000 eV and includes three parts: the zero loss peak, the low energy loss and the inner shell loss regions. We can use the microscopic approach for each portion separately to study the physical processes occurring there and yield useful analytical data.

The zero loss peak is the combination of three groups of electrons. First, there are electrons which are unscattered, passing through the specimen without any interaction with the solid. The zero loss peak, however, has a finite energy width . There are two reasons for it. The first is that the beam of incident electrons has an energy spread resulted in the inherent energy width of the electron source and instabilities in the accelerating potential, which can range from 1.5eV for a thermionic tungsten filament down to 0.3 eV for a cold field emitter. The second is the result of a definite energy resolution of the spectrometer. Typically the resolution is from 1 to 5 eV in the practical systems. Although the unscattered electrons have not interacted with the specimen, they do provide the total scattering cross section since the unscattered signal I_{un} is given by

$$\frac{I_{un}}{I} = \exp\left[-n_s \sigma_T(\theta)\right] \qquad (2.5)$$

where $\sigma_T(\theta)$ is the total cross section for scattering outside the angle θ. The angular distribution of the unscattered beam is about 1 mrad typically as shown in Figure 2.3a. Second, there are elastically scattered electrons which come from the elastic scattering events. Elastic events arise as a consequence of atom-nuclei interactions and the angular distribution of these electrons has the form :

$$\frac{I_{EL}(\theta)}{I_{un}} = \frac{1}{(\theta^2 + \theta_0^2)^2} \qquad (2.6)$$

where θ_0 is the screening parameter and $\theta_0 = 58.35\, Z^{1/3}/E_0^{1/2}$ mrad. This distribution is broad, typically 30 mrad at half height (Figure.2.3b). The third group of electrons are those , which have generated or been scattering by " phonon excitation" in the quasi-elastic events. As the result of electron-phonon interaction, electrons scattered by phonons lose an amount of energy (typically below 0.1 eV).which is so small compared with the energy spread (0.2-2eV) of the electron sources that these events cannot be distinguished from the purely elastic ones by the usual electron-microscope spectrometer system. Therefore , they are grouped with the elastically scattered electrons and the unscattered electrons together as zero-loss events . There is, however, a wealth of structure in the vibrational-loss spectrum (electron-phonon scattering intensity distribution) and it can be observed using reflected low-energy electrons (Egerton, 1986) which we will not consider in this thesis.

The low energy losses (below 50eV) constitute more than 90% of all inelastic processes. The energy lost is predominantly due to excitations of valence shell electrons

and the transitions which occur reflect the energy levels of the atoms and molecules condensed into a solid. The energy is transferred to the valence electrons either through plasma excitations in materials having a relatively high density of free electrons, or through more complicated excitations involving a mixture of single electron intraband transitions and interband transitions and collective processes. The latter situation applies to transition metals and their alloys, semiconductors and organic materials or insulators (Joy and Maher, 1980). In the region of low energy losses the results of the experiments are described by the dielectric theory. The dielectric function is used for the calculation of plasmon energy, lifetime, momentum transfer dependence and excitation probability . The angular distribution of plasmon losses is broad too and the half width being 10-20 mrad (see Figure 2.3c). The ELS in the low energy losses gives detailed information of the properties of the real plasmons and contributes considerably to the development of the plasma physics (Raether,1980).

Above about 50eV the spectrum constitutes various non-characteristic excitations, such as multiple collective excitations and single intra- or inter-band transitions of valence electrons forming a background whose intensity continuously decreases with increasing energy loss. The inner shell ionization (K, L and M shells) structures, which have well defined features ("edges") , are superimposed on this background. Since each element has unique inner shell binding energy, which corresponds to the energy loss position of its EEL spectrum, it is possible to distinguish a particular element in a environment of many elements and determine the inner shell ionization cross sections by ELS using these characteristic edges. In addition to this quantitative chemical analysis, a study of the edges also yields electronic and structural data about the specimen. It has been found experimentally (Egerton, 1975, Maher et al., 1979) that the energy differential cross section for the background has the form :

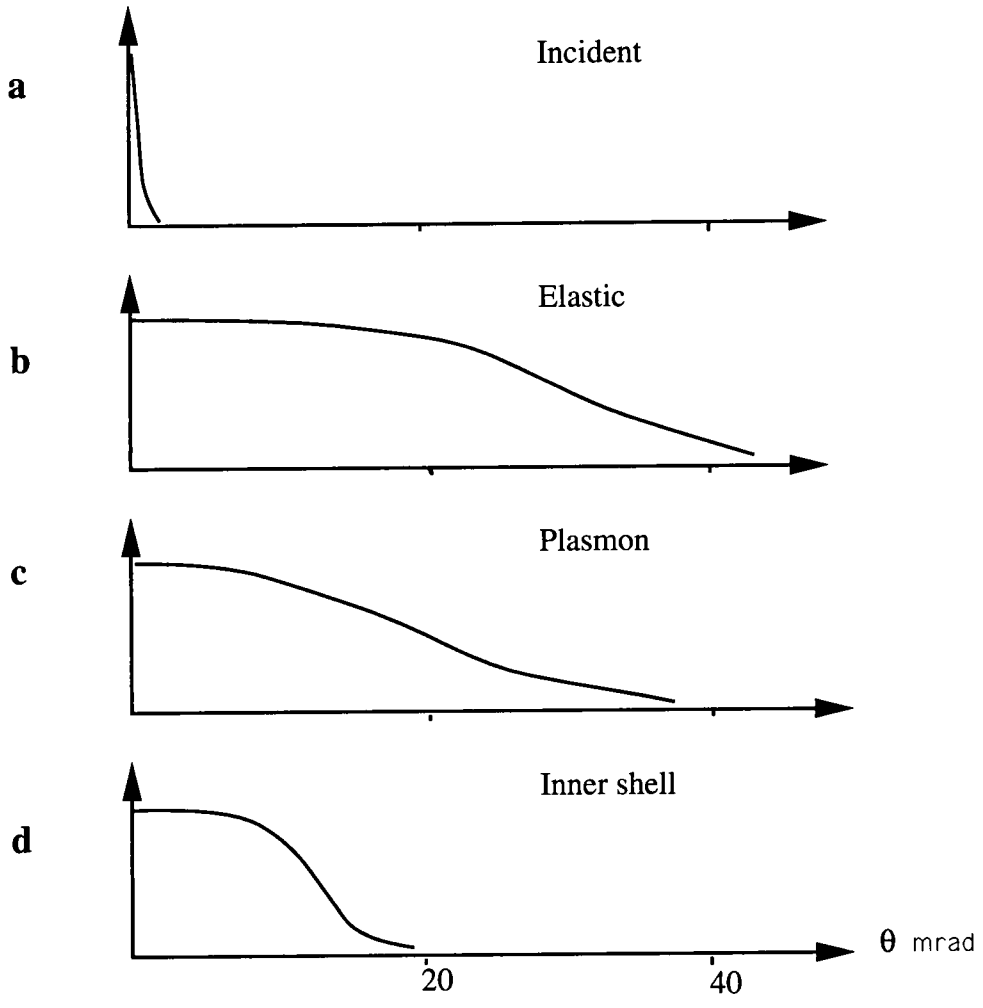


Figure 2.3. The angular distribution of (a) the incident beam, (b) elastically scattered electrons, (c) plasmon excitations and (d) inner shell losses.

$$\frac{d\sigma}{dE} = A \cdot E^{-r} \qquad (2.7)$$

where A and r are parameters depending on the acceptance angle β of the spectrometer. The most important edges for micro-analytical purposes are the K- and the L-edges. The K-edges are especially significant as they cover the elements Li to F which cannot be detected by Energy Dispersive X-ray Spectroscopy (EDXS). The differential cross section for an edge has the form (Joy, 1979) :

$$\frac{d^2\sigma}{d\Omega dE} = \frac{4a_0^2 \cdot f(E,\theta)}{(E_0/R)(E/R)} \cdot \frac{1}{\theta^2 + \theta_E^2} \qquad (2.8)$$

where $\theta_E = E/2E_0$ and R is Rydbergs constant (13.6 eV). The quantity $f(E,\theta)$ is called the " oscillator strength" and represents the number of electrons per atom that take part in the particular energy loss process. It can be seen from Eq.2.8 that the scattering is peaked with a width varying as θ_E as shown in Figure 2.3d .

Although the theoretical principle and the experimental EEL spectrum performance have been basically established as we briefly described above, to obtain the desired results such as stopping power and inelastic mean free path for a given specimen from a recorded EEL spectrum is not straightforward and there are still some important investigations need be carried out and more proper methods need be developed . For example, in the last decade a lot of attention has been paid to the methods to remove plural scattering properly form EEL spectrum including inelastic scattering angular correction (Livins et al., 1988; Wang, 1990), or both inelastic and elastic scattering angular correction (Batson and Silcox, 1983; Egerton and Wang,1990, Ho et al, 1993). Because the typical specimen thicknesses in the microscope are comparable with both the elastic and inelastic mean free paths, the scattering events are cascade processes and the inelastic and the elastic events

are mixed up , which makes the plural removal procedure very complicated. Besides the complex interaction between the electrons and the solid, there is another main limitation of EELS, that the spectrum can only be recorded up to a few keV. This means that at first it is not easy technically to analyze all the data widely spreaded from a few eV to a few keV; and the second is the core loss region for a specimen for high- or medium- atomic number elements the inner shell energy losses are far beyond this energy region .

In this thesis in the next chapter based on three dimension Poisson Statistics we developed a new method to remove plural scattering including both elastic and inelastic mixed angular correction in order to obtain more accurate single scattering information from EEL spectra. Based on this new method the electron-solid interaction in low energy loss can be experimentally determined with better accuracy. To overcome the energy range limitation of EELS we also have put our effort for the theoretical calculation for inner shell ionization processes , which allows us to combine the theoretical results for inner shells with the results from ELS low energy loss region to obtain the full scale information of the electron-solid interaction.

CHAPTER 3

ADVANCED ELECTRON ENERGY LOSS SPECTROSCOPY---- NEW WORK ON MIXED SCATTERING

3.1 ELECTRON SCATTERING THEORY

To exploit fully the information contained within the energy-loss spectrum it is necessary to study the theory of the interaction between the incident electron and the solid. For a given scattering event, the scattering cross section σ is proportional to the probability that the event occurs. Considering that the incident electron beam strikes an unit area, then σ represents the fraction of the area that produces the event of interest. In order to avoid the use of large exponents it is common to use the unit 'barn' in particle physics, where 1 barn = 10^{-24} cm^2. The average distance λ (cm), for an electron with a given energy traveling between events of a particular type, is called the mean free path . The relationship between σ and λ can be expressed as:

$$\lambda = A/ (\sigma N_0 \rho) \qquad (3.1)$$

where A is the atomic weight of the target material (g/mole), N_0 is Avogadro's number and ρ is the density (g/cm^3).

3.1.1 Elastic scattering

Analytical electron microscopy normally uses one of two elastic cross sections, either the screened Rutherford cross section or tabulated partial wave expansions of the

Mott cross section. For high energy and low atomic numbers the screened Rutherford cross section gives good results in calculations or simulations. The screened Rutherford formula has been frequently used as the elastic differential cross section in Monte Carlo simulations. For effects caused by electron diffusion and plural large angle scattering, the use of Rutherford cross section has produced rather good agreement with experiments such as the total backscattering coefficient, the energy spectrum of backscattered electrons, the depth distribution of x-ray production (Reimer and Lodding, 1984) and the parameters of secondary electron emission (Luo and Joy, 1988,1990). Because it is quite accurate for the situations that we mentioned above and is in a convenient analytic form to enable faster calculation in computer simulation with much simpler procedures, the screened Rutherford formula is widely employed in electron microscopy. Including screening effect of the orbiting atomic electrons the screened differential Rutherford cross section is (Bethe and Ashkin 1953):

$$\frac{d\sigma}{d\Omega} = \frac{Z^2\lambda_R^4}{64\pi^4 a_0^2} \frac{1}{\left[\sin^2\left(\frac{\theta}{2}\right)+\left(\frac{\theta_0^2}{4}\right)\right]^2} \qquad (3.2)$$

where Z is the atomic number ; θ_0 is the screening parameter, $\theta_0 = 0.1167Z^{1/3}/E^{1/2}$ radian; a_0 is the Bohr radius; λ_R is the relativistically corrected electron wavelength, given in centimeters, $\lambda_R = 3.87*10^{-9} / (E+9.79*10^{-4}E_0^2)^{1/2}$; E is the beam energy in keV.

For low energy (E< 20 keV)and high atomic numbers (Z>30) it is more accurate to use Mott cross section which is derived from the relativistic Dirac equation, taking into account spin-orbit coupling. For large scattering angles the Rutherford formula is only an approximation and the Mott cross section offers the results that can differ significantly

from the Rutherford values.

Mott (1929) had given the relativistic expression of the differential cross section for an electron elastically scattered with an angle θ. The solution of the Dirac equation gives the scattering cross-section for unpolarized electron as follows:

$$\frac{d\sigma(\theta)}{d\Omega} = |f(\theta)|^2 + |g(\theta)|^2 \qquad (3.3)$$

where

$$f(\theta) = \frac{1}{2ik}\sum_{l=0}^{\infty}[(l+1)\,(e^{2i\eta_l}-1) \;\; + l\,(e^{2i\eta_{-l-1}}-1)]\,P_l(\cos\theta) \quad (3.4)$$

and

$$g(\theta) = \frac{1}{2ik}\sum_{l=1}^{\infty}[-\,e^{2i\eta_l} + e^{2i\eta_{-l-1}}]\,P_l^1(\cos\theta) \qquad (3.5)$$

where $hk/2\pi$ is the momentum of the scattering electron, $P_l(\cos\theta)$ and $P_l^1(\cos\theta)$ are Legendre and associated Legendre function, respectively. If we denote μ=-l-1 or μ=l , then the phase shifts η_l and η_{-l-1} are given by

$$\tan\eta_\mu = \frac{k\cdot j_{l+1}(kr) - j_l(kr)[(W+1)\tan\phi_\mu + (l+1+\mu)/r]}{k\cdot n_{l+1}(kr) - n_l(kr)[(W+1)\tan\phi_\mu + (l+1+\mu)/r]} \qquad (3.6)$$

$j_l(kr)$ and $n_l(kr)$ are spherical Bessel and Neumann functions, respectively. ϕ_μ satisfies:

$$\frac{d\phi_\mu}{dr} = \frac{\mu}{r}\cdot\sin(2\phi_\mu) + W - V - \cos(2\phi_\mu) \qquad (3.7)$$

W and V are the total energy and the atomic potential energy respectively.Mott cross sections have been tabulated for the interesting range of energies by Riley et al.(1975). Because the energies used increase in powers of two ($E=2^n$ keV), it is not convenient to use for microanalysis. Reimer and Lodding(1984) have published the Mott cross sections for a larger number of elements in the energy range 1-10 keV in steps of 1 keV and in the range 10-100 keV in steps of 10 keV. More recently Joy's group (Czyzewski et al., 1990) has published the data of Mott elastic scattering cross sections of electrons for all elements of the periodic table up to atomic number 92 over the energy range 20eV - 20 keV and angle range 0.5 - 180^0.

The total cross section of Reimer and Lodding through all the periodic table and from 1 keV to 100 keV can be approximated by an expression of the form (Reimer and Lodding,1984; Browning et al., 1993) :

$$\sigma_T = 4.7\times10^{-18}\frac{(Z^{1.33}+0.032Z^2)}{(E+0.0155Z^{1.33}E^{0.5})(1-0.02Z^{0.5}e^{-u^2})} \ (cm^2) \qquad (3.8)$$

where

$$u = \log_{10}8\cdot E\cdot Z^{-1.33}$$

And the total Mott cross section of Czyzewski et al.(1990) is fitted by the expression :

$$\sigma_T = \frac{3.0\times10^{-18}Z^{1.7}}{E+0.005Z^{1.7}E^{0.5}+0.0007Z^2/E^{0.5}} \ (cm^2) \qquad (3.9)$$

Eq.(3.9) is valid for atomic numbers up to Z=92 and for energies from 100eV to 30 keV(Browning et al., 1993). E is the incident energy in keV for Eqs.3.8 and 3.9.

Because the data set for the tabulated Mott cross sections is large and computations tend to be slow due to the need to interpolate between data points, several empirical forms have been found for the electron elastic scattering differential cross sections as well (Browning, 1991; Browning et al.,1991,1993).

Recently we have proposed a modified Rutherford cross section (Luo and Joy, 1994) in order to provide better accuracy and a faster and more convenient computer procedure. Following the initial idea of Curgenven and Duncumb (1971) t he elastic scattering angular ϕ used to be written as :

$$\tan\left(\frac{\phi}{2}\right) = \frac{b}{2p}\cdot\left(\frac{1}{\sqrt{RND}}-1\right) \qquad (3.10)$$

where b is 0.0144Z/E and p is $0.263Z^{0.4}$. To modify this formula, we have changed p into $0.263Z^{x}$ and x is given by :

$$x = 0.4 - \frac{60}{Z\cdot\sqrt{E_0}} \qquad (3.11)$$

where E_0 is the incident beam energy.

To verify this formula we have used both the single scattering and the continuous slowing- down Monte Carlo simulations employing the modified Rutherford formula and the Mott cross section for elastic scattering calculations for Au, Ag, Cu, Al and C with

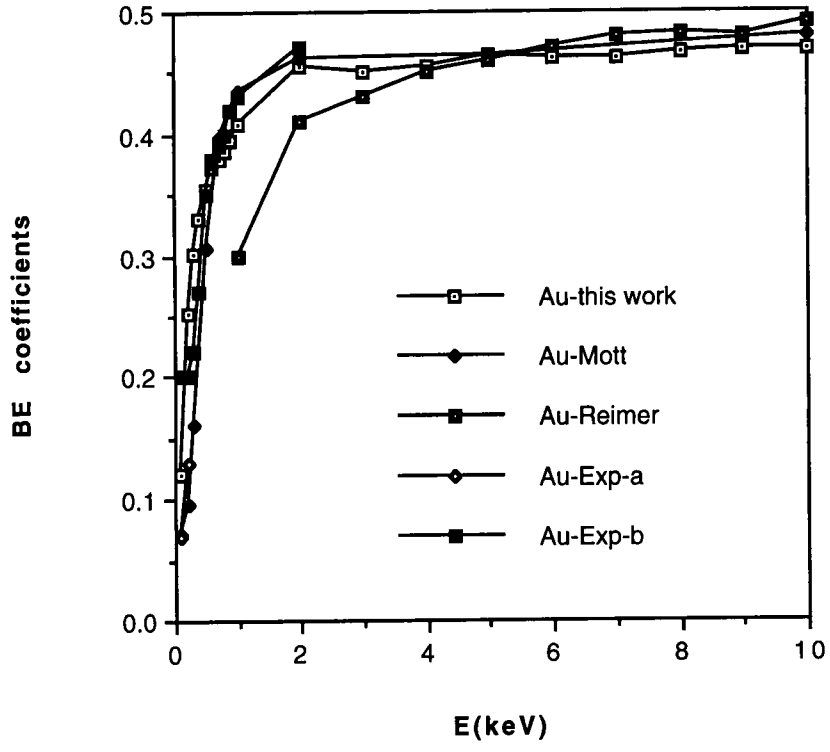


Figure 3.1 Comparison of backscattering coefficients for Au:

This work: calculated data using modified Rutherford cross section
Mott : calculated data using Mott cross section in this work
Reimer, Exp-a and Exp-b : quoted from Kotera et al.(1981)

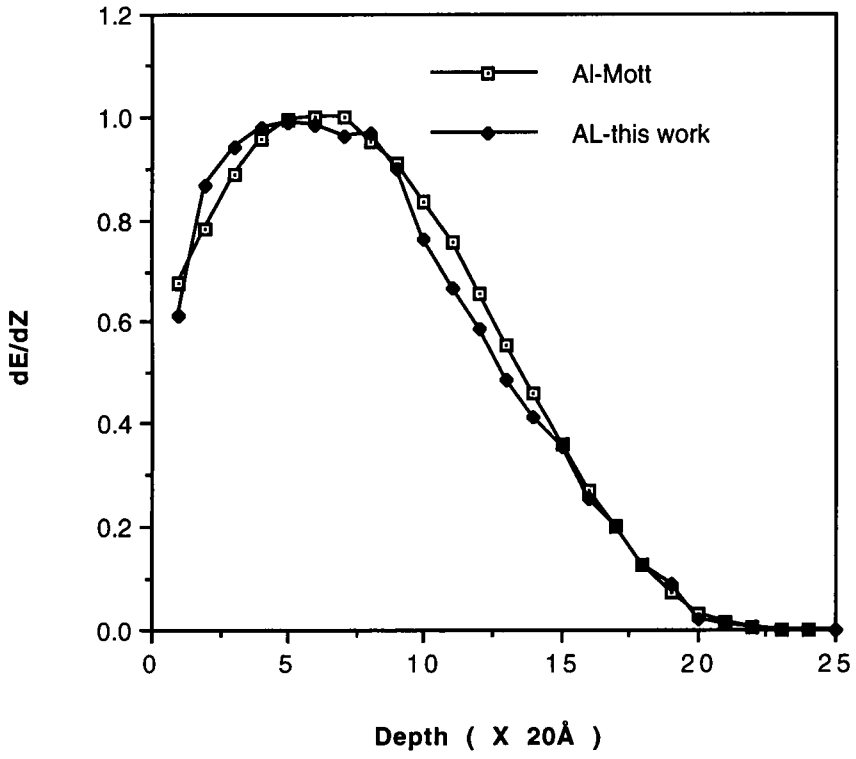


Figure 3.2 Comparison of energy deposition of depth for Al at 3 keV:
This work: calculated data using modified Rutherford cross section
Mott : calculated data using Mott cross section in this work

energies from 0.1 to 10 keV. The results indicate that the backscattered electron coefficients, the angular distribution of backscattered electrons and the energy deposition of depth are in good agreement of modified Rutherford cross section and Mott cross section (see Figures 3.1 and 3.2).

3.2.2 Inelastic scattering

During an inelastic scattering event, both energy and momentum are transfered to the target atoms or electrons while the kinetic energy of incident electrons decreases. The basic theories of inelastic scattering have been well established . The most popular of these are the Bethe theory (Bethe, 1930, Inokuti, 1971) and the dielectric theory (Ritchie, 1957).

The Bethe theory is based on Born approximation . In the Bethe theory the elements are assumed to be in atomic form and are treated on the basis of a single electron wave function undergoing a transition to the continuum. We have carried out the direct quantum mechanical calculation using Hartree-Slater model . In the Hartree-Slater model each electron is assumed to move independently of all other electrons in a time-averaged electrostatic field produced by all the nuclei and all the other electrons.Inner shell electrons have relatively large binding energies, the associated energy losses are typically some hundreds of eV corresponding to the X-ray region. Because of this strong binding to the nucleus, collective effects are generally unimportant. Inner shell ionization can therefore be described to a good approximation using a single-atom model.

The most important quantity in Bethe theory is the Generalized Oscillator Strength (GOS). The GOS describes the transfer of both energy and momentum from a fast

electron. It is necessary to calculate the initial and final state wave functions of the core electron to determine the GOS.In the Hartree-Slater method it is assumed that a central(spherically symmetric) field within the atom, and the averaged exchange potential at point r is equal to the exchange potential for an electron system whose total electronic charge density (both spins) is equal to that of the non-uniform system in question at the point r (Herman and Skillman, 1963) :

$$V^{exch} = -6\,[\,3/(8\pi)\,|\,\rho(r)\,|\,]^{1/3} \qquad (3.12)$$

Thus, the averaged exchange potential is a function only of $\rho(r)$. In a similar way it is possible to have a description of the correlation energy which is valid for a wide range of densities (Hohenberg and Kohn, 1964; Kohn and Sham, 1965; Mahan, 1981). The correlation formula proposed by Lindgren and Rosen (1970) is used in the self-consistent atomic potential.

$$V^{corel} = -\left[\, r_s + 3 + 4r_s^{0.5} - \frac{0.08}{r_s^{0.5}} \,\right]^{-1} \qquad (3.13)$$

$$r_s = \left(\frac{3}{4\pi\rho(r)a_0^3} \right)^{1/3} \qquad (3.14)$$

where $\rho(r)$ is electron density at r.

The radial wave function $\psi_i(r)$ of the ground state and the final state $\psi_f(r)$ are obtained by solving the radial Schodinger equation for a binding energy or a continuum energy E':

$$\left[\frac{h^2}{8m\pi^2}\frac{d^2}{dr^2} - V(r) - \frac{l(l+1)h^2}{8m\pi^2 r^2} + E' \right] \psi(r) = 0 \qquad (3.15)$$

where l is the angular momentum quantum number, V(r) is the sum of the nuclear coulomb potential, the total electronic coulomb potential, the exchange potential and the correlation potential. The Bethe differential cross section is :

$$\frac{d^2\sigma(E,q)}{dE\,dq} = \frac{4\pi e^4}{m\upsilon^2 E}\,\frac{1}{q}\,\frac{d f_{nl}(E,q)}{dE} \qquad (3.16)$$

where

$$\frac{d f_{nl}(E,q)}{dE} = \frac{8m\pi^2 E}{h^2 q^2}\sum_{l'} |\langle \varepsilon\, l' | \exp(i\,\mathbf{q}\cdot\mathbf{r}) | n\, l\rangle|^2 \qquad (3.17)$$

is the GOS, ε is the energy of an electron in the continuum, l' is its angular momentum quantum number, n is the principle quantum number of the bound subshell and l its angular momentum quantum number; υ is incident electron's velocity, E is the energy loss of incident electron.

The matrix elements of the GOS were determined by expanding exp(i **q**.**r**) in terms of spherical Bessel functions $j_l(qr)$.Wigner 3-j coefficients were used to evaluate the integral

$$\langle \varepsilon\, l' | \exp(i\,\mathbf{q}\cdot\mathbf{r}) | n\, l\rangle^2 = (2l'+1)\sum_{\lambda}(2\lambda+1)\left|\begin{pmatrix} l' & \lambda & l \\ 0 & 0 & 0 \end{pmatrix}\right|^2 \times\left[\int_0^\infty \psi_{nl}(r)\, j_\lambda(qr)\, \psi_{\varepsilon l'}(r) r^2\, dr\right] \qquad (3.18)$$

Thus, we can have

$$\frac{d\sigma}{dE} = \frac{4\pi e^2}{m\upsilon^2 E}\int_{q_{min}}^{q_{max}} \frac{1}{q}\,\frac{d\, f_{nl}(E,q)}{d\,E}\, dq \qquad (3.19)$$

The limits on q can be given from the energy and momentum conservation. From the energy conservation we have:

$$(E_0 + m_0c^2)^2 = (m_0c^2)^2 + h^2k_0^2\, c^2/4\pi^2 \qquad (3.20)$$

$$(E_0 + m_0c^2 - E)^2 = (m_0c^2)^2 + h^2k_1^2\, c^2/4\pi^2 \qquad (3.21)$$

where E_0 is incident electron beam energy, m_0c^2 is electron rest energy, E is incident electron energy loss. k_0 and k_1, the wave vectors of the incident electron before and after energy loss, can be obtained from Eqs.3.20, 21. Momentum conservation is incorporated to determine q_{min} and q_{max}

$$q_{min} = \sqrt{k_o^2 + k_1^2 - 2\, k_0k_1}$$

$$q_{max} = \sqrt{k_0^2 + k_1^2 + 2\, k_0k_1} \qquad (3.22)$$

The total ionization cross sections are obtained by integrating differential cross section from binding energy up to the incident energy. (In chapter 6 this method is used to compute X-ray ionization cross section.)

Another important theory in microscopy is dielectric theory(Lindhard,1954; Ritchie, 1957). Ritchie (1957) has derived an expression for the electric potential due to an electron moving with velocity **v** in a uniform infinite medium :

$$\varepsilon_0 \varepsilon(\omega, \mathbf{q})\nabla^2\varphi(\mathbf{r},t) = e\,\delta(\mathbf{r} - \mathbf{v}t) \qquad (3.23)$$

where $\varepsilon(\omega,\mathbf{q})$ is dielectric function , **q** is the wave vector, h **q** and hω are the momentum transfer and energy transfer to the electrons in the solid, respectively. In Fourier space

$$\varphi(\omega, \mathbf{q}) = -\frac{2\pi e\,\delta(\mathbf{q}\cdot\mathbf{v} + \omega)}{\varepsilon_0\varepsilon(\omega, \mathbf{q})\,q^2} \qquad (3.24)$$

where

$$\varphi(\mathbf{r},t) = \frac{1}{(2\pi)^4}\int d\mathbf{q}\int d\omega \exp[\,i(\mathbf{q}\cdot\mathbf{r} + \omega t)]\,\varphi(\omega, \mathbf{q}) \qquad (3.25)$$

Then the stopping power is given by

$$-\frac{dE}{ds} = e\,(-\nabla_s\varphi(\mathbf{r},t))\Big|_{\mathbf{r}=\upsilon t} \qquad (3.26)$$

Expressing φ in terms of its Fourier representation

$$-\frac{dE}{ds} = \frac{h^2}{4\pi^3 a_0 E_T}\int\int q_\perp \omega\,\mathrm{Im}\left[\frac{-1}{\varepsilon(\omega, q)}\right]\frac{dq_\perp\,d\omega}{q_\perp^2 + (\omega/v)^2} \qquad (3.27)$$

where

$$q^2 = q_\perp^2 + \omega^2/\upsilon^2 \quad \text{and} \quad q_\perp = 2\pi m\upsilon \sin\theta / h$$

a_0 is the Bohr radius, m_0 is the rest mass of an electron, $q_\perp$ is the component of **q** in the direction perpendicular to **v**, and $E_T = E_0 (1 + E_0 /511)/ (1 + E_0 /1022)^2$. The stopping power can also be expressed as

$$-\frac{dE}{ds} = \iint n E \frac{d^2\sigma}{d\Omega dE} d\Omega\, dE \qquad (3.28)$$

where n is the number of atoms or molecules per unit volume of the sample. Compare Eq.3.27 and 3.28 and with a small scattering angle θ we can obtain the differential cross section

$$\frac{d^2\sigma}{d\Omega dE} \approx \frac{1}{2\pi^2 a_0 n E_T} \mathrm{Im}\left[\frac{-1}{\varepsilon(\omega, q)}\right]\left(\frac{1}{\theta^2 + \theta_E^2}\right) \qquad (3.29)$$

where $d\Omega \approx 2\pi\theta\, d\theta$, $\theta_E = E / (2\gamma E_T)$ and $\gamma = 1 / \sqrt{1-(v/c)^2}$.

The single scattering distribution S(E) is:

$$S(E) = I_0 \left(\frac{\rho t N_a}{A}\right) \frac{d\sigma}{dE}$$

or
$$S(E) = \frac{I_0 t}{2\pi a_0 E_T} \mathrm{Im}\left[\frac{-1}{\varepsilon(\omega, q)}\right] \ln\left[1 + \left(\frac{\beta}{\theta_E}\right)^2\right] \qquad (3.30)$$

where ρ is the mass density, A the atomic weight and N_a the Avogadro number, β the collection semiangle. $\varepsilon(\omega, q)$ satisfies the sum rule :

$$Z = \frac{\varepsilon_0 m_0}{(\pi/2) e^2 n} \int_0^\infty \omega\, \mathrm{Im}\left(\frac{-1}{\varepsilon}\right) d\omega \qquad (3.31)$$

In eq.3.29 if the scattering angle is very small , which is corresponding to the most of the case in EELS , then $Im[-1/\varepsilon(\omega, q)]$ is approximately equal to $Im[-1/\varepsilon(\omega, 0)]$.

The $Im[-1/\varepsilon(\omega)]$ is called the energy loss function due to its proportionality to the energy loss probability and $(\theta^2 + \theta_E^2)^{1/2}$ is proportional to the momentum transfer to the specimen. In the long wavelength limit q=0 the electron dielectric function $\varepsilon(\omega, q)$ approaches the optical dielectric constant $\varepsilon(\omega)$. Comparing the results of EELS and the optical measurements (e.g., Daniels et al., 1970) although there are some differences due to the different excitation mechanisms: the external disturbed wave is the longitudinal for an electron and the transverse for a photon, their overall agreement throughout wide energy loss region provides us two opportunities. First , materials with known optical peaks can be used as calibration markers for energy loss experiments . Secondly, since ultraviolet absorption data are usually only available for few organic materials in the region above 10 eV (< 1240Å), one can use EELS to deduce optical constant and extend the known spectroscopic range up to a few keV (Isaacson and Crewe, 1975) . This technique is used in Chapter 5 to derive electron stopping power information.

3.2 PLURAL SCATTERING IN EELS AND IT'S CORRELATIONS

The qualitative and quantitative information extracted from EEL spectrum is directly connected with electron single scattering distribution as we discussed above. But the plural scattering resulted in both elastic and inelastic scattering dramatically alters the intensity distribution in an EEL spectrum from single scattering distribution with a typical thickness of a specimen in the microscopes. The most convenient and powerful method to remove the plural scattering effect is the Fourier-Log deconvolution technique. Burge and Misell (1968) and Misell and Jones (1969) provided a formulation for the calculation in terms of a logarithmic series for the single scattering solution. The formulation

of Burge and Misell has been shown by Whelan (1976) to be equivalent to the earlier results of Landau (1944) who used a Boltzmann transport equation. Johnson and Spence(1974) extended the work of Landau, Burge and Misell, obtained an equation for a plural scattering profile, i.e. the recorded spectrum R(E) can be expressed as a summation of the distributions of zero energy loss Z(E), single scattering S(E), double scattering S(E)*S(E) and so on:

$$R(E) = Z(E)*[\ \delta(E)+S(E)/I_0+S(E)*S(E)/(2!I_0^2)+S(E)*S(E)*S(E)/(3!I_0^3) + \cdots] \quad (3.32)$$

The * denotes a convolution. Taking the Fourier transform of Eq.3.32 we can get

$$R(\omega) = Z(\omega)\exp[\ S(\omega)/I_0]$$

or

$$S(\omega) = I_0 \ln[\ R(\omega)/ Z(\omega)] \quad (3.33)$$

In principle an inverse Fourier transform of Eq.3.33 can be used to give an exact single scattering distribution. However, the recorded EEL spectrum contains noise so that there is the fractional noise content in $R(\omega)$ increasing with ω and at high ω $R(\omega)$ is dominated by noise (Egerton, 1986) . Although there are several methods available for improving this problem and the differences between the true distribution and the deconvoluted one maybe small if the instrument resolution is high, no ideal single scattering distribution can be derived from this deconvolution process, as indicated by Egerton (1986).

Another method is called the convolution method which was reviewed by Daniels et al. (1970). This method is an iterative procedure for computing the twofold inelastic scattering intensity from the experimental spectrum. The iteration is started from the first channel, which is taken as single scattering intensity. The double scattering at the second channel is derived from the first channel's single intensity. The single scattering at the

second channel is obtained by subtracting the double scattering contribution from the experimental spectrum . The third channel 's double scattering intensity again can be calculated and the third channel's single scattering intensity can be obtained.. Although only the double scattering correction was carried out in Daniels' paper, the same procedure can be done for the three-fold scattering and so on. This method is based on the basic fact that the electron energy loss spectrum is a result of the convolution of elementary inelastic scattering processes. In 1976 Fields in his Ph D thesis modified Daniels' method and improved the iteration technique by including triple scattering events. Fields' method was published in a paper by Livins et al. (1988). Recently, based upon Fields' technique, Wang (1990) derived a direct convolution method to correct multiple scattering events in EELS.

Fourier convolution techniques have been developed and employed for simulation of EEL spectrum to obtain gas excitation cross section (Zanchi et al., 1990, Kihn et al. 1991) and solid specimen inelastic mean free path and stopping power (Luo et al., 1993, Joy et al. 1993b). This convolution technique can be used to remove the limitation of the deconvolution process which is influenced by the experimental spectrum noise , while in the convolution procedure the calculated results are based on the dielectric model and fitted to the experimental spectrum, so that an " ideal " single inelastic scattering can be obtained.

The Fourier convolution technique (Luo et al., 1993, Joy et al. 1993b) can be briefly described as below. In the region of low energy losses the main energy loss mechanism includes interband transitions, surface plasmon and bulk plasmon excitations. In general these individual excitation processes are overlapped in the spectrum. The single scattering distribution obtained from deconvolution processes is a result of all possible

excitations. The convolution technique makes it possible to modulate every excitation separately by the dielectric theory. The dielectric function ε can be used to describe both single excitations and collective excitations (Ritchie and Howie ,1977) ,where

$$\varepsilon = 1 + \frac{4\pi Ne^2/m_0}{\omega^2 - \omega_0^2 - i\omega\tau} \qquad (3.34)$$

Here $\omega_p{}^2 = 4\pi Ne^2/m_0$ is the bulk plasmon frequency, N is number of atoms per unit volume (for free electrons N is free electron density), ω_0 is a parameter describing the bound state (i.e; for free electrons $\omega_0 = 0$). The constant τ describes the damping suffered by the excitation. Thus the energy loss function which describes the bulk plasmon is:

$$\mathrm{Im}\{-1/\varepsilon\} = \frac{\omega\tau\omega_p^2}{(\omega^2 - \omega_x^2)^2 + \omega^2\tau^2} \qquad (3.35)$$

The energy loss function Im{-1/(1+ ε) is used to describe the surface plasmon (Plummer et al., 1992). Inner shell excitations in the low energy loss region are represented by the ' saw tooth' curves, with post-edge slopes of the form proportional to E^{-r} (Maher et al., 1979).

According to a Poisson distribution

$$I_n = (I/n!)(t/\lambda)^n \exp(t/\lambda) \qquad (3.36)$$

we can have

$$I_1 = \int_0^{\infty} \sum_i S_i(E)\, dE = I_0 t \sum_i \frac{1}{\lambda_i} \qquad (3.37)$$

From Eq.3.33 in the Fourier space the plural scattering intensity of the spectrum $J(\omega)$ is

$$J(\omega) = Z(\omega) \exp\left(\sum_i \frac{t}{\lambda_i} S_i(\omega) \right) \qquad (3.38)$$

where $Z(\omega)$ is the zero peak intensity distribution in the Fourier space , λ_i is the i-th inelastic scattering excitation mode's mean free path, $S_i(\omega)$ is the i-th single inelastic scattering distribution in the Fourier space of $S_i(E)$, which is determined by dielectric energy loss function $Im(-1/\varepsilon)$ for low energy loss area.

The first step of simulating an EEL spectrum is to use an FFT deconvolution procedure to obtain a single scattering distribution from the experimental EEL spectrum. Then, from Eq.3.30 and 3.35 choose the parameters τ, ω_X and a proportionality factor p, to fit each of the observed profiles. Finally using Eq.3.38 an FFT convolution process is employed to change the simulated single profile into a plural scattering profile for fitting to the experimental EEL spectra by adjusting these parameters iteratively. Using this simulation scheme the single scattering distribution S(E) of low energy losses is obtained.

Although the Fourier deconvolution and the convolution procedures are very powerful techniques in EELS, and the Fourier deconvolution was widely used in the past two decades, its theoretical basis builds on the condition that all the scattering electron are collected, i.e., only for the 100% collection of the transmitted electrons, the EELS

spectrum can be expressed as the well accepted form

$$J(E)= I_0 \sum_{n=1}^{\infty} \frac{1}{n!} \left(\frac{t}{\lambda} \right)^n S_i^{(n)}(E) \qquad (3.39)$$

where J(E) is the EEL intensity, $I_0 = I \exp(-t/\lambda_i)$, λ_i is the inelastic mean free path, $S_i^{(1)}(E)$ is the single inelastic scattering distribution and $S_i^{(n)}(E)$ is the n-th order of inelastic scattering distribution. Due to the finite collection angle of the spectrometer the angular distribution and correction are necessary and the inelastic angular scattering correction (Livins et al., 1988 ; Wang , 1990) or both the inelastic and elastic scatterings' correction (Batson and Silcox, 1983; Egerton and Wang, 1990) have been carried out in the last decades.

3.3 NEW APPROACH ON MIXED SCATTERING

In EELS studies plural scattering introduces unwanted artifacts into the energy-loss spectrum not only due to the inelastic scattering but also the elastic scattering. In an elastic scattering event the electron energy remains unchanged but the direction of the trajectory is altered . In an inelastic scattering event the electron transfer some energy to the sample, this results both in a reduction of the kinetic energy of the electron and a change in the direction of its travel. Since the total mean free path is about several hundred Å for all elements at 100-200 keV, an electron is likely to undergo plural scattering in passing through a typical specimen. It is necessary to remove plural scattering from a experimental spectrum including both elastic and inelastic scattering.

Techniques to remove plural scattering in microanalysis have previously been

developed and applied to the experimental electron energy loss spectrum. These techniques are either based on convolution (Misell and Jones, 1969; Daniels et al, 1970; Livins et al., 1988 ; Wang , 1990, Luo et al., 1993, Joy et al., 1993b) or Fourier transform deconvolution method (Johnson and Spence, 1974; Egerton, 1986, Crozier and Egerton, 1989 , Luo et al., 1991, Joy et al., 1990). The quantitative calculation of both elastic and inelastic angular scattering distributions is not considered in the most of these methods. In the last two decades the Fourier transform techniques combined with one-dimensional Poisson statistics (see Eq.3.37) have been considered as the best suited to cope with EELS (Egerton et al., 1985) because of the ready availability of fast Fourier transform algorithms that minimize the processing time required, but this technique involves the inelastic energy loss only. Livins et al.(1988) and Wang (1990) have considered the inelastic scattering angular correction.Recently Egerton and Wang (1990) have investigated both the inelastic and elastic scattering events for an electron energy loss spectrum recorded with an angle-limiting aperture. However,their method is based on the assumption that elastic and inelastic scattering processes are independent.

Strictly speaking, if all of the scattering electrons can be collected by the electron spectrometer, the Fast Fourier deconvolution transform techniques are valid and maybe are the best methods. In practice, the spectrometer is usually performed with some form of angle limiting collection aperture. On the other hand, the characteristic energy loss distribution results in both inelastic and elastic scattering events. Due to the fact that there has been no systematic study of both inelastic and elastic scattering angular correction, in this thesis we propose a new quantitative method for the determination of the single-scattering profile from the electron energy loss spectrum, which contains contributions from both elastic and inelastic plural angular scattering events.

Our new method (Luo and Joy, 1994b) is based on the three dimensional Poisson statistics (Batson and Silcox, 1983 , Jeanguillaume et al. , 1992 and Ho et al. , 1993) :

$$P(E,\theta)=I_T\sum_{n=0}^{\infty}\frac{1}{n!}\left(\frac{t}{\lambda_e}S_e(\theta)+\frac{t}{\lambda_i}F(E)\cdot S_i(\theta)\right)^{(n)}\exp\left(-\frac{t}{\lambda_T}\right) \qquad (3.40)$$

which involves the inelastic single scattering energy loss function F(E), the inelastic single scattering angular distribution function $S_i(\theta)$ and the elastic single scattering angular distribution function $S_e(\theta)$. Where I_T is the total incident electron intensity; t is the sample thickness; λ_i , λ_e and λ_T are inelastic , elastic and total scattering mean free paths; $S_i(\theta)$ and $S_e(\theta)$ and F(E) are all normalized ; $P(E,\theta)$ is the plural scattering distribution. (n) denotes the n-th order of convolution and the express for it is :

$$S^{(n)}(\xi)=\int_{-\infty}^{+\infty}S^{(1)}(\xi')\cdot S^{(n-1)}(\xi-\xi'))d\xi' \qquad (3.41)$$

It is easy to show that if we integrate Eq.3.40 over the entire solid angle the elastic scattering factor is cancelled out, then this 3-Dimension Eq.3.40 becomes 1-Dimension Eq.3.39 which is the theory basis of widely used Fourier deconvolution method. Eq.3.40 very clearly shows how the recorded EEL spectrum is formed from both inelastic and elastic scattering. The EEL spectrum is the result of mixed inelastic and elastic scattering events and the inelastic and elastic scattering can not be treated as independent each other, and the elastic scattering contribution can be ignored for a practical collection aperture.

In our calculation procedure, Rutherford cross section (Eq.3.2) is used for the

single elastic scattering angular distribution .

Ignoring the Cerenkov radiation loss, Fano's formula for inelastic scattering angular distribution is :

$$\frac{d^2\sigma}{d\Omega dE} = F(E)\cdot\frac{1}{\theta^2+\theta_E^2} \qquad (3.42)$$

where $\theta_E = E/(2\gamma E_T)$, $E_T = m\upsilon^2/2$, and $\gamma = 1/(1-\upsilon^2/c^2)^{1/2}$. In this work, the energy loss E is up to 100 eV, within this region the angular distribution $S_e(\theta) = 1/(\theta^2+\theta_E^2)$ is almost independent of the energy loss E.Therefore, we take the bulk plasmon energy loss for all E in θ_E.

This method is tested for aluminum at 100 keV with collection semi-angle 5 mrad. The convolution order is up to 10 and the scattering angle is up to 300 mrad and 600 mrad respectively, which are accurate enough for this spectrum. Initially, an FFT deconvolution procedure is imployed to obtain the single inelastic scattering distribution F(E) without angular correction as a test function. Further, using Eq.3.40 an iterative convolution process is carried out to combine the single scattering energy and angular distributions F(E), $S_i(\theta)$ and $S_e(\theta)$ to a plural scattering spectrum $P(E,\theta)$. Considering that some electrons have been scattered elastically or inelastically through an angle greater than β which is the collection semi-angle of the aperture and then elastically or inelastically back into the aperture, a careful calculation of angular distribution is performed as shown in appendix A. Finally the theoretical spectrum $P(E,\theta)$ is modified by the finite resolving power of the analyser according to the convolution integral:

$$G(E,\theta) = \int_{-\infty}^{+\infty} P(E',\theta)\cdot R(E-E')dE' \qquad (3.43)$$

where $G(E,\theta)$ is the theoretical EEL intensity with energy and angular distribution, and $R(E)$ is the intrinsic instrumental broadening function which is experimentally determined and mathematically normalized. By adjusting $F(E)$, t/λ_e and t/λ_i this procedure is continued until the calculated resultant spectrum $G(E,\beta)$ fits the experimental , While $G(E,\beta)$ is:

$$G(E,\beta) = \int_{0}^{\beta} G(E,\theta)d\theta \qquad (3.44)$$

The Figure 3.3 shows that our calculated result is in good agreement with the experiment in the plasmon region as well as in the zero loss peak area. Fig.3.4 is the comparison of the single scattering distributions F(E)s with and without angular correction (Egerton, 1986, Luo et all, 1993). From Figure 3.4 we see there is no double plasmon peak if both the elastic and inelastic angular corrections are considered in this method. The double plasmon, results in the FFT deconvolution procedure which does not include angular correction (Egerto, 1986, Luo et al., 1993), may indicate that the traditional FFT deconvolution procedure may not completely remove the plural scattering from the experimental spectrum. The conclusion from our result , that the double plasmon excitation has low probability in aluminum when $t/\lambda>3$ is consistent with Egerton and Wang (1990) and the theoretical prediction by Ashley and Ritchie(1970).

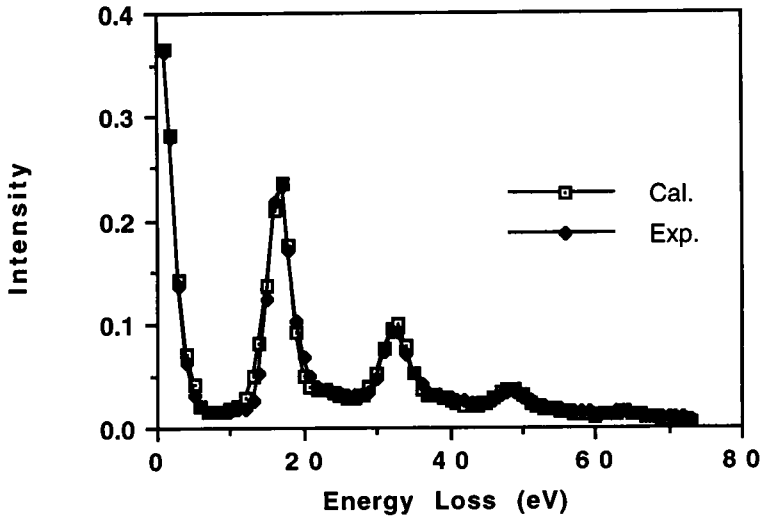


Figure 3.3 Comparison of calculated and experimental EELS for aluminum at 100 keV with semi-collection angle 5 mrad.

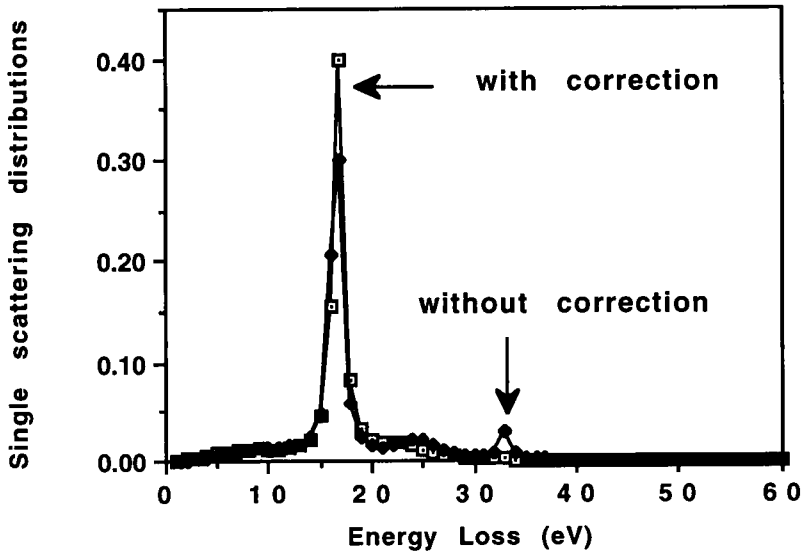


Figure 3.4 Comparison of single scattering distributions with and without mixed angular correction.

3.4 LOCAL THICKNESS DETERMINATION BY EELS

In analytical electron microscopy, it is often important to know the local thickness of a sample. The conventional method used for measuring specimen thickness by EELS is (Egerton, 1986, Leapman et al., 1984, Egerton and Cheng, 1987):

$$\frac{t}{\lambda_i} = \ln\left(\frac{I_T}{I_0}\right) \tag{3.45}$$

where t is the specimen thickness, λ_i is the total inelastic mean free path, I_T is the total intensity in an EEL spectrum, and I_0 is the zero loss peak intensity. This is rigorously correct only if the electrons are collected over all scattering angles and all energy losses(Ho et al., 1993). However, in most experiments only a fraction of the scattered electrons are collected due to a limited collection semi-angle. To overcome this problem we propose a new method (Luo et al., 1994b) based on three-dimension Poisson statistics which takes into account both the inelastic and elastic mixed angular correction as we discussed above. The Rutherford cross section (Bethe and Ashkin, 1953) is used for the single elastic scattering angular distribution $S_e(\theta)$ and the total elastic mean free path. The inelastic scattering angular distribution is proportional to $1/(\theta^2+\theta_E^2)$, where θ_E is the characteristic inelastic scattering angle. The inelastic mean free path is calculated by an empirical formula proposed by Egerton and Cheng (1987). The first step is to obtain a single scattering distribution F(E) by an FFT deconvolution procedure (Egerton, 1986), together with λ_i, λ_e, as test parameters. Next an iterative convolution process is carried out to combine the single scattering energy loss F(E) and angular distributions, $S_i(\theta)$ and $S_e(\theta)$ to give a plural scattering spectrum $P(E,\theta)$. Through repeated iterations F(E) and t are adjusted until the calculated spectrum fits the experimental spectrum.

This approach has several advantages. First, multiple inelastic, elastic and mixed scattering of the incident electrons can be taken into account simultaneously. Second, the procedure is applied to the low energy loss region only, thus avoiding the problems associated with recording and processing spectra from core loss regions. Third, no specific parameters such as optical refractive index are needed.

The aluminum films were produced and the experimental data collected as described below and follow techniques previously described (Blackson et al. 1993). Aluminum films were deposited simultaneously onto freshly cleaved rock salt and disk of cured epoxy resin. The rock salt was dissolved in water and the Al film was picked up on 400 mesh TEM grids.The cured epoxy with aluminum film was cross sectioned using ultramicrotomy techniques and the thickness of aluminum was measured using transmission electron microscopy. The electron microscopy was performed on an Hitachi 800 TEM equipped with a Gatan EELS.

The calculated thickness for the two Al films are 600Å and 1600Å respectively and are in good agreement with our direct TEM measurements of the films. Figure 3.5 shows the calculated EELS spectra are in good agreement with our experimental data for two samples. To check this technique we combined the single scattering distribution obtained from our calculations and the thickness values reported by Egerton (1986), to simulate an EEL spectrum. The resulting spectrum is in good agreement with Egerton's (1986) experimental EELS data as shown in Figure 3.6.

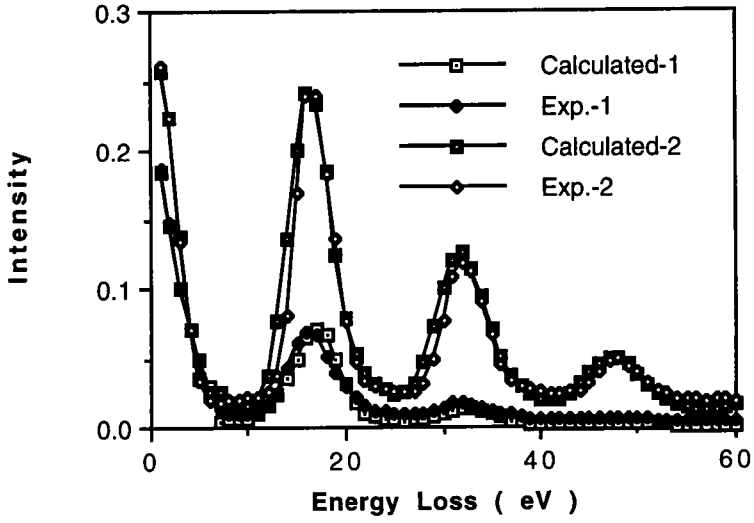


Figure 3.5 Comparison of experimental and calculated spectra for Al . 1 and 2 are EELS for two different thickness samples .

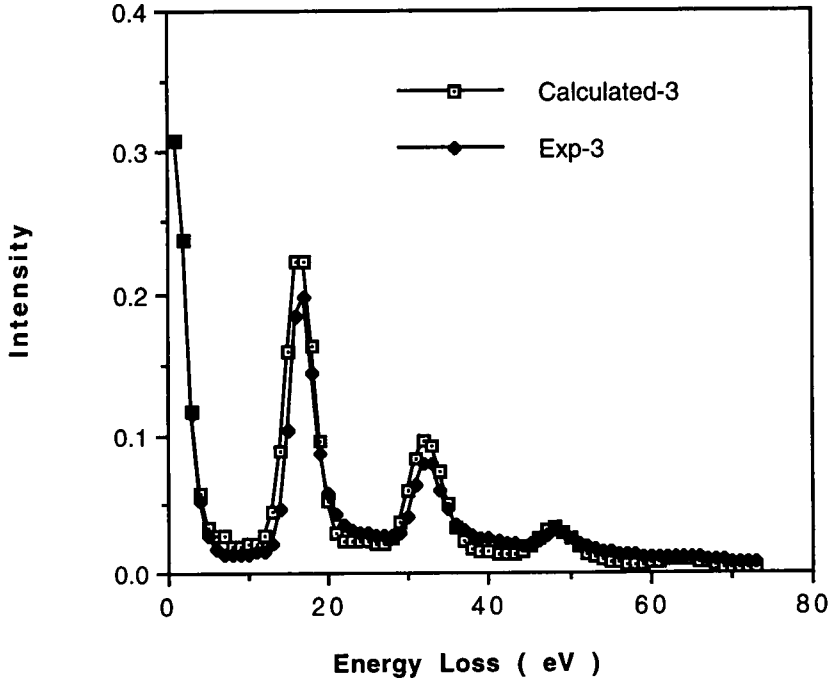


Figure 3.6 Comparison of experimental data-3 (Egerton, 1986) and the calculated spectra-3 for Al in this work.

CHAPTER 4

MONTE CARLO CALCULATIONS OF SECONDARY ELECTRON EMISSION

4.1 INTRODUCTION

With the advent and wide availability of powerful computers, the methodology of computer simulations has become a ubiquitous tool in the study of microscopy and microanalysis. The basic idea in these methods is that with a computer one may follow explicitly the trajectories of the incident beam electrons in the microscope. Because the system (the given specimen and the electron beam) is appropriately constructed, i.e., physically boundary conditions and the proper physical models for electron-specimen interactions are employed, the trajectory will serve to simulate the behavior of a real assembly of electrons, and the statistical analysis of the trajectories will determine meaningful predictions for properties of the electron signals such as backscattered electrons (BSE) and the secondary electrons (SE).

One of the very earliest published papers on ' Monte Carlo' methods (Kahn 1950) provides an excellent statment of the basis of the method : " By applying random sampling techniques to the problem (of interest) deductions about the behavior of a large number of particles are made from the study of comparatively few. The technique is quite analogous to public opinion polling of a small sample to obtain information concerning the population of the entire country". The spirit of Monte Carlo method is the use of random sampling to solve a problem in a scientific fields (which can be math, physics, chemistry , and so on). The first published example of the use of random numbers to solve a problem is probably

that of Buffon who in his 1777 volume " Essai d' Arithmetique Morale " described an experiment in which needles of equal length were thrown at over a sheet marked with parallel lines. By counting the number of intersections between lines and needles Buffon was able to derive a value for π . Subsequently other mathematicians and statisticians followed Buffon's lead and made use of random numbers as a way of testing theories and results. During the Manhattan Project, which led to the development of the first atomic bomb, John von Neumann, Stanislav Ulam, and others made innovative use of both random number sampling and of game-playing simulations involving random numbers as a way of studying physical processes as diverse as particle diffusion and the probability of a missile striking a flying aircraft, and it was during this period that these techniques were first dubbed " Monte Carlo methods" (Metropolis and Ulam 1949; McCracken, 1955).

Although Monte Carlo methods had been applied to many other phenomena it was not until the work of Hebbard and Wilson (1955) that the method was successfully employed for charged particles. Later work by Sidei et al. (1957), Leiss et al. (1957) led to a major paper by Berger (1963) which laid the groundwork for future developments. Simultaneously, in England, M. Green, a physics graduate student in Cambridge working for V. E. Cosslett, was persuaded to investigate the application of von Neumann's Monte Carlo method, and the university's EDSAC II computer, to the scattering of electron beams. Taking experimental data on the scattering of electrons in a 1000 Å film as a starting point, Green (1963), and later Bishop (1965) were able to derive the electron backscattering coefficient, and the depth dependence of characteristic X-ray production, from a bulk sample, and demonstrate good agreement with measured values.

By 1976 the use of this technique was sufficiently common for a conference on the "Use of Monte Carlo Calculations in Electron Probe Microanalysis and Scanning Electron

Microscopy" to be held at the National Bureau of Standards in Washington D. C.. The proceedings of that meeting (Heinrich et al. , 1976) still form one of the basic resources for information in this field, and programs , algorithms and procedures developed by the NBS group have formed the starting point for many of the programs in current use.

The importance of these methods is that in principle, they provide accurate results for the BSE and SE signals in scanning electron microscopes. Monte Carlo methods can be used to simulate the primary electrons and the secondary signals energy distributions, angular distributions and depth distributions and other properties under investigation thus, they provide indispensable bench marks for microscopy and microanalysis. There are, however, important limitations. The finite capacity of computers (even for a supercomputer) , for example, in both memory and time, implies that one may consider only a finite number of electrons (both incident electrons and secondary signals in particular SEs) and one may follow trajectories of only finite length.

The Monte Carlo method is a method for performing a random walk in the specimen. The averages over these statistical trajectories correspond to equilibrium ensemble averages. In microscopy, each incident electrons is traced during its many collisions until it loses its energy or escapes from the specimen, and in each step of the traced electrons the scattering angle is predicted on the basis of theoretical probability distributions or empirical models (Joy, 1991).

For the incident beam electrons and the the electrons in the specimen, the total number of possible configurations is an astronomically large number, and straightforward sampling of these configurations is impractical. There are different types of Monte Carlo methods available as introduced below. Our Monte Carlo scheme is biased to probe the

statistically important regions of the specimen for secondary electron (SE) cascade processes and only the incident and backscattered electrons trajectories are traced. The secondary electron simulation is considered in a statistical way to overcome the computer limitations.

Advances in electron-optical and vacuum design have recently resulted in the availability of scanning electron microscopes with a potential spatial resolution of better than one nanometer. This level of performance has, in turn, stimulated renewed interest in the use of, and the limits to, secondary electron imaging in the scanning electron microscopy (SEM). This chapter describes a Monte Carlo simulation which attempts to calculate from a detailed model of the electron beam interaction the properties of the secondary electron signal, such as its magnitude, and its angular and depth distribution, which are important in interpreting SE images.

The phenomenon of secondary electron emission was discovered in 1902 (Austin and Starke,1902) and has since been the subject of numerous experimental and theoretical investigations. Important pioneer studies were performed by Bethe (1941), and Salow (1940), leading to the development of more detailed phenomenological models by Baroody (1950), Jonker (1952) and Dekker (1958).Wolff (1954) proposed the use of the Boltzmann transport equation to describe the process of secondary electron generation through the cascade, and many subsequent treatments such as those of Cailler and Ganachaud (1972), Bindi et al. (1980 a,b,c) , Schou (1980,1988), Rosler and Brauer (1981a,b,1988), Devooght et al. (1987) have used the Boltzmann equation for the calculation of SE.

Other treatments have also proved to be useful. For example Chung andEverhart (1974,1977) used a simple exponential decay law and quantum theory to calculate the form

of the emitted secondary electron energy distribution. Techniques based on some form of Monte Carlo simulation have also been widely applied. Koshikawa and Shimizu(1974) proposed a model in which the primary beam is assumed to penetrate directly to some maximum depth L without suffering any energy loss, and then generate secondaries whose subsequent multiplication through the cascade process is followed by the Monte Carlo simulation . This model is simple to compute but only account for the secondaries (SE1) generated by the incident beam since the later progress, and possible backscattering, of the primary electron is not followed. Joy (1984,1985) incorporated the exponential decay law into a single-scattering Monte Carlo simulation for the special case in which secondary generation was assumed to arise solely from knock-on collisions producing fast (i.e high energy) secondary electrons. This model followed the trajectories of both the primary and the secondary electrons, but because of the limitations of calculating time the secondaries were only tracked until their energy fell below 200 eV.Secondaries of energy lower than this value were assumed to escape according to the exponential decay law. Ding and Shimizu (1988) proposed a theoretical model based on the combined use of Gryzinski's inner-shell electron excitation function and the dielectric function for taking account of the valence electron contribution in inelastic scattering processes. Luo et al. (1987), and Luo and Joy (1988) adopted a hybrid model of the exponential decay law and cascade process and combined this with a Monte Carlo simulation of the primary electron trajectory, but were restricted to the calculation of secondaries with energies below 2 keV only.

In most previous papers (with the exception of that by Joy 1984,1985), and especially in those employing some form of Monte Carlo simulation (e.g. Chung and Everhart 1974,1977, Koshikawa and Shimizu 1974, Bindi et al .1980 a,b,c; Rosler and Brauer 1981a,b, 1988, Devooght et al . 1987, Ding and Shimizu 1988) the energy of the

secondaries was restricted to a maximum value of 100 eV. This assumption is not, however, accurate especially at high incident beam energies where a significant fraction of fast secondaryelectrons may be generated. Therefore in this present work,secondary electrons with energies ranging from zero to half the incident beam energy have been included in the cascade process calculation. In addition a more detailed analysis of the excitation of SE y both the incident and the backscattered electrons has been made in order to achieve better agreement between theory and experiment as well as a better explanation of the variation of the relative yield or β coefficient with the variation of the incident energy.

4.2 MODEL FOR SECONDARY ELECTRON PRODUCTION

Construction of the model for secondary electron production involves three distinct steps, determining the trajectory of the incident electron, computing the rate of secondary electron generation along each portion of this trajectory, and finally calculating the fraction of secondary electrons which escape from the solid after a series of cascade process. In this chapter the primary electron trajectory is computed using a plural scattering Monte Carlo model . The electron range for a given beam energy is obtained from the modified Bethe stopping power equation (Bethe ,1930 , Joy and Luo, 1989) discussed in Chapter 5) :

$$\frac{dE_0}{dS} = -\frac{78500}{E_0}\frac{Z\rho}{A}\ln\left[\frac{1.166(E_0 + kJ)}{J}\right] \qquad (4.1)$$

where E_0 is the incident electron energy, Z and A are the atomic number and the atomic weight, respectively, S is the length of the path along the trajectory , ρ is the density; J is the mean ionization potential,and k has a value of 0.851 for Au, 0.852 for Ag, 0.83 for Cu and 0.815 for Al. This equation is accurate down to 50 eV. Its values for Au, Ag, Cu and

Al are typically within 10% over the range 50-200eV, and within better than 5% from 200eV to 10 keV compared with published values from Tung et al.(1979). Below 50 eV the stopping power is obtained from the data of Tung et al.(1979). Following Berger and Seltzer (1964) J can be approximated as

$$J = 9.76Z + \left(\frac{58.5}{Z^{0.19}}\right) \qquad (4.2)$$

or, alternatively, experimental values from Berger and Seltzer (1982) can be used. For the elements considered here the computed and experimental values differ by at most 2%.The range, determined from an integration of equations (4.1) and (4.2), is then divided into 50 steps of equal length for the Monte Carlo model of the primary beam interaction. The simulation uses the plural scattering approximation (Joy 1987) and employs the screened Rutherford cross section to determine the elastic scattering. This model has been shown to produce good data for all the elements and energies considered here. Typically 5000 trajectories (at normal incidence) were computed for each data point to ensure good statistical accuracy.

The second step is to compute the rate of production of secondary electrons along the trajectory determined as discussed above. The model in this paper takes into account all possible creation processes of SE resulting from the interaction of primary electrons and backscattered electrons with free as well as bound (core) electrons. In addition the contribution to secondary production from the volume plasmon decay is included, but only for the case of Al since there is no correspondingly good model for the plasmon interaction in Au,Ag and Cu. In every case the secondaries produced are allowed to have any energy up to the incident energy. The differential cross section for production of SE from valence and d electrons is given (Luo et al.,1987) by the relation:

$$d\sigma(E) = \frac{\pi e^4 dE}{E_0 E^2} \qquad (4.3)$$

The calculated lowest energy of internal SE is chosen as $E_F+\phi$ (E_F is Fermi energy and ϕ is workfunction) so that these SE can cross the surface potential barrier and enter the vacuum state as pure secondaries.

Gryzinski's function (Gryzinski,1965) is employed to describe the excitation of the core electron:

$$d\sigma(E) = \frac{\pi e^4}{E_0 E^2}\left(\frac{E_0}{E_0+E_j}\right)^{\frac{3}{2}}\left(1-\frac{E}{E_0}\right)^{\frac{E_j}{E_j+E}}\left\{1-\frac{E_j}{E_0}+\frac{4}{3}\frac{E_j}{E}\ln\left[2.7+\left(\frac{E_0-E}{E_j}\right)^{\frac{1}{2}}\right]\right\} dE \quad (4.4)$$

in (4.3) and (4.4) E is the energy loss of the primary electron during the inelastic event, E_0 is the energy of primary electron and E_j is the binding energy of the core electron.

For Al we have adopted the theoretical analysis made by Chung and Everhart (1977). The differential inverse mean free path or probability per unit length for creating SE's by volume-plasmon decay is:

$$\frac{d(1/\lambda)}{dE} = \lambda_{eff}^{-1}(E_0,\theta_1)D(E,h\omega_p,\Gamma_v) \qquad (4.5)$$

where

$$\lambda_{eff}(E_0,\theta_1) = \frac{2a_0E_0}{h\omega_p}\left[\ln\left(\frac{\theta_1^2+\theta_E^2}{\theta_E^2}\right)\right]^{-1} \qquad (4.6)$$

and $D(E,h\omega_p,\Gamma_v)$ which describes plasmon decay via one-electron transitions is

$$D(E,h\omega_p,\Gamma_v)=\left\{\sum_{\vec{G}} n_{\vec{G}}G\,|W_{\vec{G}}|^2\left[\tan^{-1}\left(\frac{E-E_0^G-h\omega_p}{\Gamma_v\sqrt{2}}\right)-\tan^{-1}\left(\frac{E-E_F-h\omega_p}{\Gamma_v\sqrt{2}}\right)\right]\right\}$$

$$\times\left\{\pi\sum_{\vec{G}} n_{\vec{G}}G\,|W_{\vec{G}}|^2(E_F-E_0^G)\right\}^{-1} \qquad (4.7)$$

and

$$E_0^G=\frac{(h\omega_p-h^2G^2-4\,|W_{\vec{G}}|^2)}{2h^2G^2/m} \qquad (4.8)$$

where $h\omega_p$ is the plasmon energy, a_0 is the Bohr radius (Eqs. 3.5 to 3.8 are from Chung and Everhart, 1977). Chung and Everhart (1977) assumed that for $E_0< 2$ keV, $q_E=q_0/K_0$, $(q_1^2+q_E^2)^{1/2}= q_1/K_0$, $q_1 = 2$ nm $^{-1}$,and $q_0 = 1.5$nm $^{-1}$. We have used this data for energy E_0 up to 3 keV. For calculation of $D(E,h\omega_p,\Gamma_v)$ we have followed the procedures of Ashcroft and Sturm (1971) and Koyama and Smith (1970), considering only the eight equivalent reciprocal-lattice vectors $\mathbf{G}_{111}$ and $\mathbf{G}_{200}$ for Al with $n_{111} = 8$ and $n_{200} = 6$.

In addition to the SE produced by the incident primary electrons as a result of the volume plasmon decay, the contribution of secondaries excited from volume plasmon decay by the internal SE in the cascade process has also been calculated (Scheinfein et al.,1993). The contribution to secondary production of the surface plasmon decay is so small that it can be neglected (see Chung and Everhart 1977).

An assumption in most SE theories is that secondary escape is governed by a function of the type

$$p_Z = A_1 \exp(-z/\lambda) \qquad (4.9)$$

This is the so-called straight-line approximation (Dwyer and Matthew, 1985), and implies the assumptions that the emerging secondaries are unscattered on their way to the surface and that any scattering of an excited SE with the electron gas in the solid produces absorption; i.e. only those electrons that are not scattered between their points of excitation and the surface can escape (Chung and Everhart, 1974). In fact the scattering of excited SE does not produce absorption of all these SE. To improve this approximation, Chung and Everhart (1977) included the contribution of single scattered SE, but their theoretical values are still too low by roughly a factor of 3 . In this paper the calculation of slow SE has been performed with a hybrid model of the exponential decay law and cascade process.

The hybrid model of the exponential decay law and cascade process can be summarized as follows. The probability of a SE arriving at the surface without any inelastic collision with the electron gas is

$$1/2 \exp(-z/\lambda(E)\cos 45^0) \qquad (4.10)$$

where 45^0 is an average escape angle, z is the depth at which the SE is produced, and $\lambda(E)$ is the inelastic mean free path for secondary electrons with energy E which, in metals, can be expressed (Seah and Dench,1979) as :

$$\lambda(E) = a\left\{ \frac{538}{(E-E_F)^2} + 0.41[a\,(E-E_F)\quad]^{1/2} \right\} \qquad (4.11)$$

where a is the thickness of a monolayer of the target in nanometers. If, as proposed by

Bindi et al (1980 c), we replace the term ($E-E_F$) in formula (4.11) with ($E-E_F-2$) then this expression for $\lambda(E)$ gives the same values as theirs . Because (4.11) is valid for secondary energies up to 10 keV only, we restrict ourselves to incident energy below this value although , in principle , our method could equally well be used for higher incident energies (for example 30 keV).

The cascade process is described as follows: The probability $P_{z'}$ for a SE with energy E to travel from z to z' without any inelastic collisions is

$$1/2 \exp (- |z-z'| / \lambda(E)\cos 45^0) \qquad (4.12)$$

The probability $P_{z'+\Delta z'}$ for the SE to travel from z to $z' +\Delta z'$ without any inelastic collision is

$$1/2 \exp (- |z-(z' +\Delta z')|/ \lambda(E)\cos 45^0) \qquad (4.13)$$

so that between z' and $z'+\Delta z'$ the probability for the SE to interact with another electron is

$$\Delta P_{z'} = P_{z'}- P_{z'+\Delta z'} = P_{z'} \Delta z'/ \lambda(E)\cos 45^0 \qquad (4.14)$$

$\Delta P_{z'}$ is then the probability for the SE to travel from z' to $z'+\Delta z'$ to take part in the cascade process.

In this present work, two previous limitations on the computation have been removed:

1. The restriction that the energy of every secondary electron in cascade process lies

below 100 eV has been removed.

2. The contribution to the emitted secondary yield of the internal SE is now estimated by integrating over the full beam range rather than just including the contribution over some arbitrary "maximum depth " as has been done previously (e.g Koshikawa and Shimizu 1974). The elimination of this restriction is especially important when internal secondary electrons of high energy (i.e. above a few hundred eV) are being considered.

Wolff (1954) pointed out that the phenomenon of SE emission can be thought of as occurring in two distinct stages. The first of these is the production of internal secondaries by collisions between the fast primary electrons and those electrons bound in the metal. The second stage is the subsequent cascade process in which these secondaries diffuse through the solid, multiplying and losing energy as they travel, until they either sink back into the sea of conduction electrons or reach the surface with sufficient energy to emerge as true SEs. Although secondaries with energies ranging from 0 to half the beam energy are considered by our theory, it is necessary to divide them into two groups having energies below, and above, 100eV. As shown by Wolff (1954) and Amelio (1970) an investigation of the screened Coulomb interaction reveals that, in the case of electron-electron collision, the scattering is spherically symmetric in the center of mass system up to about 100eV (for an appropriately chosen cutoff distance) after which it is more accurately described by Rutherford scattering. It is clear that the modification of the scattering symmetry from a spherical behavior to a Rutherford behavior is a smooth monotonic transition. However, such an ideal description is very difficult to achieve theoretically. Therefore, a cutoff energy (100eV) is defined above which the scattering is strictly Rutherford and below which the scattering is strictly spherical. In the work of Koshikawa and Shimizu (1974), the assumption that the scattering angle is spherically symmetric in the centre-of-mass system up to about 100 eV is also used. They did not consider the case

of SE with energies higher than 100eV.Below 100 eV the SE's scattering is considered to be strictly spherical. As shown by Koshikawa and Shimizu(1974), with the assumption of spherical scattering in the centre-of-mass system, E' the energy of an electron after scattering, is given as

$$E' = E_0 R^{1/2} \qquad (4.15)$$

where R is a random number and E_0 is the energy of an electron before scattering. Thus for each electron with an initial energy E_0 (<100 eV) undergoing the cascade process, two SEs appear after a collision with energy E' and E" such that

$$E" = E_0 (1 - R^{1/2}) \qquad (4.16)$$

where E" is the energy of the excited SE. It can be shown (Luo et al. 1987) that the probability p(E") of producing a new SE with energy in the energy interval [E", E"+dE"] is

$$dE"/E_0 \qquad (4.17)$$

This generation probability is valid for secondaries with energies less than 100 eV. The new secondaries excited in cascade process are considered to come from valence electrons only.

Above 100eV the scattering is considered as strictly Rutherford. Because the SE's energy is now higher, not only valence but also core electrons can be excited as new secondaries in the cascade process. The cross-section for an inelastic collision to produce a

new SE with energy in the energy interval [E[j], E[j]+dE[j]], excited from valence or d-shell electron by a SE with high energy E (>100eV), is given by formula (4.3). The cross-section for an inelastic collision to produce a new SE with energy in the interval [E[j], E[j] + dE[j]], but excited from core electrons by a SE with high energy E (>100 eV), is decided by formula (4.4) where E is the energy loss of the original SE. Relative to the bottom of the valence band we have

$$E = E[j] + Ej - (E_F + \phi) \qquad (4.18)$$

where as before E_j is the binding energy, E_F is Fermi energy and ϕ is the work function.

In an inelastic collision, a new SE produced by an internal SE with a high energy E[i] (>100eV) can be excited from all possible electron shells and can have all possible energies as long as the energy loss of the original SE is less than its energy E[i] before collision. Following Koshikawa and Shimizu (1974), we assume that for each electron entering the cascade process, two SEs appear: the original secondary which has lost some energy, and a new secondary. The total probability of creating a new SE in such an inelastic collision should be unity, so we therefore have:

$$X\left\{ cn[1]\sum_{j=1}^{i-1} d\sigma_v[j] + cn[2]\sum_{j=1}^{i-1} d\sigma_d[j] + \sum_{k=3}^{\text{all shells}} cn[k]\sum_{j=1}^{i-1} d\sigma_c[j] \right\} = 1 \qquad (4.19)$$

where the X is the normalization factor, i or j is the number of energy interval of SE, cn[1] is the number of valence electrons, cn[2] is the number of d shell electrons and cn[k] is the number of the k-th shell core electrons; $d\sigma_v[j]$ is the inelastic cross-section for a SE with energy E[j] excited from a valence electron, $d\sigma_d[j]$ is the inelastic cross-

section of a SE with energy E[j] excited from d -shell electrons, and $d\sigma_c[j]$ is the inelastic cross-section of a SE with energy E[j] excited from the k-th shell core electron, respectively.

After an inelastic collision, the probability of producing a new SE with energy E[j] (j can vary from 1 to i-1,i.e. E[j] can take all possible energy from 0 to E[i] the energy of the original SE) by an original SE with high energy E[i] from valence, d and core electrons respectively is:

$$cnv[i,j] = X\, cn[1]\, d\sigma_v[j] \qquad (4.20)$$

$$cnd[i,j] = X\, cn[2]\, d\sigma_d[j] \qquad (4.21)$$

$$cnc[i,j] = X \sum_{k=3}^{\text{all shells}} cn[k] \sum_{j=1}^{i-1} d\sigma_c[j] \qquad (4.22)$$

The quantity cn[i,j] = cnv[i,j]+cnd[i,j]+cnc[i,j], is the number of SEs with energy in the energy interval [E[j], E[j]+dE[j]] excited from all possible shell electrons by an original SE with an energy E[i] >100eV in an inelastic collision , that is to say cn[i,j] is the probability of producing a new SE with energy E[j] in an inelastic collision by an original SE with an energy E[i] >100eV . At the same time the energy of original SE becomes (E[i]-E), where E is its energy loss in the collision. Here cn[i,j] is calculated using the Rutherford scattering model. From this we can calculate the contribution of the internal SEs with high energy (>100eV) to the production of new SE in the cascade process.

In our model, the calculation of SE emission is separated into three stages :

(1) the production of internal SE with all possible energy (from 0 up to half the incident energy) along the path of the primary electron and the backscattered electron;

(2) the cascade process. The exponential decay law is adopted in the cascade process to describe the both the probability of the SE travelling through the solid to reach the surface (equation 4.10) as well as to calculate the probability of the SE reaching somewhere else in the solid to take place in an inelastic collision (equation 4.14). In the inelastic event if the energy of original SE is higher than 100eV then cn[i,j], when using the Rutherford model is used to calculate the production probability of the new SE, otherwise in the spherical scattering approximation dE[j]/E[i] is used for this purpose, where E[i] is the energy of the original SE and E[j] is the energy of the new SE. E[j] can be any value from 0 up to E[i] and the new SE can be excited from any possible electron shell in cascade process.

(3) the transmission of the SE through the surface potential barrier.

The maximum depth from which the SE are emitted is usually quoted as being about 5 nm below the surface in the case of metals (Koshikawa and Shimizu,1974), but this value does not take into consideration the contribution of internal secondaries generated with high energy deep in the sample. For a more accurate computation we need to know the contribution of the region deeper than this maximum depth for SE emission, especially when the incident energy of the primary electrons is higher than 2 keV. In this calculation therefore we divided the sample into two parts, one a region from 0 to 14 nm below the surface, which was subdivided into 7 layers, each 2 nm thick, and a second region stretching from 14 nm to the electron range.

The trajectory and the energy of both primary electrons and backscattered electrons

as they travel the layers between 0 to 14 nm is recorded, so that the number of SE1 and SE2 electrons with all possible energies and excited from all possible electron shells can be calculated. (Here we define the SE1 as the SE excited by primary electrons, and the SE2 as the SE excited by backscattered electrons.) Below a depth of 14 nm, since this exceeds the usual maximum depth for SE emission, the calculation is not performed in as much detail as for the depth range from 0 to 14 nm. We estimate the average path and energy of primary and backscattered electrons using the data derived for the range 0 to 14 nm, and assuming that the situation for primary or backscattered electrons is the same at all depths below 14 nm. It is useful to have a look at electron distribution in the region below 14 nm and for this purpose we find the Monte Carlo simulations very useful (Joy 1984). Typical trajectory plots show that in the region below 14 nm in addition to the fractional number η of electrons which are backscattered through the region there is also some fraction $(1-\eta)$ of electrons which reach the end of their range and come to rest in the sample. These electrons can still generate a lot of secondaries which are emitted from the sample directly or through cascade process to produce new SE in the layer near the surface. In order to estimate the magnitude their contribution to the emitted SE yield, we take the factor 0.5η as the effective size of this component in the depth range below 14 nm. Although this assumption is not strictly accurate, because the real scattering processes are complicated, since the generation occurs at depths much below the main region for SE production it is sufficiently accurate to provide a correction which helps to give values for the SE yields which are in better agreement with experimental data than was previously possible. Using this simplification the number of SE1 and SE2 generated below 14 nm which are excited by primary and backscattered electrons from all possible electron shells, and for the entire energy range, can be calculated.

The calculation of cascade process is made for the entire depth region from the

surface to the limit of the electron range and as the secondary falls from high energy down to low energy. Some of these SEs with high energy travel to the surface by the exponential decay law, the rest of them takes part in the cascade process to produce new secondaries and, at the same time, loses some energy and so falls into a lower energy interval. This process will continue until we reach the lowest energy interval ($E_F + \phi + 0.2$ eV) of the SE computation, where 0.2eV is the energy interval at ($E_F + \phi$).

The SE elastic scattering process is assumed to be isotopic because the mean free path of the slow SE becomes as small as the order of atomic distance, leading to an isotopic diffusion (Samoto and Shimizu 1983). Thus, all directions of motion of an internal SE at the surface are equally probable .In order for the SE with energy E at the surface to escape, we must have $E > (E_F+\phi)$. The maximum allowable value of escape angle α is determined by taking the normal component of momentum, $p\cos\alpha$, equal to a value

$$P_c = \sqrt{2m(E_F+\phi)} \qquad (4.23)$$

Then the total escape probability p(E) of a SE with energy E at the surface is :

$$P(E) = \frac{\int_0^{\alpha} \sin\alpha \, d\alpha \int_0^{2\pi} d\varphi}{2\pi} = 1 - \cos\alpha = 1 - \frac{P_c}{P} = 1 - \sqrt{\frac{2m(E_F+\phi)}{2mE}}$$

$$= 1 - \sqrt{\frac{(E_F+\phi)}{E}} \qquad (4.24)$$

4.3 RESULTS AND DISCUSSION

The model described here has been applied to the study of secondary electron emission from Au, Ag, Cu and Al, and has been used to calculate the most important parameters of the emission including the total SE yield as a function of incident energy, and the energy distribution of the emitted secondaries. the fractional contribution to the yield from SE1 electrons (i.e those produced by incident electrons only), and the β coefficient which measures the relative efficiency of primary and backscattered electrons at production of secondaries (the definition of β is just given below).

Secondary electrons are conventionally taken to be those emitted from the sample with energies less than 50 eV. Depending on the material examined the most probable secondary energy is between 1 and 3 eV (Seiler 1983). Because of their low energy the volume from which SE can mainly escape is limited to some region a few nanometers in depth below the surface. Consequently the secondary yield can be subdivided into two components (Drescher et al. 1970), SE1 which contains those electrons produced as the incident beam passes downwards though the surface escape region, and SE2 which contains those generated as backscattered electrons pass the sample on their way back to the surface. Thus the total secondary yield δ can be written as:

$$\delta = SE1 + SE2 \qquad (4.25)$$

which can rewritten as

$$\delta = SE1 (1 + \beta \eta) \qquad (4.26)$$

where η is the bulk backscattering coefficient for the target and β is the factor which represents the relative efficiency of the backscattered electrons in generating secondaries. Because the backscattered electrons are lower in energy than the primary electrons,and since they approach the surface over a range of angles, β is always greater than unity. The β-factor, defined in equation (4.26) , is the ratio of the secondary yield per backscattered electron compared to the secondary yield per incident electron (Kanter 1961). It is an important quantity in SE imaging because its value will determine the fractional content of the high resolution SE1 electrons in the total secondary signal. A high value of β implies that SE1 contrast will be weak in relation to the backscatter generated, and consequently low resolution, SE2 component. Because in this paper the BS and SE yields have been calculated simultaneously, β can be determined by applying equation (4.26) .

The variation of the calculated SE yield in terms of the incident primary energy is shown in Figures 4.1 to 4.4 for Au, Ag, Cu and Al respectively. The calculated secondary yield δ, the partial secondary yield δSE1, the backscattered electron yield η , primary electron step length, and the β coefficient are all shown in Tables 4.1 to 4.4 for Au, Ag, Cu and Al respectively. In Tables 4.5 and 4.6 the calculated results for the SE yields and the β coefficient are compared with experimental measurements and the other theoretical predictions, and it can be seen that there is good overall agreement between theoretical and experimental magnitudes . For Cu and Au there are few experimental values obtained at 1 or 2 keV with which to compare the calculated data except those of Bindi et al.(1980a). Our calculated data are in excellent agreement with these experimental results, and this may be because all possible creation mechanisms for secondary electrons, especially the contribution from internal SE with energies higher than 100eV are now considered. In figures 4.1 through 4.4 the decreased trend of the SE yields for Au, Ag, Cu and Al with the increased incident energy is in agreement with the previous theoretical

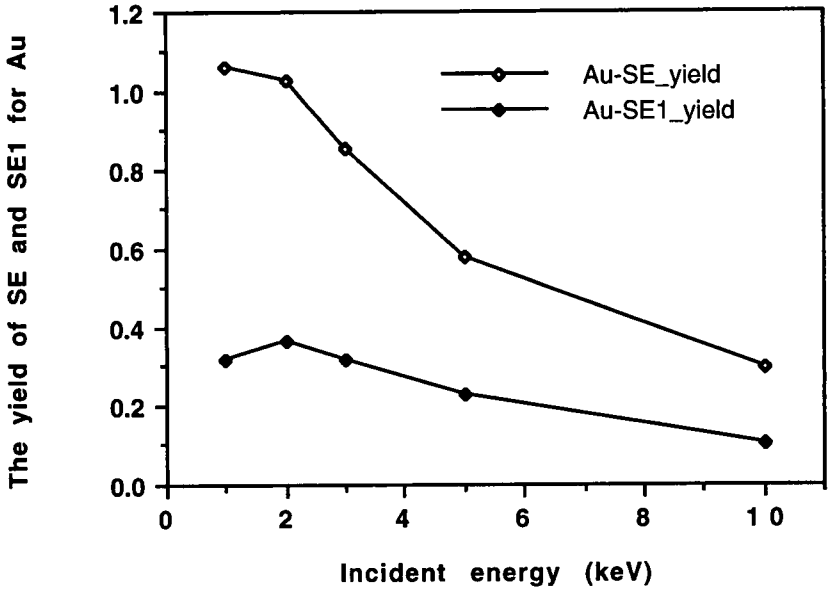


Figure 4.1 The variations of the yield of SE and SE1 with beam energy for Au.

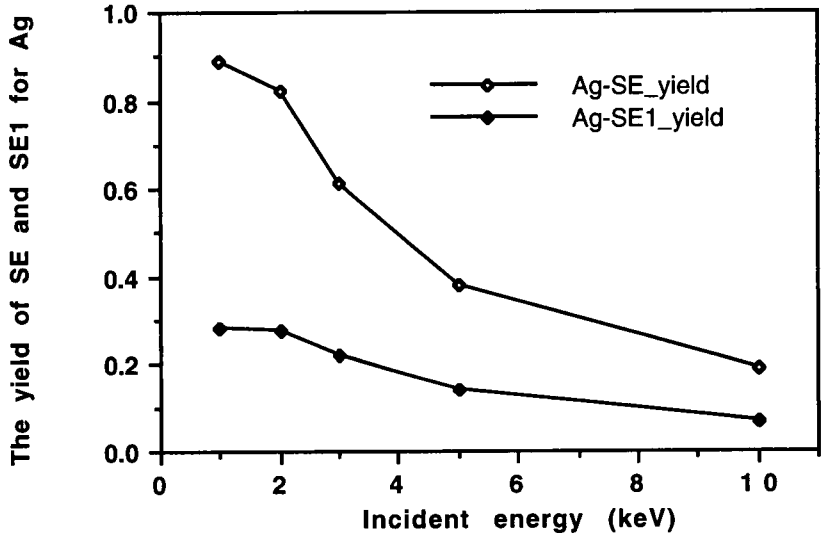


Figure 4.2 The variations of the yield of SE and SE1 with beam energy for Ag.

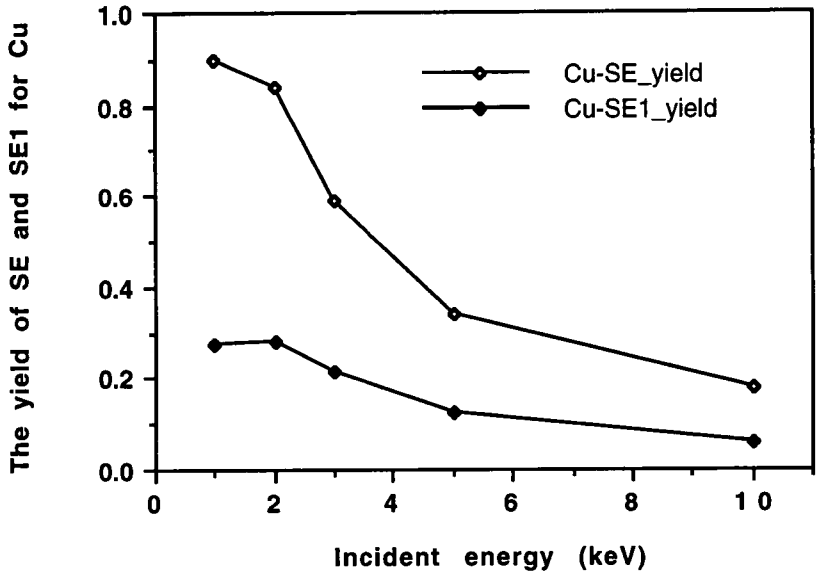


Figure 4.3 The variations of the yield of SE and SE1 with beam energy for Cu.

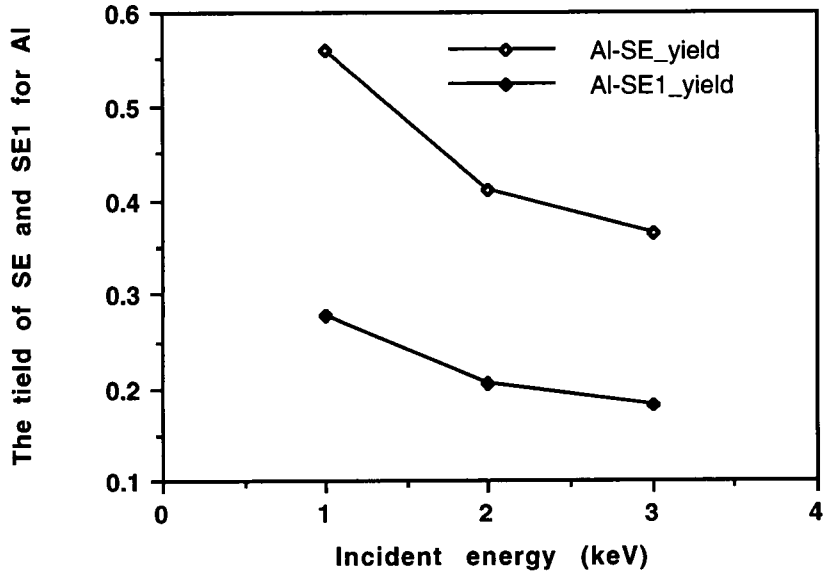


Figure 4.4 The variations of the yield of SE and SE1 with beam energy for Al.

Table 4.1 Calculated data for Au

Incident energy (keV)	1	2	3	5	10
Step (nm)	0.25	0.71	1.31	2.81	7.90
BS yield	0.451	0.457	0.457	0.457	0.459
SE yield	1.064	1.030	0.8574	0.5812	0.2935
SE1 yield	0.3144	0.3623	0.3147	0.2272	0.1057
ß-factor	5.14	4.31	3.77	3.41	3.87

Table4. 2 Calculate data for Ag

Incident energy (keV)	1	2	3	5	10
Step (nm)	0. 33	0. 94	1.73	3.66	10.9
BS yield	0.376	0.364	0.368	0.364	0.370
SE yield	0.891	0.820	0.612	0.382	0.192
SE1 yield	0.282	0.275	0.222	0.142	0.067
ß-factor	5.74	5.45	4.78	4.65	5.03

Table4.3. Calculated data for Cu

Incident energy (keV)	1	2	3	5	10
Step (nm)	0.30	0.84	1.52	3.37	10.4
BS yield	0.287	0.278	0.291	0.295	0.283
SE yield	0.896	0.839	0.590	0.339	0.177
SE1 yield	0.276	0.281	0.213	0.125	0.0583
ß-factor	7.85	7.15	6.10	5.85	7.19

Table 4.4 Calculated data for Al

Incident energy (keV)	1	2	3
Step (nm)	0.68	1.94	3.66
BS yield	0.163	0.159	0.160
SE yield	0.559	0.411	0.363
SE1 yield	0.278	0.205	0.182
ß-factor	6.20	6.31	6.20

and experimental data.

In figures 4.5 through 4.7 are shown the normalized secondary electron energy distribution curves at 1 keV for Au, Cu and Al respectively together with some experimental data and other selected calculated data. The comparison between theoretical and experimental distribution energy curves, normalized for the maximum peak height, together with the comparison of all other data can lead to the conclusion that the present approach can be successfully used to describe SE phenomenon.

Aluminium, a simple, nearly-free-electron metal, has become a standard material for the theoretical treatments and there is a large quantity of experimental data available on its secondary electron properties. Our model incorporates the theory for the volume plasmon contribution to secondary electron yields (although only at 1 or 2 keV) and the contribution of internal SE with energies higher than 100 eV in cascade process. It represents some more complete study for Al at 1 or 2 keV than before. Good agreement is found between our theoretical results and the wide range of experimental data available for Al, for the SE yield and for the energy distribution as well as the β coefficient (see Tables 4.5, 4.6 and Figure.4.7) .

Figures. 4.8 to 4.11 plot the computed β-factor as a function of the incident energy from 1 up to 10 kev for Au, Ag, Cu and from 1 to 3 keV for Al respectively. There is a clear variation of β with beam energy for Au, Ag and Cu : from 1 to 5 keV there is a linear decrease of β and from 5 to 10 keV a linear increase. The lowest value of β occurs at 5 keV suggesting that this incident energy may be the optimum one for secondary imaging. Tables 4.5 and 4.6 show our calculated data values for δ and β with comparison with experimental results. It can be seen that all of t hem are in good agreement with the

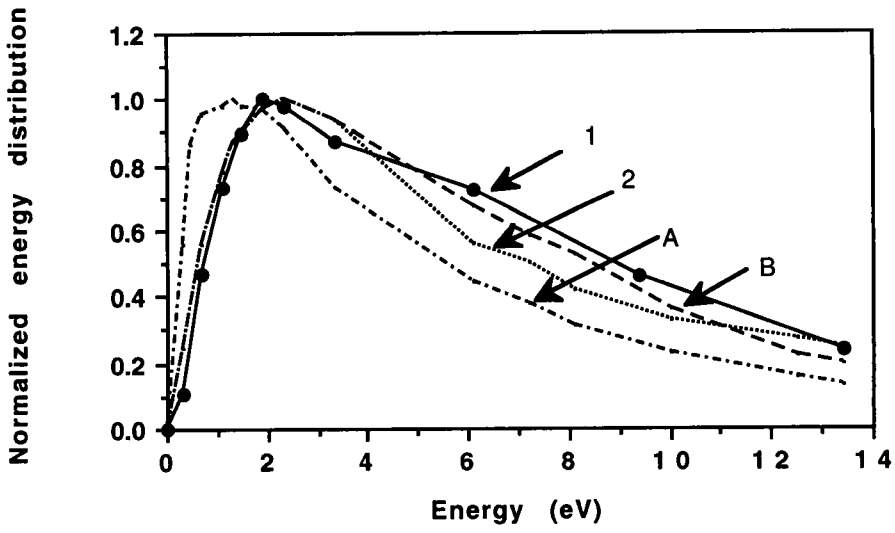


Figure 4.5 Normalized secondary electron energy distribution curves for Au at 1 keV. Curve 1 : present model Curve 2 : model by Bindi et al.(1980a)
Experimental curves : A : Bindi et al.(1980a)
B : Pillon and Roptin's(quoted from Bindi et al., 1980a)

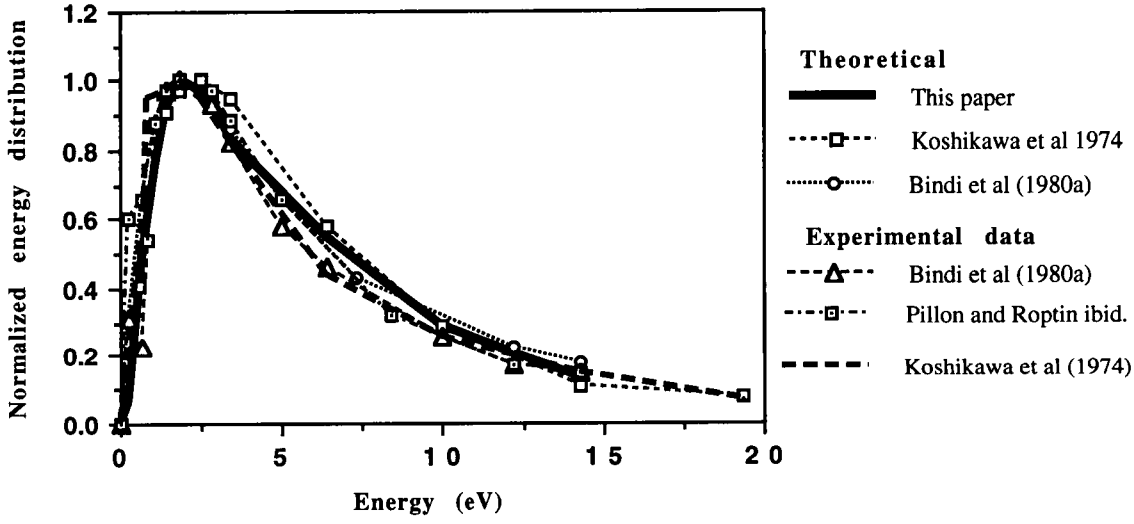


Figure 4.6 Secondary electron energy distribution curves for Cu at 1 keV.

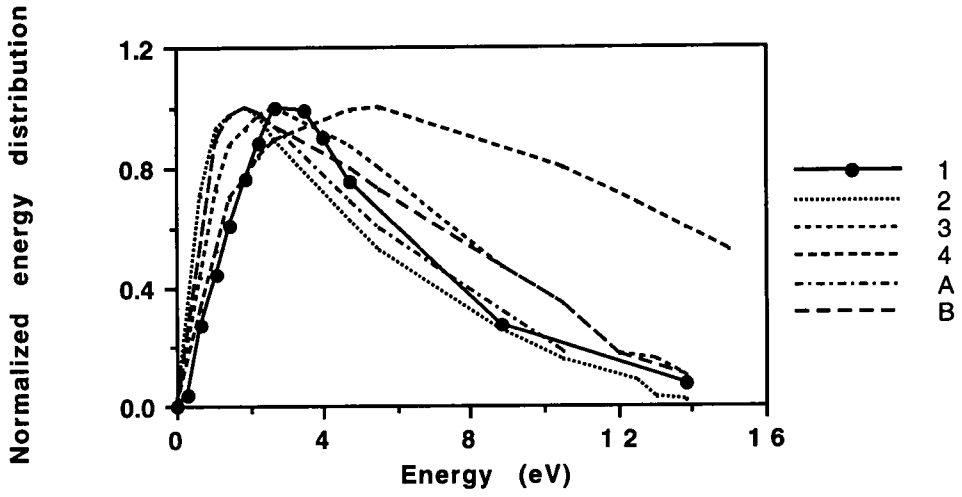


Figure 4.7 Comparison of theoretical and experimental normalized energy distributions of SE for Al at 1 keV.
Theoretical curves: 1. present calculations
2. Bindi et al. (1980 b)
3. Chung and Everhart (1977)
4. Amelio (1970) with corrections
Experimental curves : A: Bindi at al. (1980 b)
B: Roptin (1975)

experimental data available. The variation of β with energy can be explained as following:

(1) As the incident energy is reduced from 5 down to 1 keV , the average energy of the backscattered electrons falls more quickly than incident electron does, leading to an improvement in their efficiency for generating the SE2 component.

(2) In addition for the energy range between 5 to 1 keV, as the incident energy decreases the range and hence the step length of the incident electrons also decreases , thus the average generation depth of the backscattered electrons is nearer to the surface. For example, for Au at 5 keV the incident electron's step length is 2.8 nm, and since each

Table 4.5 The yield of SE for Cu, Au and Al

Incident energy (keV)		1	2	3	5
Cu	Calc.	0.896(ours) 0.18*	0.839(ours)		
	Exp.	0.86-1.07*	0.13*(1.8keV)		
Au	Calc.	1.064(ours) 0.28*	1.030(ours) 0.26*	0.857(ours)	0.581(ours)
	Exp.	1.23-1.36 * 1.48**	1.15-1.18 * 1.02**	0.84**	0.64**
Al	Calc.	0.559(ours) 0.52## 0.38Δ 0.37ΔΔ 0.52,0.57ΔΔ	0.411(ours) 0.35## 0.18Δ 0.22Δ 0.25,0.27ΔΔ	0.363(ours) 0.26##	
	Exp.	0.57Δ 0.60ΔΔ 0.48,0.50# 0.45***	0.39Δ 0.23*** 0.45ΔΔΔ		

* Bindi et al. (1980 a)

** Rothwell (1987)

*** Bronshtein and Fraiman(1961)

\# Roptin (1975)

Δ Bindi (1978)

ΔΔ Bindi et al . (1980 c)

ΔΔΔ Thomas and Pattinson (1970)

Schou (1988)

Table 4.6 The ß-factor for Au and Al

Incident energy (keV)		1	2	3	10
Au	Calc.	5.14(ours)	4.31(ours)	3.77(ours)	3.87(ours)
	Exp.		4.2**	2.5**(2.6keV)	1.9*(9.3keV)
			3.9**(1.8keV)		
				2.8**(2.4keV)	1.7*(11keV)
			2.9**(2.2keV)		
Al	Calc.	6.20(ours)	6.31(ours)	6.20(ours)	
		5#			
	Exp.	4.6-7.2#	3.5***		
		7.9##	4, 6***		
		5.9###	5.85##		
		6.3####	3.8####		

* Drescher et al (1970)

** Bronshtein and Denisov (1967)

*** Rosler and Brauer (1981b)

\# Bindi et al. (1980 b)

Bronshtein and Fraiman (1961)

Lanteri et al. (1975)

Thomas and Pattinson (1970)

incident electron has 50 steps before its energy become zero a BS electron could generated as deep as 140 nm beneath the surface. But at 1 keV, the corresponding step length is only 0.25 nm, and so generation region for BS electrons is limited to a depth of 12.5 nm. It is clear that at 1 keV the BS electron should have relatively higher efficiency at generating secondaries than at 5 keV because its path is nearer to the surface so that the secondaries excited by the BS electrons can reach the surface more easily.

(3) In the energy range from 5 to 10 keV, the average depth of the BS electrons is deeper as the range of the incident electrons increases. However the contribution of SE with high energy (which can be as high as the half incident energy) excited by BS electrons in the region below the 14 nm boundary also becomes more important as the incident energy increases and this again leads to an increasing trend in β The probability of producing SE with high energy is, of course, low but those SE's are carrying the majority of the energy lost by BS electron in the interaction .These SE's with high energy are generated far from the surface, and so their probability of escaping is small. Consequently their energy is mainly lost in the cascade process to produce new SE with lower energies until their energy becomes zero . Figures 4.12 to 4.14 shows some experimental data by Joy (1970) and Reimer and Drescher (1977) . Their experiments demonstrate that a portion of the SE can be generated from deeper than a few nanometers and the higher the incident energy the greater the depth of SE excitation and escape. When the incident energy is higher the contribution of SE generated in deeper region should not be ignored. In this paper the number of SE excited from BS electrons both in the region down 14 nm, and below 14 nm are calculated. The number of SE both of high (>100eV) and low (<100eV) energy are also calculated together with the number of SE multiplying in the cascade process. Besides the number of SEs which are multiplying in the cascade process between 0 to 14 nm considered as previously, the multiplication of the number of SE which generated below 14 nm but which travel to the 0-14 nm region to take part in cascade process, together

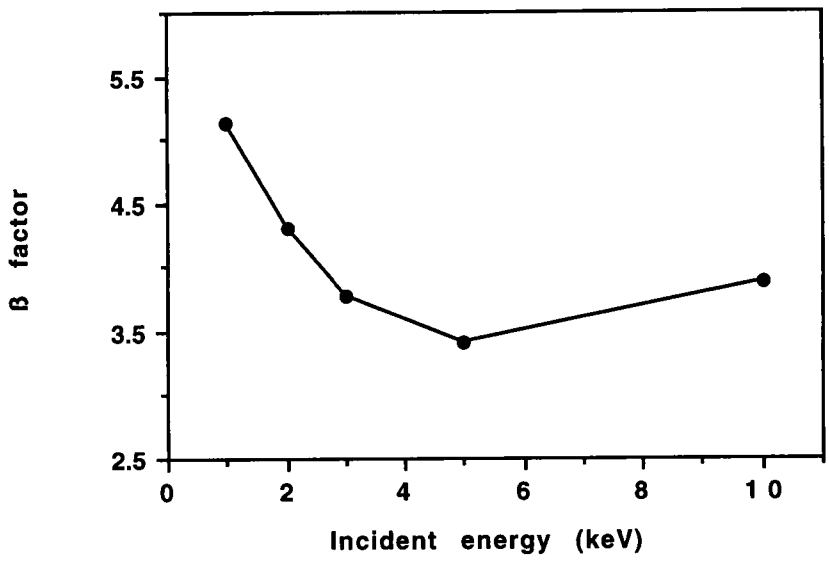


Figure 4.8 The variation of the β-factor with beam energy for Au.

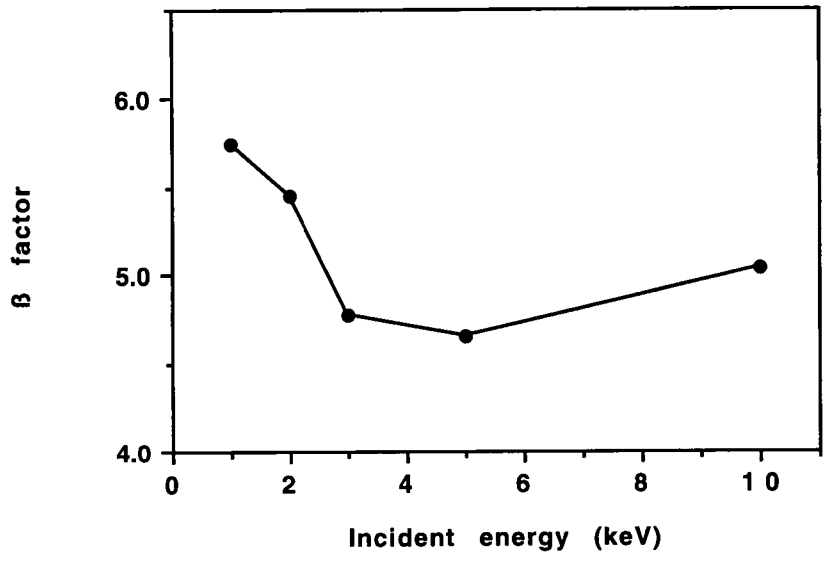


Figure 4.9 The variation of the β-factor with beam energy for Ag.

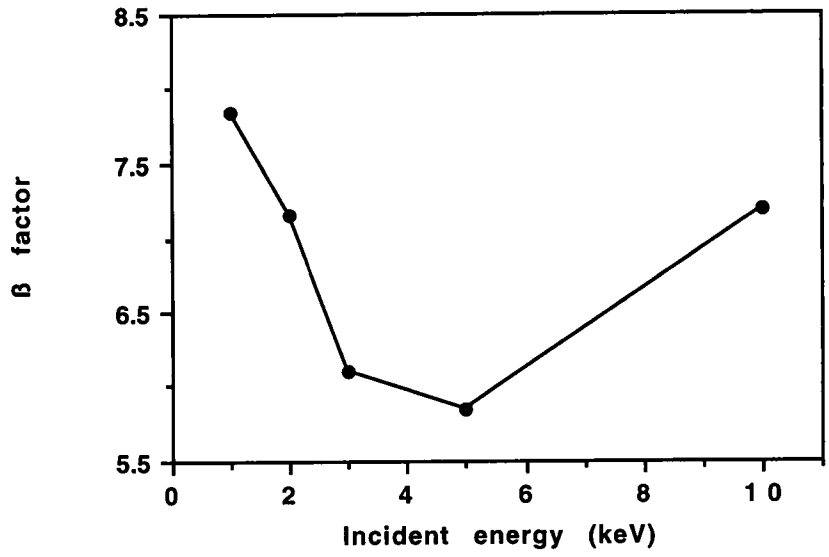


Figure 4.10 The variation of the β-factor with beam energy for Cu.

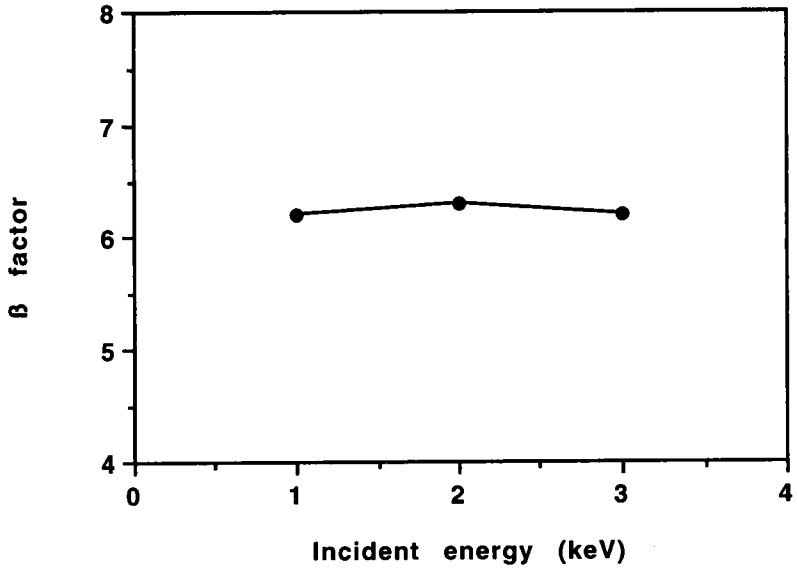


Figure 4.11 The variation of the β-factor with beam energy for Al.

with the number of SEs generated below 14 nm which can directly reach the surface as true SE , both tend to cause an increase in the yield of type SE2 secondaries and so raise the β-factor. The higher is the incident energy, the more the fraction of emitted SE which are excited by the high energy internal SE at depths below 14 nm in the cascade process, so the higher the β-factor is. Hence the observed increase in the β-factor from 5 to 10 keV.

For Al the calculation is valid at 1,2 and 3 keV for plasmon calculation (Chung and Everhart, 1977) so we calculate up to 3 keV only. From 1 to 3 keV the β-factor's value has no variation but is in good agreement with the experimental data available. For Al the β-factor has its own curve different from Au, Ag and Cu , most probably because of the plasmon calculation included, which is important for a nearly-free- electron metal such Al. According to theoretical calculations and experimental data for SE, the angular distribution obeys the cosine law (Jonker 1951, Koshikawa and Shimizu 1974, Bindi et al. 1980 a,c , Rosler and Brauer, 1981b). However the origin of this result has not received much discussion. A pure cosine distribution for SE can be obtained from an assumption of the isotropic distribution of internal SE. This distribution mainly results from the elastic collisions of the SE. For SE because of the mean free path of the slow SE as small as the order of atomic distance, it leads to an isotropic diffusion.

Let it be supposed that:

1. For an internal SE after an elastic collision all directions of motion are equally probably. i.e., for internal SE there is not memory of its previous direction of motion in elastic scattering process.
2. The mean free path of elastic collision is $\lambda_e(E)$ for a given energy E of SE. On a rough average an elastic collision will happen for a SE travelling a distance $\lambda_e(E)$ along a given

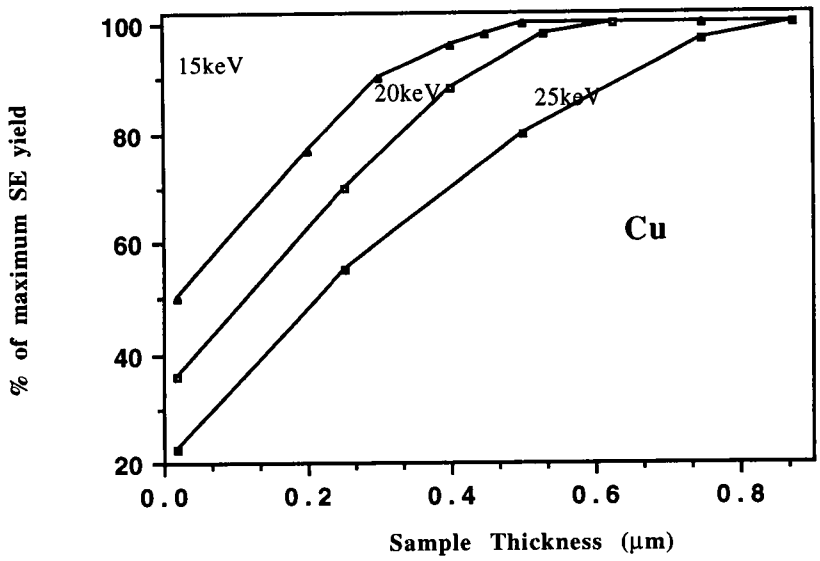


Figure 4.12 Variation of SE yield with thickness. The experimental data for Cu is from Joy (1970).

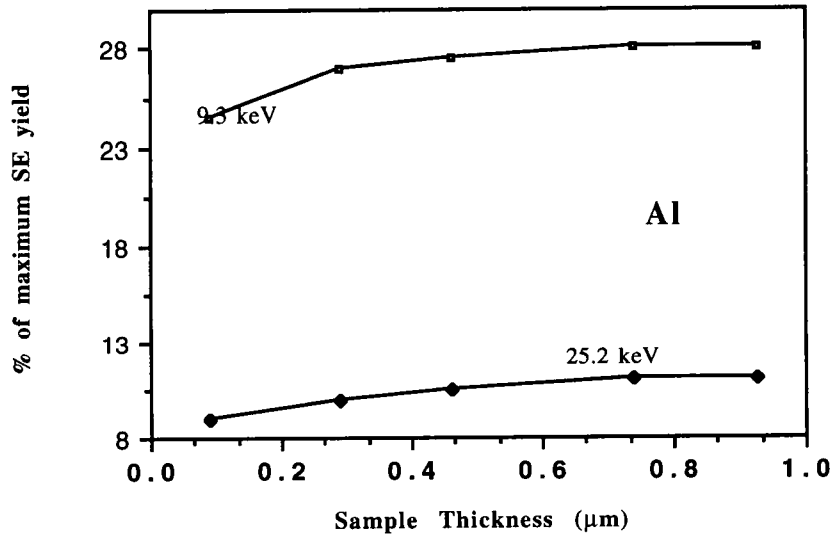


Figure 4.13 Variation of SE yield with thickness. The experimental data for Al is from Reimer and Drescher (1977).

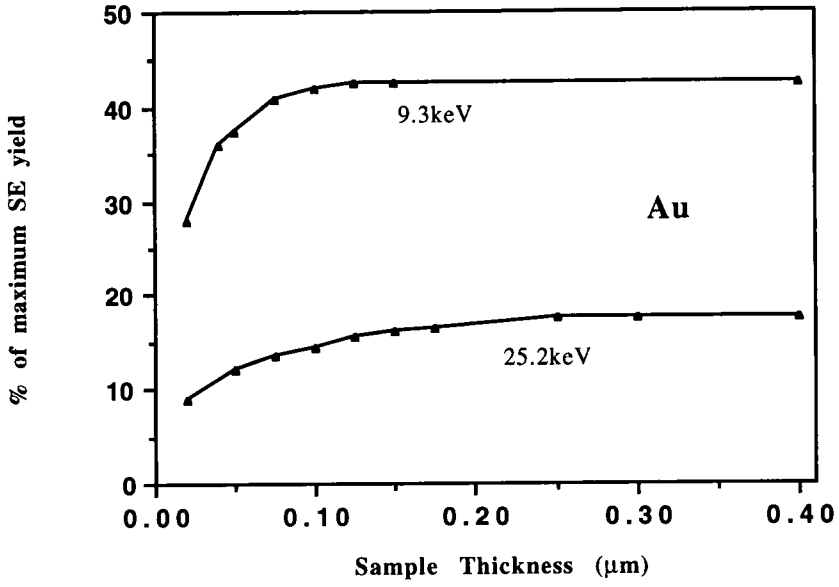


Figure 4.14 Variation of SE yield with thickness. The experimental data for Au is from Reimer and Drescher (1977).

direction.

According to our assumptions at the surface for a SE with energy $(E_F+\phi)<E<(E_F+\phi+50eV)$ there are isotropic distribution of its motion direction and homogeneous density. Although after every elastic scattering for a SE the direction of motion at the surface is isotropic, but with more accuracy the number of SE at different escape angle θ in unit solid angle striking the inside surface is different.

From Figure.4.15 we can see that at the layer of thick $\lambda_e(E)$ after all elastic collision all SE with energy E only along $\theta=0^0$ can keep this direction to strike surface, along direction $\theta>0^0$ because its path is longer than $\lambda_e(E)$, along this path there will be new elastic collision before the SE strike the surface at angle θ. Then these SE with energy E at

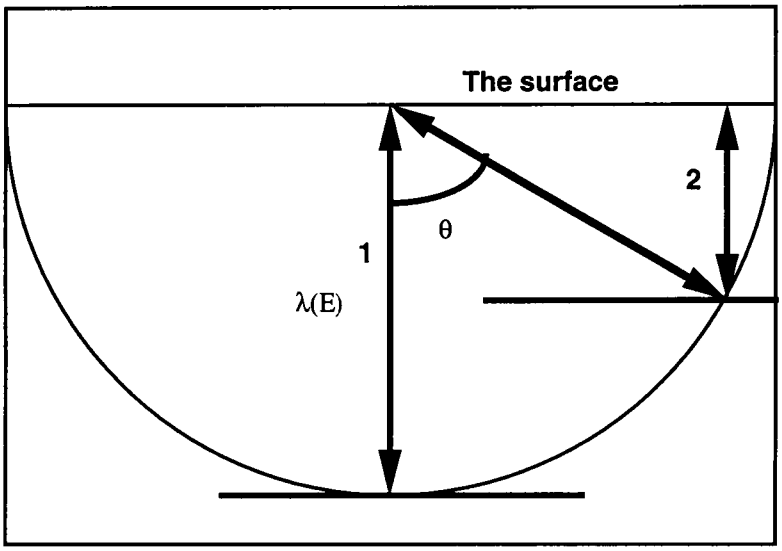


Figure 4.15 Variation of layer thickness with escape angle θ, in which the SE witha given energy E at escape angle θ after a elastic collision can strike the surface retaining its escape angle

1: the layer thickness λ(E) when θ=0

2: the layer thickness λ(E)cosθ when escape angle is θ.

escape angle θ only in the layer of thickness $\lambda_e(E)\cos\theta$ can strike the surface at the original escape angle θ after an elastic collision .The larger θ becomes therefore the thinner the layer thickness must be . Because the direction and density of SE with energy E is isotropic and homogeneous respectively, the number of SE striking the surface at various escape angle θ is proportional to the layer thickness $\lambda_e(E)\cos\theta$. Then for the intensity of SE with given energy E and at given escape angle θ striking the surface we have the relation

$$I(\theta) = I(0^0)\cos\theta \qquad (4.27)$$

where $I(\theta)$ is the number of SEs with energy E at a given escape angle θ in unit solid angle striking the surface, $I(0^0)$ is the number of SE with energy E at angle 0^0 in unit solid angle striking the surface. Hence from this we can see that the cosine law results from the isotropic elastic scattering directly. From Jonker (1952) it can be seen that if inside the sample the current striking the surface follows a cosine law, i.e. if we have Eq.4.27 then a cosine law will be followed outside too. This means the surface barrier will not change the shape of the angular distribution.

From Jonker's (1952) calculation we have:

$$I_0(\theta) = I_0(0^0)\frac{\cos\theta_0}{\sqrt{1-\sin^2\theta_0/n^2}} \qquad (4.28)$$

where $I_0(\theta)$ and $I_0(0)$ are the current density of SE outside the sample at angle θ and 0^0 respectively, $n = \{ [E-(E_F+\phi)]/E \}^{1/2}$, E is the energy of internal SE. For true SE , its energy is from $E_F+\phi$ to $E_F+\phi+50$ eV and from the energy distribution curve we can see the most of SE with energy near $E_F+\phi$, so in fact the isotropic distribution model's

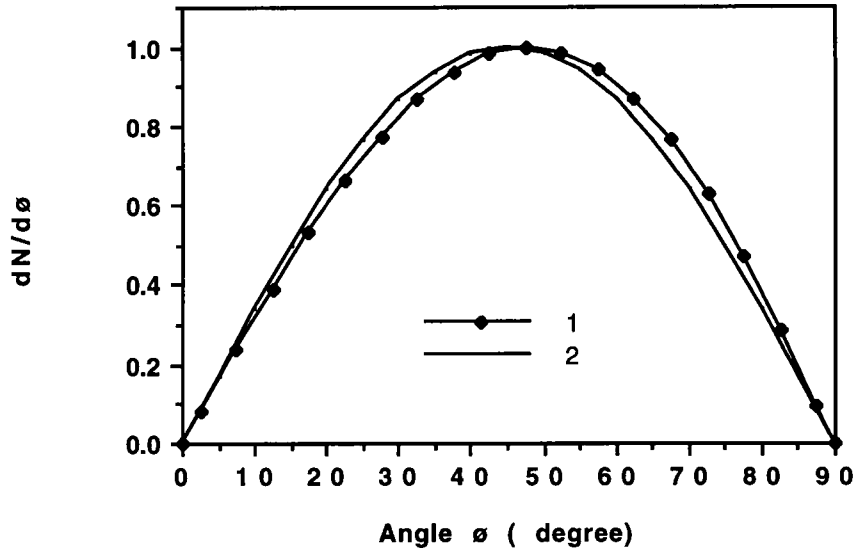


Figure 4.16 Comparison of our angular distribution calculated by isotropic distribution model of internal SE and the cosine law for Al at 2 keV.
1: our calculation 2: Cosine Law

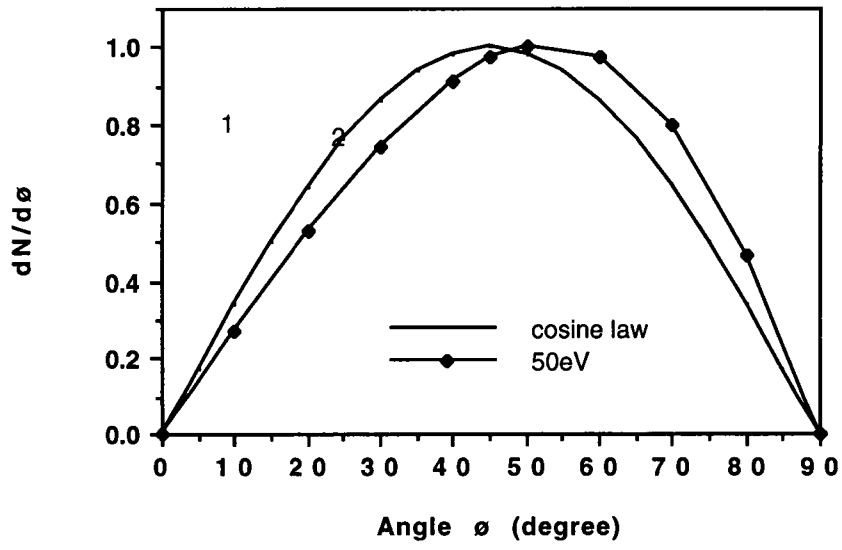


Figure 4.17 Comparison of our angular distribution calculated by isotropic distribution model of internal SE with energy 50 eV and the cosine law for Au .
1: Angular distribution of SE with energy 50 eV 2: Cosine Law

discrepancy (Luo and Joy 1988) to cosine law is very little as shown in Figure 4.16. However at the highest energy, 50 eV, the difference is rather larger (Figure 4.17) but the number of SE with 50 eV is small so that for the integrated SE emission the angular distribution still obeys the cosine relation.

It is true that , if inside the sample the SE current striking the surface follows a cosine law, a cosine law will hold outside too (Jonker 1952). However up to now we have ignored the influence of the inelastic scattering upon the angular distribution of internal SE. This influence will be discussed as follows.

Figure 4.18 shows the inelastic and elastic mean free path curves varying with energy of SE for Al. For a SE with small energy its inelastic mean free path is rather big. Therefore it is the elastic mean free path which determines the angular distribution mainly. But for those SE with energy near 50 eV , its inelastic mean free path becomes so small that it is comparable with the elastic mean free path . Under elastic scattering the density of SE with given energy at the surface layer is homogeneous, while for inelastic scattering the density of SE with given energy at the surface layer at various escape angle is different. Because of the exponential decay law, the larger the value of the escape θ the longer the path length to the surface so leading to a smaller density of SE with a given energy at escape angle θ at the surface. From this we can see that for those SEs for which the inelastic mean free path is comparable with the elastic mean free path, the cosine law does not hold. In this case we can expect that the distribution curve at high escape angle θ will lie inside the circular profile of the cosine law . This results from exponential decay in inelastic scattering.Figure 4.19 shows the angular distribution of SEs ,which are influenced by the inelastic scattering and which deviate from cosine law. This shape resembles some experimental curves of angular distribution for SE with higher energy obtained by

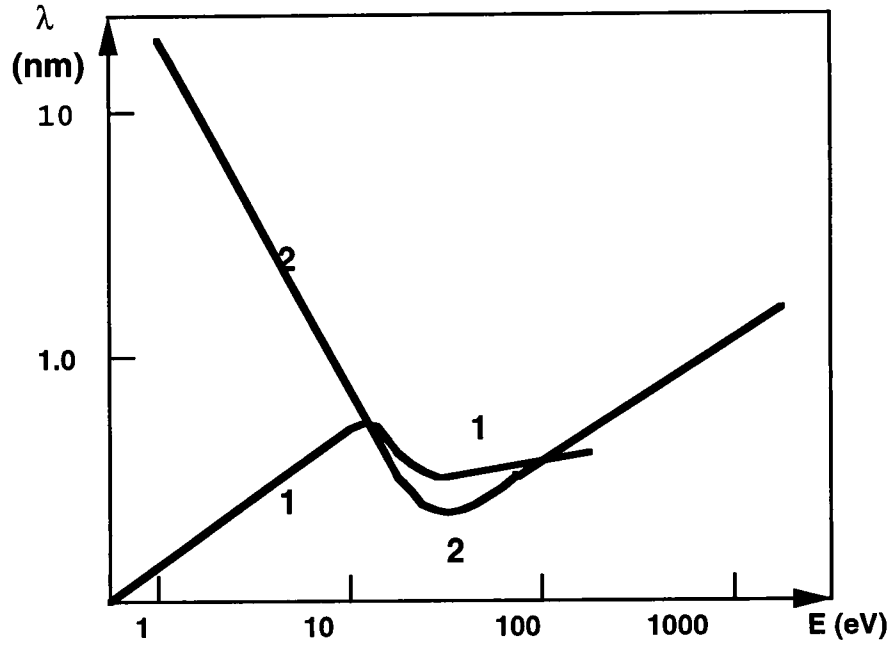


Figure 4.18 Comparison of curves of inelastic and elastic mean free path varying with energy of SE for Al (quoted from Bindi et al. 1980c and Ganachaud and Cailler 1979 respectively).
1.elastic mean free path
2.inelastic mean free path

Jonker (1951). It can also be noted that this analysis of angular distribution for SE can be used for BS electron in a similar fashion . For BS electrons with high energy arriving at the surface after a lot of elastic and inelastic scattering, the directions of motion will be isotropic and hence the angular distribution of BS electron will obey the cosine law too.

4.4 CONCLUSIONS

In this chapter a theoretical analysis of SE emission, including for the first time the contribution from internal SEs with high energy and emerging from significant depths below the surface, has been carried out. This treatment has been applied to Au, Ag,Cu and Al over a wide incident energy range. Because of the complexity of the calculations , previous Monte Carlo simulations have usually only calculated internal secondary electrons with energies up to 100 eV in cascade process. We have sought to overcome this difficulty by invoking a normalization factor X based on Rutherford theory and have successfully removed the limitation. The exact details of individual inelastic scattering are considered by our new model since a direct simulation of each individual inelastic scattering process is probably the best way to treat the production of new SE in cascade process. We have found that the contribution of SEs with high energy and the SEs emerging from deeper than the usual exited depth are important mechanisms of SE generation and contribute to the variation of β-factor , especially at higher incident energies.

The agreement between theory and experimental data is satisfactory, suggesting that the present model is successful one and is capable of considerable accuracy. This Monte Carlo calculation has also provided us a more detailed consideration of the signal-to-noise ratio in SEM study. The calculation has given the function of β-factor with the incident energy and suggests maybe that the signal-to-noise has the lowest value at 5 keV at normal

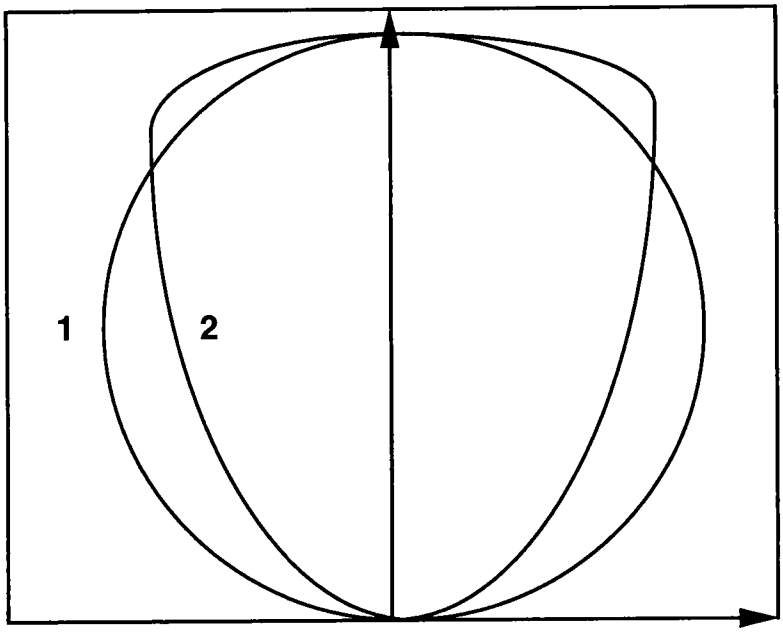


Figure 4.19 The discrepancy in the angular distribution caused by inelastic scattering.
1. Cosine Law distribution
2. The distribution as influenced by inelastic scattering

incidence Another advantage of using our method is that one can easily extend it to another metals, semiconductors,insulators as well as compound materials and at more high incident energy as long as an adequate knowledge of the binding energy and the form of $\lambda(E)$ is given.

Our discussion of angular distribution of secondary emission points out that, for true SE of low energy (e.g., for E=2 eV), the cosine law angular distribution is followed well , and that this is a direct consequence of elastic scattering within the specimen., For those SEs with higher energy the deviations from the cosine law are caused by the influence of inelastic scattering. If both elastic and inelastic scattering are considered then the angular distribution of SE does not follow the exact cosine law . Because of the λ_e is as small as the atomic distance for ture SEs , the angular distribution is determined within a very thin surface layer of thickness λ_e.

In our model, we have made several simplifying approximations, e.g. the BS electron trajectory distribution below 14 nm. However, the satisfactory agreement obtained between theory and experiment for the total yield of SE, the yield of SE1 ,the energy distribution and the β-factor for the four elements considered suggests that the theory we have outlined provides a good working physical picture of SE emission.

CHAPTER 5

STOPPING POWER DETERMINATION

5.1 INTRODUCTION

In Physics, Chemistry, Biology and Medicine, it is very important to have accurate information about the stopping power of various media for electrons. The stopping power is defined as the average energy loss of energetic electrons per unit pathlength along their trajectories due to inelastic Coulomb collisions with atomic electrons of the specimen . Electron stopping power is one of the most important parameters which describe the interaction of an electron with a solid since it determines the range of the electron for a given incident energy , as well as the yield, spatial and lateral distributions of the various emissions such as X-rays, secondary electrons and electron hole-pairs associated with the incident electron.

In 1895 a German physicist P. Lenard studied the absorption of cathode rays by exposing thin foils to the rays (Gray, 1958).This is the one of the first experiments examining the process of electrons through solid media. Lenard found that the general law of absorption of cathode rays (i.e. electron beam) can be expressed by the relation $I=I_0e^{-at}$, where I is the intensity of the transmitted electrons, I_0 is the incident electrons, t is the foil thickness and a is the absorption coefficient. In 1911 Rutherford developed a model of scattering of alpha rays , successfully explained the experimental results and concluded that the collisions of alpha or beta particles with matter are essentially identical except for differences due to the differences in mass and charge. In 1915 Bohr proposed a theory of the rate of energy loss dE/dS on the basis of classical notions, and in 1930 Bethe (1930)

presented a quantum mechanical theory of the stopping power. Several decades have passed and Bethe's theory still is the foundation of this field and widely used in a variety of fields. The magnitude and variation of electron stopping power is well established for energies in the range greater than about 10 keV (NBSIR , 1982; ICRU Report 37, 1984, Nieminen, 1988) and for a detailed discussion of stopping power theory there are many comprehensive reviews in the literature: Bohr (1948), Bethe and Ashkin (1953), Fano (1963) and Inokuti (1971).

The energy of 10 keV is a commonly accepted lower limit for the applicability of the Bethe theory (NBSIR , 1982; ICRU Report 37, 1984). Above 10 keV the stopping power can be expressed by straightforward analytic expressions . The most widely used analytical expression for the stopping power has been that due to Bethe (1930, Bethe and Ashkin, 1953) :

$$-\frac{dE}{dS} = \frac{2\pi e^4 nZ}{E} \ln\left(\frac{1.166E}{I}\right) \qquad (5.1)$$

where E is the instantaneous energy of the electron, S is the path length along the trajectory, n is the density, I is the mean ionization potential of the sample . The value of I can be found from tabulated values (e.g., ICRU 1984) or approximated from an analytical fit (Berger and Selzer, 1964) giving :

$$I = \left[9.76\,Z + \frac{58.5}{Z^{0.19}} \right] \text{(eV)} \qquad \text{for } Z \geq 13$$

$$I = 11.5\,Z \text{ (eV)} \qquad \text{for } Z \leq 12 \qquad (5.2)$$

I is therefore typically of the order of a few hundred electron volts.

For incident energy higher than 30 keV taking into account relativity and spin effects as well as exchange effects the stopping power is expressed as (ICRU 1984) :

$$-\frac{dE}{dS} = \frac{2\pi N_a r_e^2 m_0 c^2}{\beta^2}\frac{\rho Z}{A}\left[\ln\left(\frac{T}{I}\right)^2 + \ln\left(1+\frac{\tau}{2}\right) + F(\tau) - \delta\right] \qquad (5.3)$$

where β is the velocity of the incident particle divided by the velocity of light, r_e is the classical electron radius, $r_e^2 = 7.940775 * 10^{-26}\ cm^2$, T is the kinetic energy of the incident electron, τ is the ratio of the kinetic energy of the incident electron to its rest energy, $\delta/2$ is the density-effect correction for which a detailed discussion is given in ICRU (1984) and will not discussed in this thesis. $F(\tau)$ is given by:

$$F(\tau) = (1-\beta^2)\left[1 + \frac{\tau^2}{8} - (2\tau+1)\ln 2\right] \qquad (5.4)$$

The applications of these expressions to Monte Carlo simulations of electron solid interactions have been found to give good results over a wide range of energies. For E>> I the Bethe formula is well behaved predicting a stopping power which varies monotonically with a limiting slope of about $E^{-0.8}$, but as E falls to the condition where E ~ I, then the value of the stopping power becomes dominated by the logarithmic term. Consequently the stopping power rises to a maximum, which occurs when E ~ 2.5 I and then falls rapidly to zero when E=I/1.166. For still lower values of E the equation then predicts a negative stopping power, which is clearly nonphysical. There is now, however, increasing interest in the use of low energy (less than 10 keV) electron beams for such purposes as scanning electron microscopy and microanalysis, critical dimension metrology, and electron lithography.

5.2 AN EMPIRICAL STOPPING POWER RELATIONSHIP FOR LOW ENERGY ELECTRONS

There are basically two ways to overcome this problem. The first one is using empirical and semi-empirical formulas which are widely used in the microanalysis in particular Monte Carlo calculations. The most popular solution to this difficulty has been that proposed by Rao-Sahib and Wittry(1974). A tangent drawn to a plot of the Bethe formula's profile has been used to extrapolate the stopping power to incident energies below the singularities in Eq.5-1. On this approximation the stopping power is given by:

$$-\frac{dE}{dS} = 624\,\frac{\rho\, Z}{A\sqrt{EI}} \qquad \text{for } E<6.34I \qquad (5.5)$$

where the symbols have the same meaning as in Eq.5.1 and the E and I are in eV, S in Å , ρ , the density is in g/cm^3. This expression is well behaved for all non-zero electron energies and has the desired properties of being a function of the same parameters as the original Bethe expression and being readily calculable. An alternative parabolic extrapolation has been suggested by Love et al.(1978). Although the Rao-Sahib and Wittry (1974) and Love et al.(1978) expressions extend the usefulness of the Bethe expression to low energies and avoid the mathematical problems of the original equation, they have no inherent physical significance and are not particularly accurate. For example, for energies of a few hundred electron volts or less the Rao-Sahib Wittry expression overestimates the stopping power by a factor of two or more times and so quantities which are related to the stopping power, such as the electron range, secondary electron, and x-ray yields, will be in error.

As shown by several authors (e. g., Reimer and Stelter 1986, Ritchie et al. 1969, Shimizu and Ichimura , 1981) a more general version of the Bethe equation can be obtained by writing it in the form :

$$-\frac{dE}{dS} = 785 \frac{\rho Z}{A E} \sum_{n,l} \frac{f_{n,l}}{Z} \ln \frac{2E}{A_{n,l}} \qquad (5.6)$$

where for the target atom whose l-th shell contains n electrons, $f_{n,l}$ is the oscillator strength and $A_{n,l}/2$ is the ionization energy of the shell. This form of the Bethe expression makes it clear how the overall stopping power is the sum of core ionization, plasmon, and conduction electron excitations. In practice $f_{n,l}$ is equated to the number of electrons in the shell or, for the outermost shells, to some effective number of electrons. Eq.5.6 can thus be rewritten as :

$$-\frac{dE}{dS} = 785 \frac{\rho Z}{A E} \sum_{i} \frac{Z_i}{Z} \ln \frac{E}{E_i} \quad \text{eV/Å} \qquad (5.7)$$

where Z_i is the occupancy of the i-th shell (as tabulated, e.g., in Reimer and Stelter 1986), and E_i is the corresponding binding energy (Shimizu and Ichimura, 1981). This expression can then be evaluated for any given energy E. The summation is only carried out over those terms i for which $E>E_i$, thus all the terms are positive or zero so the equation does not exhibit the inversion of Eq.5.1, and the expression can be used down to an energy equal to the ionization energy of the outermost occupied shell of the atom (i. e., the energy at which the last term in the summation of Eq.5.6 becomes zero). Stopping powers derived from

this equation are in excellent agreement with those computed from other models (e. g., Ashley et al. 1979, Tung et al. 1979). However, evaluating Eq.5.7 for any specific energy and atoms is a lengthy process, since for heavier atoms many shells must be considered, and it is difficult to modify the equation. It is also necessary to use empirical numbers for shell occupancy to get correct values to allow for the use of a compound material as the target. Thus, while this version of the Bethe equation provides a benchmark value for the stopping power over the energy range of the interest, it is not in an ideal form for inclusion in a general purpose Monte Carlo simulation.

Based on the physical idea of Eqs.5.6-7, we (Joy and Luo ,1989) have given an empirical stopping power relationship for low energy electrons to overcome the limitations of Rao-Sahib Wittry expression. The basic consideration is that when the incident electron energy is decreasing so is the number of atomic electron involved in the excitation . Therefore the mean ionization potential I is no longer a constant but has an energy dependence. The original Bethe expression can be modified to incorporate this energy dependence by writing it in the form:

$$-\frac{dE}{dS} = 785 \frac{\rho Z}{A E} \ln\left[\frac{1.166(E + k I)}{I} \right] \quad eV/Å \qquad (5.8a)$$

which can equivalently by written as:

$$-\frac{dE}{dS} = 785 \frac{\rho Z}{A E} \ln\left[\frac{1.166 E}{I'} \right] \quad eV/Å \qquad (5.8b)$$

where

$$I' = \frac{I}{1 + k \cdot I/E} \qquad (5.8c)$$

and the variables have the same meaning as in Eq.5.1. k is a variable whose value depends on the material examined but which is always close to, but less than, unity. In this manner some rudimentary form of energy dependence for I is incorporated into the equation since for high energies I' asymptotically approaches I , but for small energies, such that E << I then I' is smaller than I and varies about linearly with E. The general form of this variation in the magnitude of the mean ionization potential is consistent with recent theoretical analyses of stopping power measurements in both water and some rare gases (La Verne and Mozumder 1983, 1985).

The expressions 5.8 a and b possess some useful properties :

1. They retain the generality and convenience of the original Bethe expression in requiring only one parameter I to describe the interaction with a complex target.
2. For E >> I the stopping power variation has the same form and magnitude as for the standard Bethe expression of Eq.5.1.
3. The inversion of the original Bethe expression at E ~ I is now absent and the expression does not change sign until E << I , the exact energy depending on the value of k.
4. Stopping powers predicted by the expressions are in close agreement with values predicted from Eq.5.7, and from data such as that of Tung et al. (1979), for all energies E > 50 eV and for a wide range of elements.

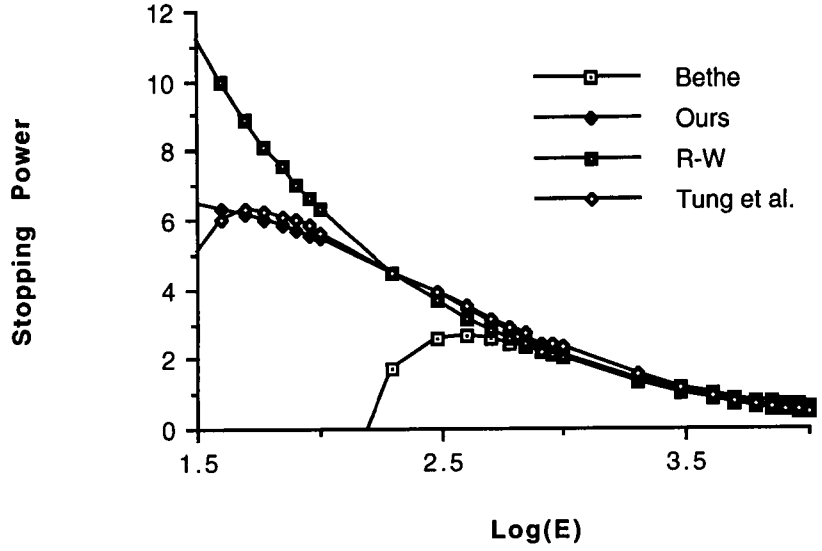


Figure 5.1 Stopping power of aluminum calculated from Eq.5.8a (Joy and Luo,1988),Bethe (1930), Tung et al. (1979) and Rao-Sahib and Wittry(1974).

The agreement between Eqs.5.8a or 5.8b and other calculations of stopping power can be optimized by selecting the magnitude of the variable k. For the elements C, Al, Si, Ni, Cu , Ag and Au, the variation of stopping with energy was calculated using Eq.5.7. The binding energy values E_i were taken from the data in Siegbahn et al. (1967) for all except the valence and d-electron shells. For the purpose of this study, d-electrons (in Cu, Ag and Au) were regarded as valence electrons. The effective binding energy E_v of these was determined by writing (Shimizu and Ichimura, 1981):

$$\left(\frac{dE}{dS}\right)_{total} = \left(\frac{dE}{dS}\right)_{core} + \left(\frac{dE}{dS}\right)_{valence} \qquad (5.9)$$

since the Bethe formulation includes electron-electron and plasmon excitations. Hence Eq.5.1 with the total stopping power, and the components of Eq.5.7 with the individual

contributions we can write

$$z_v \ln E_v = Z \ \mathrm{Ln}\, I - \sum_{i \neq v} z_i \ln E_i \qquad (5.10)$$

thus

$$E_v = \left[\frac{I^Z}{\prod_{i \neq v} E_i^{Z_i}} \right]^{1/Z^v} \qquad (5.11)$$

Table 5.1 gives the best fit k values for the seven elements tested. These values were deduced by comparing data obtained using Eq.5.7 with the modified Bethe expressions (Eqs. 5.8a or 8b) and applying a least-squares fitting criterion to find the optimum value of k. The I values used were obtained from Eq.5.2.

Table 5.1

Element	C	Al	Si	Cu	Ni	Ag	Au
k value	0.77	0.815	0.822	0.83	0.83	0.852	0.851

With these values of k, the agreement between the stopping powers predicted by the modified Bethe expressions and those predicted by the more elaborate expression of Eq.5.7 is excellent at all energies above about 50eV. In addition, as demonstrated by Figure 5.1, a comparison of stopping powers calculated from Eq.5.8a with published values from Tung et al.(1979), Rao-Sahib Wittry and Bethe(1930), shows that the modified Bethe expression produces values which are typically within 10% over the range 50-200 eV,

and within better than 5% from 200eV-10keV, of Tung et al.(1979) data. For elements, and for compounds, for which no comparable stopping power data are available to permit the value of k to be optimized, a value of 0.85 can be used. Because k appears only as part of the sum term inside the logarithm, the computed stopping power even at low energies , is not strongly sensitive to the value of k used, and even in the case of carbon, for which a best fit value of k=0.77 is available, substitution of the value k=0.85 causes less than 10 % error at any energy. The expressions of Eq.5.8a,b can more accurately represent the stopping power down to the energy at which the incident electron becomes, by the usual definition (e.g., Seiler 1983), a secondary electron. Therefore, a general expression of Eq.5.8a, b for all elements can be given as:

$$-\frac{dE}{dS} = 785\,\frac{\rho Z}{AE}\,\ln\left(\frac{1.166E}{I} + 1\right) \quad \text{eV/Å} \qquad (5.12)$$

The use of this improved stopping power expression permits more accurate modeling of all types of electron beam interactions at low energy. An example of the effect that the choice of energy loss model makes can be seen in Figure 5.2, which plots the electron range as a function of beam energy for C, Cu, and Au using the original Bethe plus Rao-Sahib Wittry model (Eq.5.1and 5.3) and the modified Bethe expression (Eq.5.8) In both cases, the range R at energy E has been computed from the relation:

$$R = \text{residual range at 50 eV} + \int_{0.05}^{E}\left[1 / \left(\frac{dE}{dS}\right)\right]dE \qquad (5.13)$$

where the residual range at 50 eV is the figure quoted by Tung et al. (1979) for the element of interest, or can be estimated using the result (Nieminen 1988) that below 50 eV the

stopping power for all materials varies as $E^{5/2}$. It can be seen that the improved model predicts electron ranges for energies below a few keV which are significantly larger than those of the other model, which overestimates the stopping power at low energies, especially for heavy elements. Similarly, significant changes can be seen in the computed values of the secondary electron yield and the $\phi(\rho Z)$ curve for x-ray production at low energy (Joy, to be published).

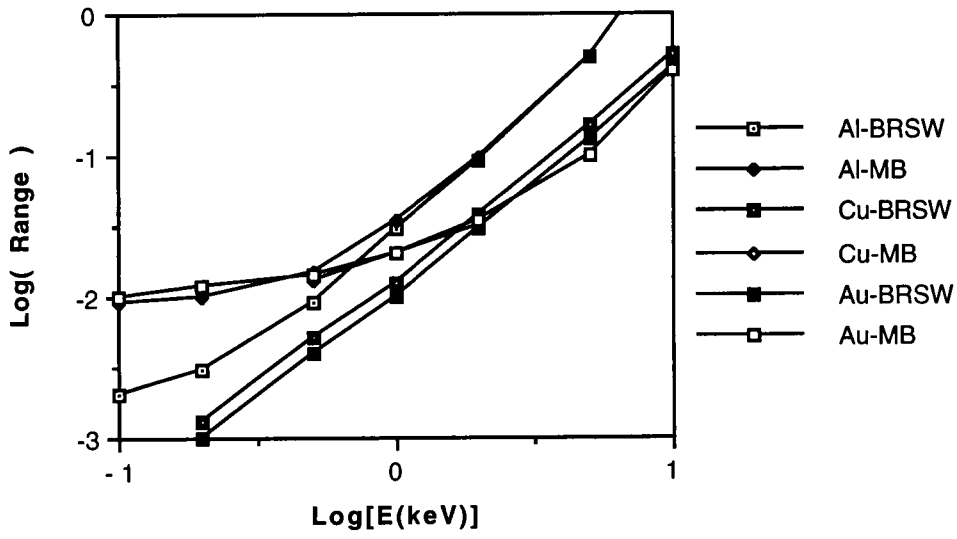


Figure 5.2 Variation of electron range with incident energy for Al, Cu, and Au as computed from the original Bethe model extended by the Rao-Sahib Wittry extrapolation (BRSW) and from the modified Bethe (MB) equation.

The revised Bethe expression discussed here is a semiempirical modification for which no theoretical basis is claimed, although the physical basis of the alteration is that it incorporates an energy variability into the value of the mean ionization potential I. For high

electron energies the model predicts stopping powers which are the same as those of the original Bethe expression whose accuracy is now well established. For low beam energies, however, the modified equation predicts stopping powers which are substantially more accurate than those of the original model since they agree well with stopping power estimates from other calculations. The revised equation avoids the unfortunate mathematical behavior of the standard Bethe expression at low energies while retaining the compactness, and convenience, of that expression. It is therefore well suited for application in Monte Carlo simulations of electron-solid interactions at low energies.

The second method to obtain the stopping power at low energies is to calculate it based on some theoretical model. Almost all of these calculations have been based on the approach of Lindhard (1954), Fano (1956), and Ritchie (1957, 1959). As we mentioned before, the stopping power of the specimen is expressed in terms of a complex dielectric function $\varepsilon(\omega,\mathbf{k})$ which depends on the momentum transfer $\hbar\mathbf{k}$ and the energy transfer $\hbar\omega$. The stopping power is proportional to the double integral, with respect to k and ω, over the quantity $(\omega/k)\mathrm{Im}[-1/\varepsilon(\omega,k)]$ (NBSIR , 1982; ICRU Report 37, 1984) .

Ashley, Ritchie and collaborators have developed a statistical model, in which the dielectric function is calculated according to Lindhard's local plasmon approximation for free electron gas in metals , and an insulator model developed by Tung et al.(1976a) for insulators and semiconductors. Since the seventies, they have been using a variety of models, adapted to a variety of materials, taking into account single-electron excitations as well as collective excitations (i.e. plasmons). Whenever possible, experimental optical data, which were obtained from optical measurements or EEL spectrum, were used to obtain the dielectric function in the limit of zero momentum transfer $\varepsilon(\omega,0)$. It was still necessary, however, to obtain $\varepsilon(\omega,k)$ for non-zero k through theoretical extrapolation, guided by the

requirement that very large energy transfers should be described by the Rutherford cross section, or by the Moller cross section when exchange is taken into account. The contribution of inner shell electrons to the stopping power has been calculated using theoretical atomic generalized oscillator strengths (NBSIR, 1982; ICRU Report 37,1984).

The stopping power data have been calculated by Ashley et al.(1975) for Al and Al_2O_3; Tung et al (1976a), for Al_2O_3; Ashley et al. (1976a) and Tung et al. (1979) for Al, Si, Ni, Cu, Ag and Au; Ashley et al. (1976b) for Ge and GaAs; Tung et al. (1976b) for Si and SiO_2 ; Ashley et al. (1978) for polystyrene; Ritchie et al. (1978) for water; Ashley et al.(1979) for Al; Paiter et al. (1980) for polyethylene; Ashley (1980) for various organic solids, Ashley and Anderson (1981) for SiO_2; and Ashley (1982) for water; Williams et al.(1989) for polymethyl methacrylate (PMMA) ; Ashley (1988a) for C, Al, Cu, Ag, Au, water, polythylene, and PMMA; Ashley (1988b) for poly (butene-1-sulfone)(pbs). Other calculations based on the use of Lindhard's statistical model have been reported by Sugiyama (1976).

5.3 EXPERIMENTAL DETERMINATIONS OF ELECTRON STOPPING POWER AT LOW ENERGIES

Although detailed theoretical investigations of the stopping power in the low energy loss region have been made as we briefly discussed above, for the practical purposes of modeling, for example, electrons interactions in electron lithography at low incident beam energies, it is necessary to be able to obtain accurate stopping power data for a wide variety of materials many of which are either proprietary or of significant chemical complexity. In such cases the chance of finding the required data already in the literature is small, and

the resources and data required to perform an ab initio computation of the stopping power using some suitable theoretical model may not be available. We have therefore developed a practical approach which permits the stopping power to be derived by straightforward experimental techniques from any material which can be examined in an electron microscope.The approach uses electron energy loss spectroscopy (EELS) and sum rules to derive the dielectric response of the specimen and hence the stopping power, but has analogies with optical methods (Ashley, 1988).

5.3.1 Outline of method

The simplest expression for the stopping power can be written in the form of Eq.5.1. In this form the Bethe equation has been widely used because it requires only one parameter, I , to describe all of the inelastic interactions of the electron with the solid. The application of Eq.5.1 is limited, however, to energies $E >> I$ where core ionization processes dominate and where the Born approximation is valid. At low energies two problems arise, firstly the Born approximation may not be valid and, secondly, E, the energy of the electron may be smaller than the critical excitation energy for one or more of the shells of the atom. Consequently the value of the mean ionization potential I must change, as must the apparent atomic number of the material. It is therefore more appropriate to write Eq.5.1 in the form (Ritchie et al., 1969; Powell, 1982):

$$-\frac{dE}{dS} = \frac{2\pi e^4 n\, N_{eff}(E)}{E} \ln\left(\frac{1.166E}{I_{eff}(E)}\right) \qquad (5.14)$$

where $I_{eff}(E)$ and $N_{eff}(E)$ are respectively the effective values of the mean ionization potential, and the number of electrons from the atom or molecule participating in the

process, at the energy E. This modified form of the Bethe equation has a concise form and clear physical interpretation. At high energies $N_{eff}(E) = Z$ and $I_{eff}(E) = I$, but at low energies both $N_{eff}(E)$ and $I_{eff}(E)$ will fall with E. The task is therefore to find $N_{eff}(E)$ and $I_{eff}(E)$ by some suitable experimental procedure.

Inelastic electron scattering in solids can be described macroscopically in terms of a complex dielectric constant $\varepsilon(\omega,k)$ dependent on frequency ω and momentum-transfer k. For k=0 the dielectric constant is related to the familiar optical constants and can be written in the form

$$\varepsilon(\omega, 0) = \varepsilon_1 + i\ \varepsilon_2 \qquad (5.15)$$

The differential inelastic scattering cross section, and hence S(E) the single scattering electron energy loss spectrum, is then proportional to $\mathrm{Im}[-1/\varepsilon(\omega,k)]$ i. e.(Pines, 1969),

$$S(E) \propto \frac{1}{k^2}\ \mathrm{Im}\left[\frac{-1}{\varepsilon(E, k)}\right] \qquad (5.16)$$

where

$$\mathrm{Im}\left[\frac{-1}{\varepsilon}\right] = \frac{\varepsilon_2}{\varepsilon_1^2 + \varepsilon_2^2} \qquad (5.17)$$

is known as the energy loss function. (Note that in the energy region below about 100 eV $(\varepsilon_1^2 + \varepsilon_2^2)$ is usually appreciably different from unity, and hence there is a large difference between electron energy-loss and optical absorption spectra, but at higher energy loss where losses are predominantly due to core-electron excitations $\varepsilon_1 \sim 1$ and $\varepsilon_2 << 1$ so

that $Im[-1/\varepsilon] \sim \varepsilon_2$ and hence electron energy loss spectra become similar to X-ray absorption spectra). An experimental electron energy loss spectrum can therefore be used to derive the dielectric function, although it might be expected that this will be slightly different from that found by an optical method.

From a microscopic point of view the single scattering electron energy loss spectrum S(E) can also be expressed in the form (Bethe, 1930, Inokuti, 1971) :

$$S(E) = \frac{\text{constant}}{E} \times GOS \qquad (5.18)$$

where GOS is a generalized oscillator whose strength is a property of the scattering center. The properties of this oscillator can then in turn be expressed in terms of the quantities $N_{eff}(E)$ and $I_{eff}(E)$ that we require. Hence a comparison of Eqs.5.16 and 5.18 permit $N_{eff}(E)$ and $I_{eff}(E)$ to be evaluated as a function of the energy loss E.

5.3.2 Experimental procedure

An electron energy loss spectrum (EELS) is obtained from the material of interest. In our case this is done at 200 keV on an Hitachi H800 transmission electron microscope using a Gatan 607 electron spectrometer, or a Philips CM20 with a GATAN PEELS spectrometer. The EEL spectra are collected in serial mode (i.e., sequentially scanning data at increasing energy loss) within a maximum acceptance aperture angle of 10 mrad and with an energy resolution of 3 eV. The analyzed area can range from 100 Å to as large as 0.5μm in diameter. In order to obtain sufficiently good signal statistics the sample is

chosen to be typically 1000-2000Å in thickness, hence some fraction of the electrons suffer plural scattering. In order to obtain the true single scattering profile S(E) the digitally recorded spectrum is therefore deconvoluted using a matrix arithmetic modification of standard Fourier procedures. A deconvolution procedure is also used to improve the effective energy resolution of spectrum to about 1 eV. The experimental spectra are typically recorded for energy losses only in the range 0 to 500 eV in order to minimize the total time required to collect the data. Although the signal at 500 eV loss is only about 0.01% of that in the elastic (zero loss) peak it is still well above the statistical noise floor of the recording equipment so the continuum tail of the deconvoluted spectrum is extrapolated to noise level using the power law approximation (Maher et al., 1979):

$$S(E) = A\ E^{-r} \qquad (5.19)$$

where the constants A and r are found by a logarithmic least-squares fitting procedure to the spectrum.

The imaginary part of the dielectric function can be found using the relation:

$$S(E) = \frac{I_0 t}{\pi a_0 m_0 \upsilon^2} \mathrm{Im}\left[\frac{-1}{\varepsilon(E)}\right] \ln\left\{1 + \frac{\chi^2}{\theta_E^2}\right\} \qquad (5.20)$$

where I_0 is the intensity of the zero loss peak, t is the sample thickness, υ is the electron velocity, a_0 and m_0 are respectively the Bohr radius and mass of the electron, χ is the semi-collection angle of the spectrometer,

$$\theta_E = \frac{E}{\gamma m_0 \upsilon^2} \quad \text{and} \quad \gamma^2 = \frac{1}{1-\beta^2}$$

The Kramers-Kronig transform is then applied to obtain Re (ε(E)) the real part of the dielectric function, and the real and imaginary parts are then normalized from the sum rule:

$$1 - \mathrm{Re}\left[\frac{1}{\varepsilon(0)}\right] = \frac{2}{\pi}\int_0^{\infty} \mathrm{Im}\left[\frac{-1}{\varepsilon(E)}\right]\frac{dE}{E} \qquad (5.21)$$

For a metal the left hand side of Eq.5.21 is unity, while for an insulator Re[1/ε(0)] is $1/\varepsilon_1(0)$. The data is now in its final form and $N_{eff}(E)$ and $I_{eff}(E)$ can be found from the sum rule relations:

$$N_{eff}(E) = \left(\frac{2m_0}{h^2e^2n}\right)\int_0^{E/2} E'\,\mathrm{Im}\left(\frac{-1}{\varepsilon(E')}\right)dE' \qquad (5.22)$$

and

$$\ln\left(\frac{I_{eff}(E)}{2R}\right) = \left(\frac{8\pi}{h^2\omega_p^2}\right)\int_0^{E/2} E'\ln\left(\frac{E'}{2R}\right)\mathrm{Im}\left(\frac{-1}{\varepsilon(E')}\right)dE' \qquad (5.23)$$

where E is the energy loss, and $\omega_p=(4\pi e^2nN_{eff}/m_0)^{1/2}$.

The EELS data is read directly from the multi-channel analyzer into a standard personal computer (typically an Apple Macintosh II) which performs all of the operations discussed above. The program is given as Appendix B.

5.3.3 Practical applications

As a practical demonstration of this method data was obtained for vitreous ice,

which is the phase formed when water is cooled at a sufficiently high rate > 10^6 deg K/s). This form of ice is an important component in the electron microscopic study of biological materials since it forms the matrix within which the tissue of interest is held. It was found possible to obtain spectra of sufficient quality for incident beam exposures of less than 50 el/Å^2 , a dose too low to cause any radiation damage to the ice at the sample temperature of 100 K. Figures 5.3 and 5.4 show the curves for $N_{eff}(E)$ and $I_{eff}(E)$ derived from the data. Both parameters show a steady rise in value from close to zero at the lowest energy for which reliable data can be computed, to a saturation condition at an energy around 1 keV. For comparison values of $N_{eff}(E)$ and $I_{eff}(E)$ derived for liquid water (Zeiss et al., 1975) from optical and model dielectric function data are shown. It can be seen that the general forms of both sets of data are similar although there are some detailed discrepancies. In particular the electron data does not show as pronounced a structure in the low energy (< 100eV) region. Some of these may be due to the different nature of the two procedures used, and it is also possible that the phase change from vapor to ice might have some effects at low energies. The saturation value of I_{eff} at 74 eV derived from the EELS data is however, in excellent agreement with other estimates e.g., 71eV (La Verne and Mozumder, 1983), 72eV (Zeiss et al., 1975), 75eV (Ritchie et al., 1978).

Figure 5.5 shows the resultant stopping power curve derived from this data and an application of Eq.5.13. For comparison the "standard" Bethe relation of Eq.5.1 is also shown. Over the energy range from 5 keV to 20 keV the agreement between the EELS derived data and optical data (Ashley, 1982) is excellent, the peak stopping power (at about 100 eV) being only 5% higher than the value quoted by Ashley. Given the small volume of material (~10^{-16} cc) and the very low electron dose used for the production of the original EELS data this demonstrates that this technique can be given results which compare well with those obtained by the more macroscopic optical methods.

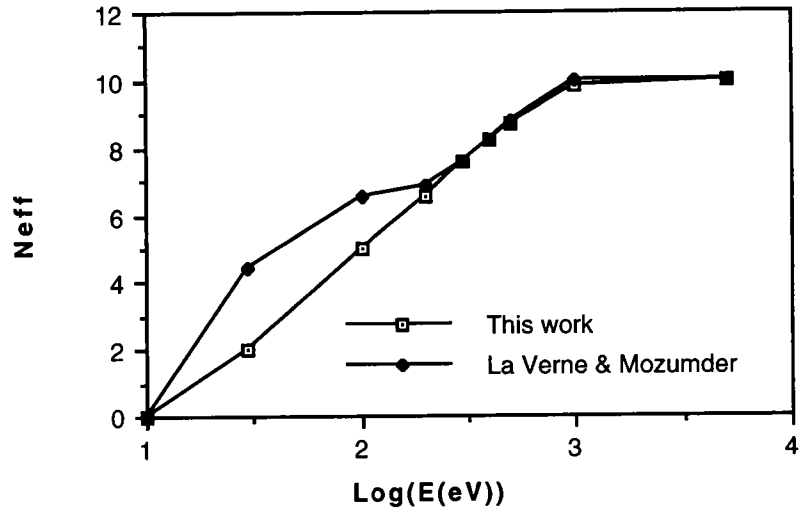


Figure 5.3 Experimentally determined variation of N_{eff} with energy for vitreous ice The optical data (La Verne and Mozumder,1983) for liquid water is shown for comparison.

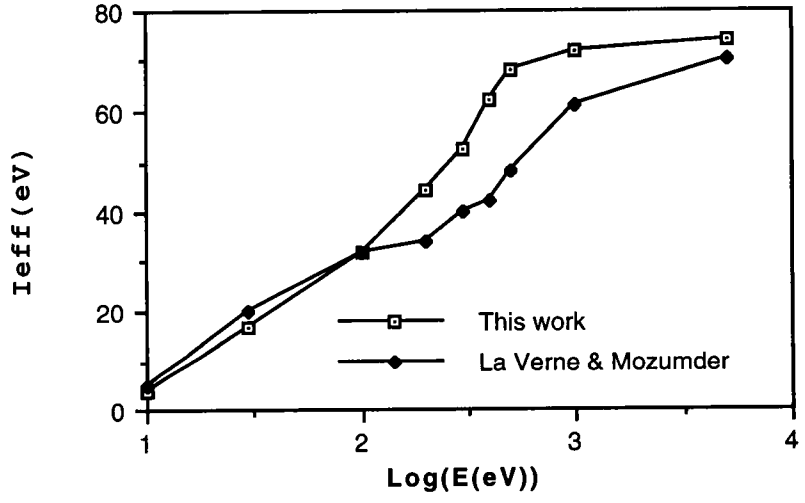


Figure 5.4 variation of I_{eff} with energy for vitreous ice (open squares, our experiment). The optical data (La Verne and Mozumder, 1983) for liquid water is shown for comparison (closed squares).

To illustrate the practical technological application of this approach Figures 5.6 and 5.7 show a corresponding set of N_{eff} and I_{eff} and stopping power data for device quality GaAs. The form of the N_{eff} and I_{eff} curves versus energy shows again there is not an obvious saturation of the oscillator strengths for the individual shells. Instead the oscillator strength distribution for one shell overlaps with that from another shell to give a smoothed variation with energy. The oscillator strength, and the corresponding I_{eff} value, do not finally saturate until an energy of about 2.5 keV reflecting the higher average values of the core critical ionization potentials compared with the data for ice. The saturated value of is found to be 342 eV which is in close agreement with the value of 340 eV predicted by the usual (Berger and Seltzer, 1964) analytic fit. Monte Carlo predictions of the electron range and energy deposition obtained using the stopping power data of Fig.4.8 have been found to be in good agreement with independent estimated of these quantities derived from electron beam metrology studies.

The experimental method reported here permits stopping power data to be obtained from femto-gram amounts of elements and compounds. In those cases where suitable theoretical or macroscopic experimental data for comparison is available the results obtained by the method discussed here have been found to be in good agreement for both absolute magnitude and the form of the energy variation. We have derived data for more than a dozen materials of the type used in semiconductor device fabrication and data for others is now being accumulated. At present most simulations in use for the modeling of electron lithography, critical dimension metrology, and imaging assume that the stopping power can be computed from Eq.5.1, with values of I derived from the Berger and Seltzer expression, although the data presented here shows that for any energy below about 5 keV this is likely to be in error. Because the N_{eff} and I_{eff} curves versus energy are monotonic

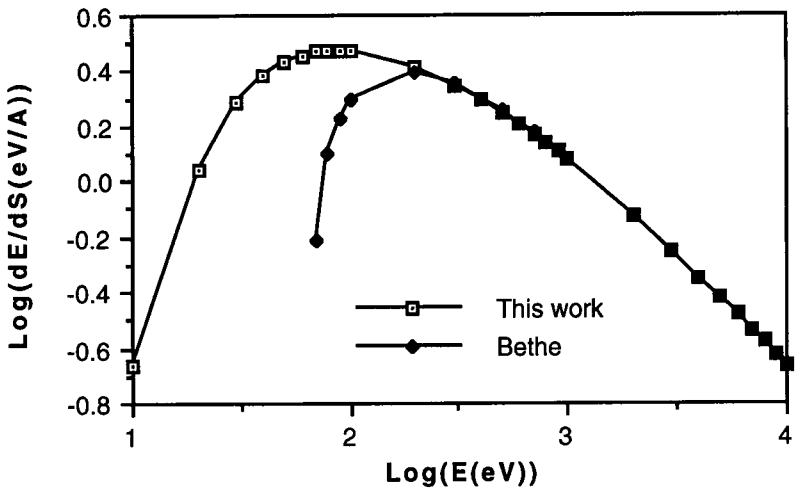


Figure 5.5 Comparison of our experimentally determined stopping power for vitreous ice with Bethe equation data.

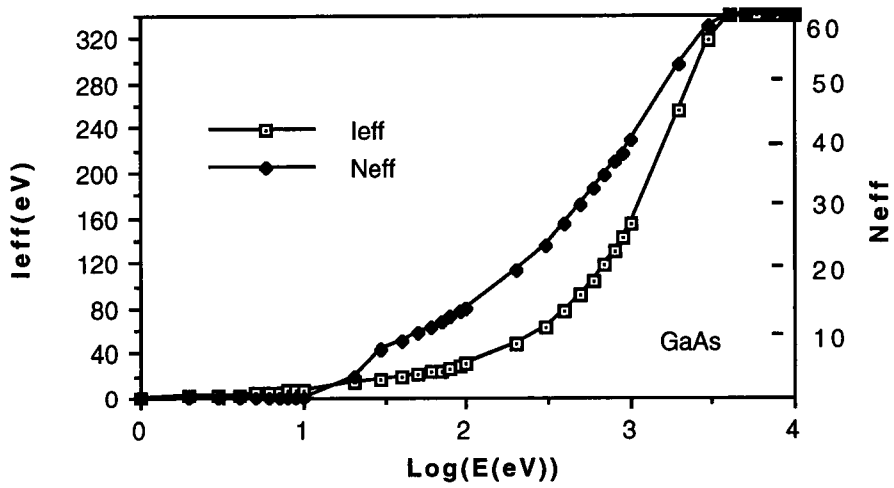


Figure 5.6 Experimentally determined variation of N_{eff} and I_{eff} for GaAs (dielectric function from Daniels et al.,1970).

we believe that it should be possible to parametrize this data to facilitate the use of Eq.5.14 and hence to provide accurate stopping power values for the values of incident electron energy now of interest.

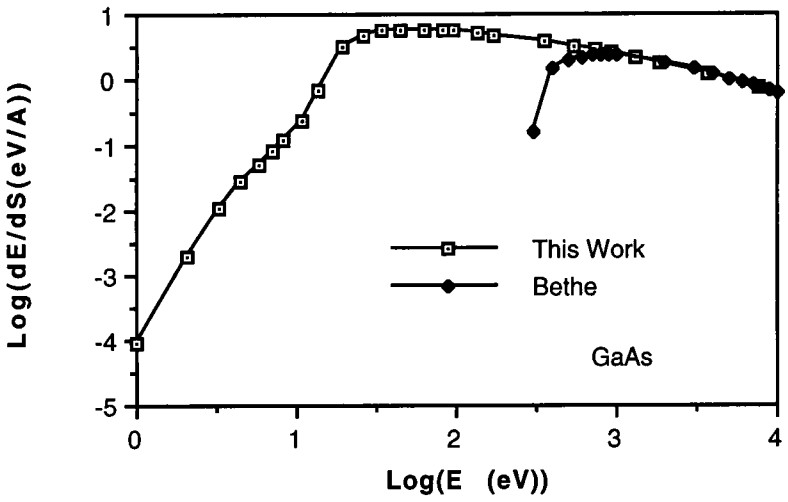


Figure 5.7 Comparison of our computed stopping power for GaAs from dielectric function (Daniels et al., 1970) and the Bethe equation's.

Figures.5.8 - 5.32, 5.35-5.36 are experimentally determined stopping powers for a variety of materials including:

Compound : SiO_2, Al_2O_3, InSb, GaSb, ZnSe, MoS_2, MgO, SiC;

Elements : C, Al, Si, Ti, V, Cr, Mn, Fe, Co, Ni, Cu, Ge, Pd, Ag, Pt, Au, Pb;

Superconductor: $Bi_{1.8}\,Pb_{0.3}Sr_2Ca_2Cu_3O_{10}$;

and others : Guanine and DNA .

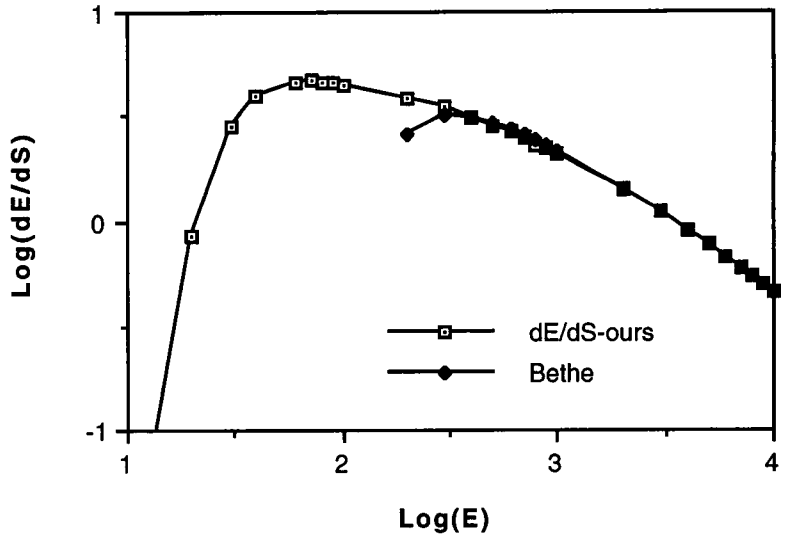


Figure 5.8 Comparison of our computed stopping power for SiO_2 from dielectric function (Daniels et al., 1970) and the standard Bethe equation's.

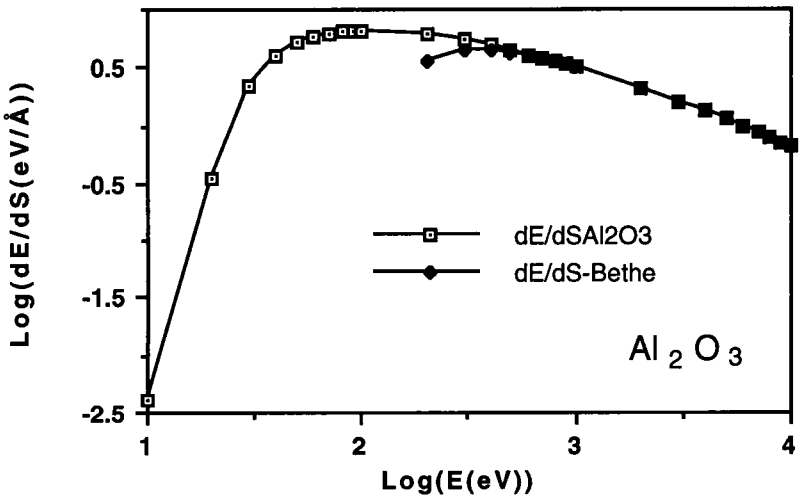


Figure 5.9 comparison of our stopping power data calculated from dielectric function (Ashley,1982) and the standard Bethe equation's for Al_2O_3.

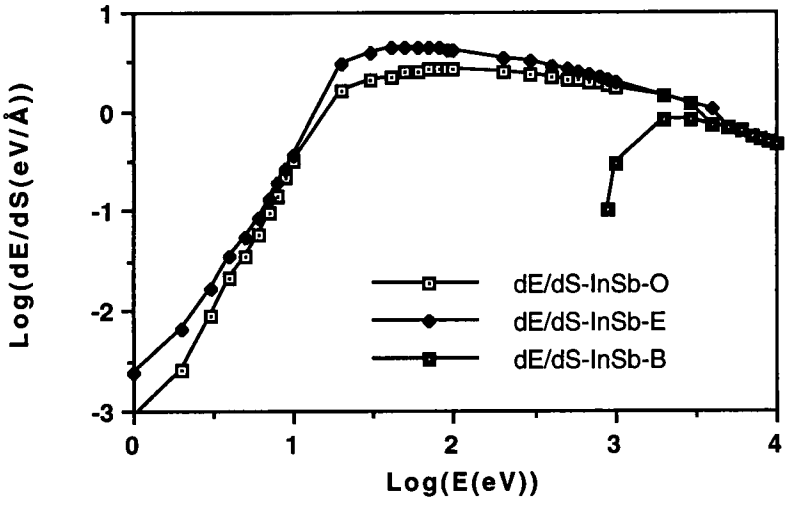


Figure 5.10 Experimentally determined stopping power using this method for InSb. O: form optical data; E: from EELS, B: from standard Bethe equation for InSb. The dielectric function is from Daniels et al.(1970).

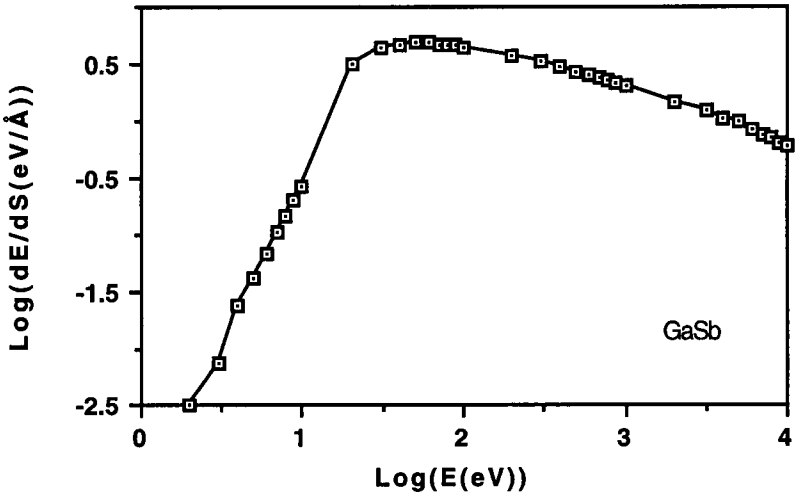


Figure 5.11 Experimentally determined stopping power using this method for GaSb. The dielectric function is from Daniels et al.(1970).

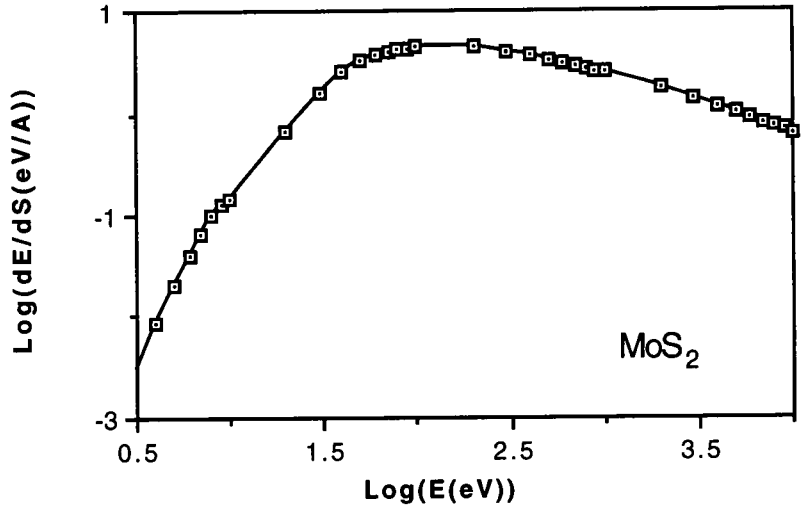


Figure 5.12 Stopping power for MoS_2 (data from our experiment).

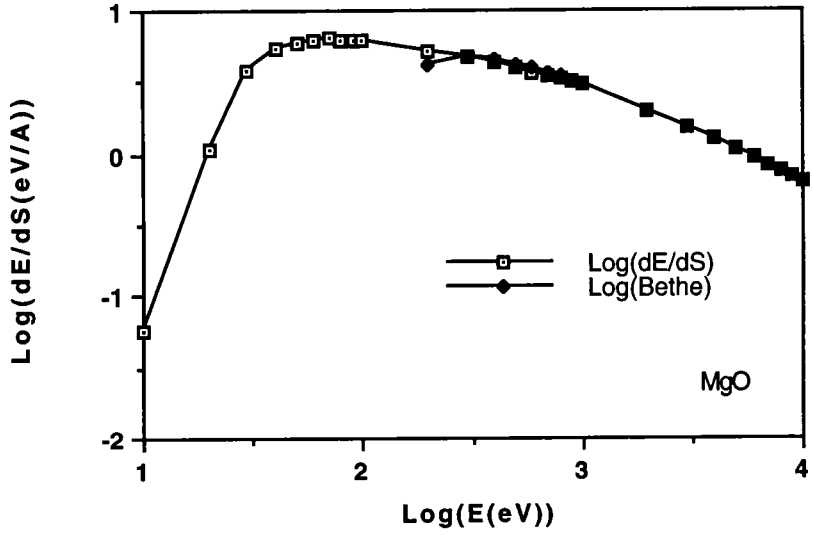


Figure 5.13 Stopping power for MgO calculated from dielectric function (Ashley, 1982).

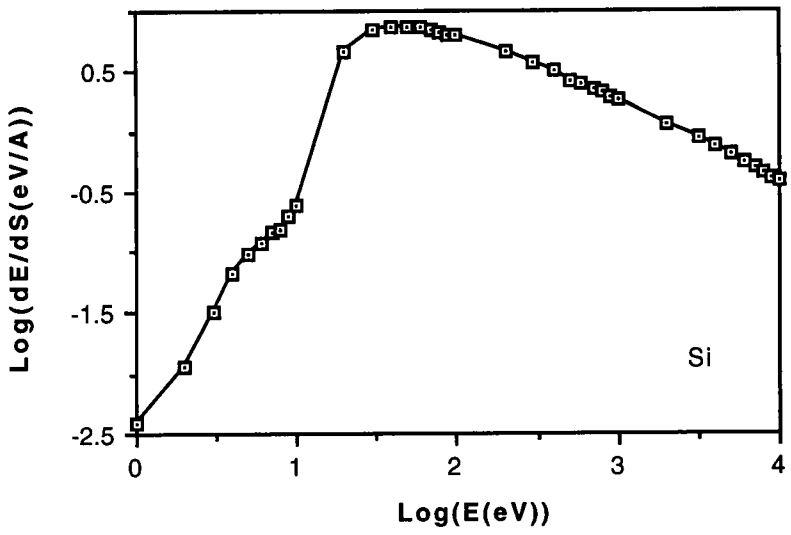


Figure 5.14 Stopping power for Si (data from our experiment).

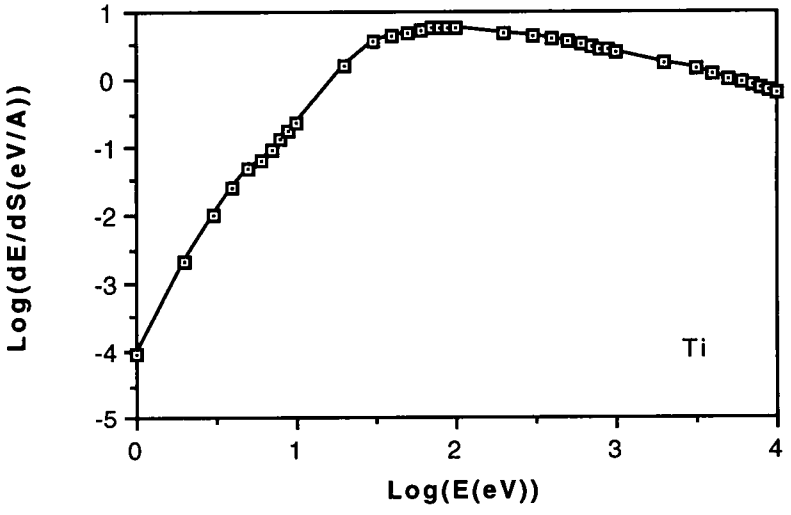


Figure 5.15 Stopping power for Ti , calculated from dielectric function (Tougaard, 1988) .

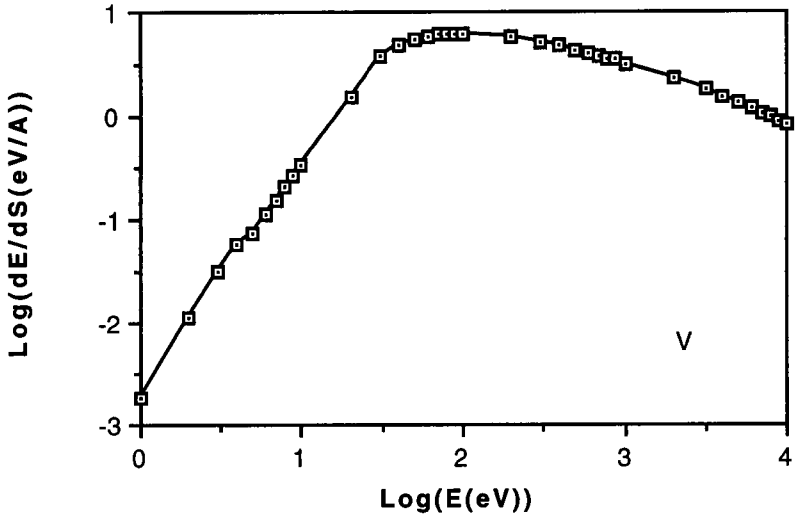


Figure 5.16 Stopping power for V, calculated from dielectric function (Tougaard, 1988)

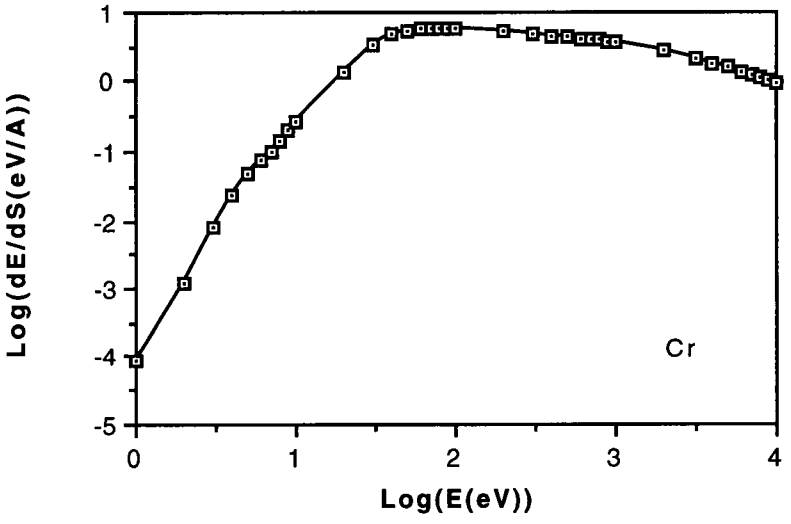


Figure 5.17 Stopping power for Cr (data from our experiment).

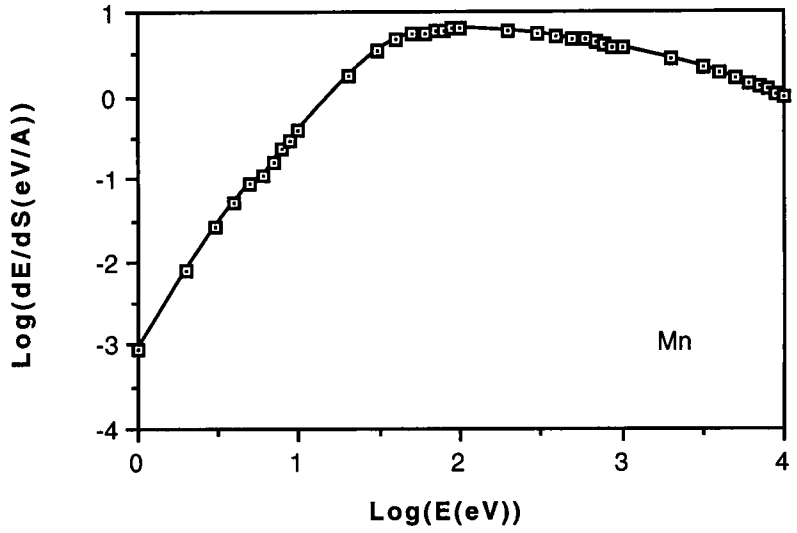


Figure 5.18 Stopping power for Mn, calculated from dielectric function (Tougaard,1988) .

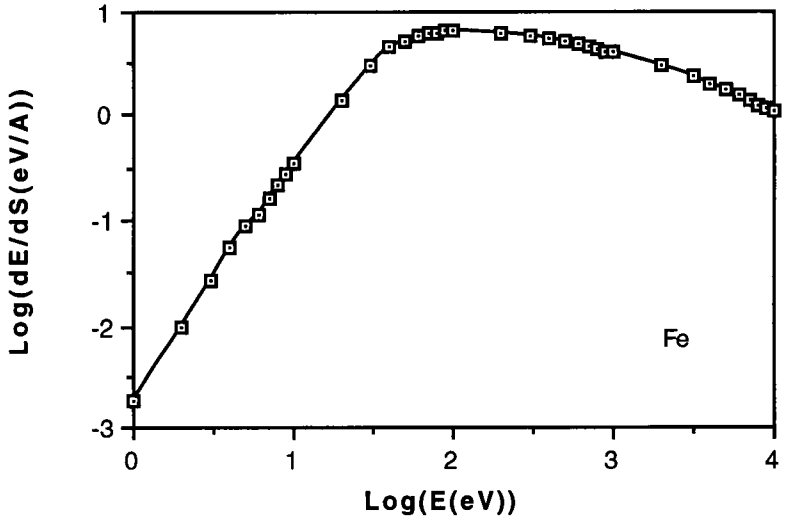


Figure 5.19 Stopping power for Fe, calculated from dielectric function (Tougaard, 1988) .

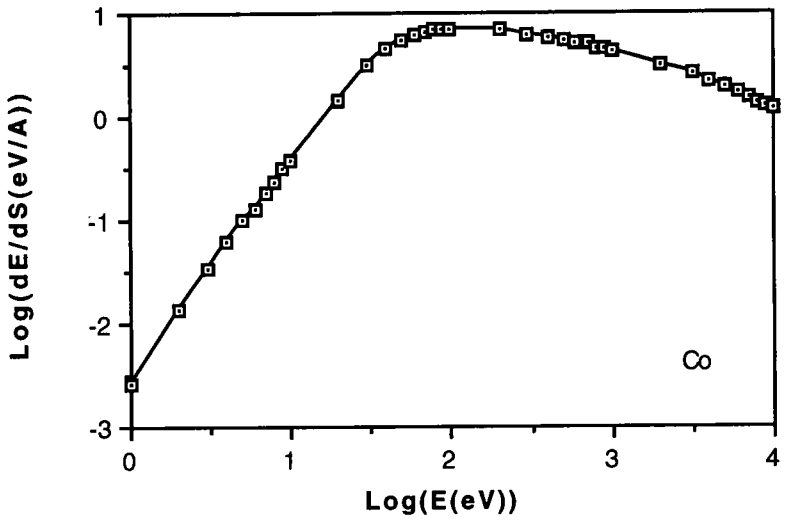


Figure 5.20 Stopping power for Co, calculated from dielectric function (Tougaard, 1988) .

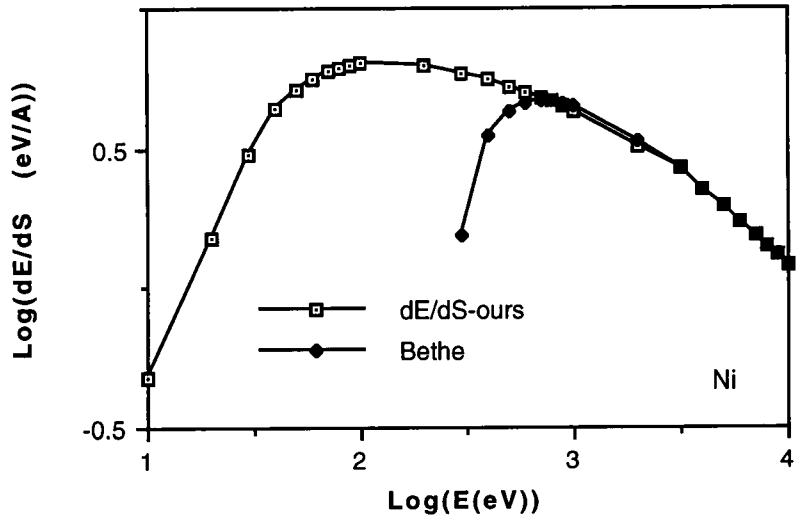


Figure 5.21 Stopping power for Ni calculated from dielectric function (Tougaard, 1988) .

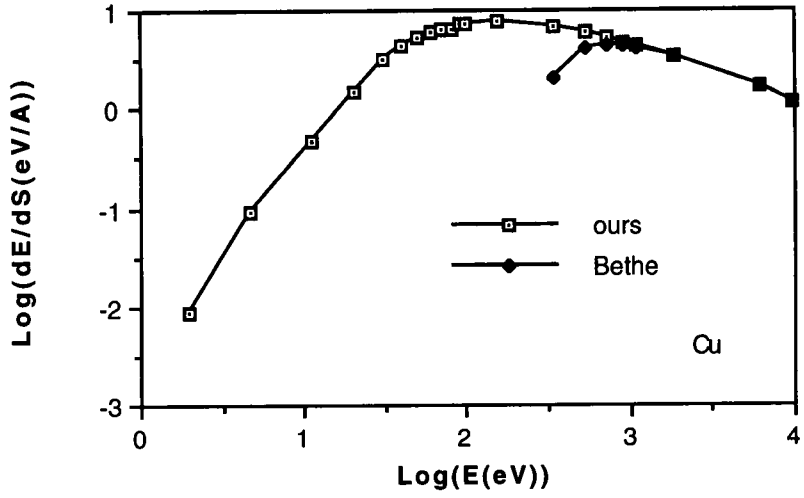


Figure 5.22 Stopping power for Cu (our experiment data). The curves are our stopping powers and the calculated from Bethe equation, respectively.

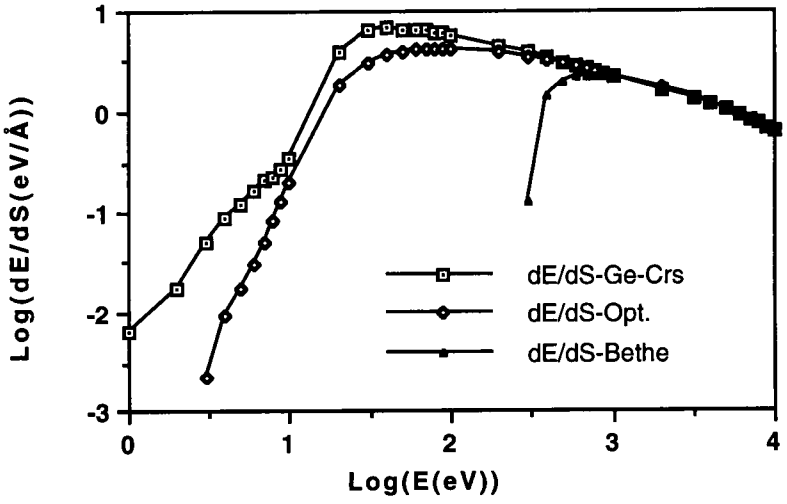


Figure 5.23 Stopping power for Ge. The curves are stopping power for a crystalline specimen, the stopping power computed from optical data (Daniels et al. 1970); and calculated from the Bethe equation, respectively.

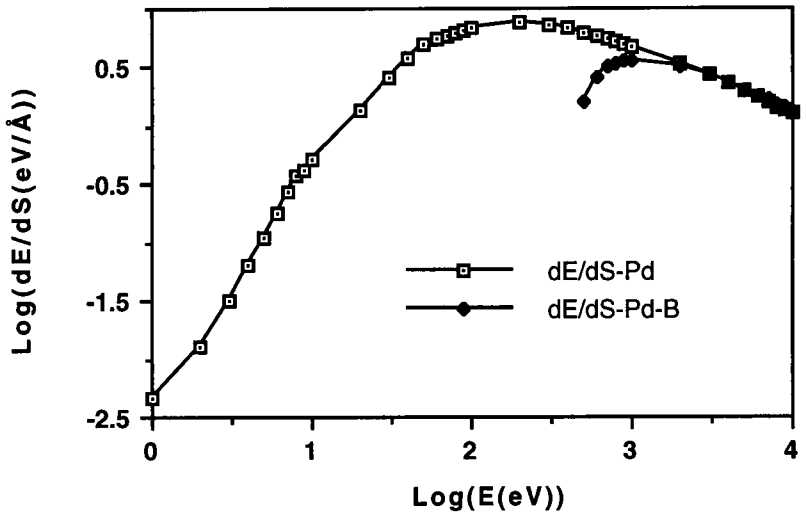


Figure 5.24 Stopping power for Pd (our experiment data). The curves are our stopping power and the calculated from Bethe equation, respectively .

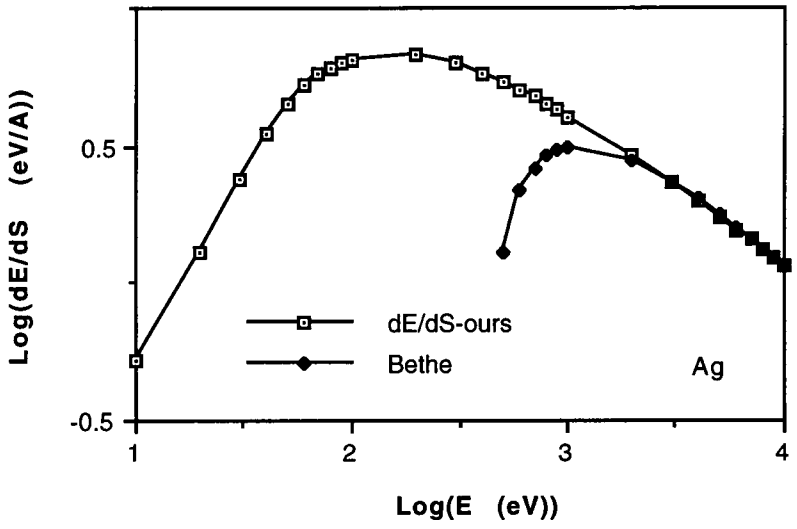


Figure 5.25 Stopping power for Ag (dielectric function from Daniels et al., 1970). The curves are our calculated stopping power, and the one from Bethe equation.

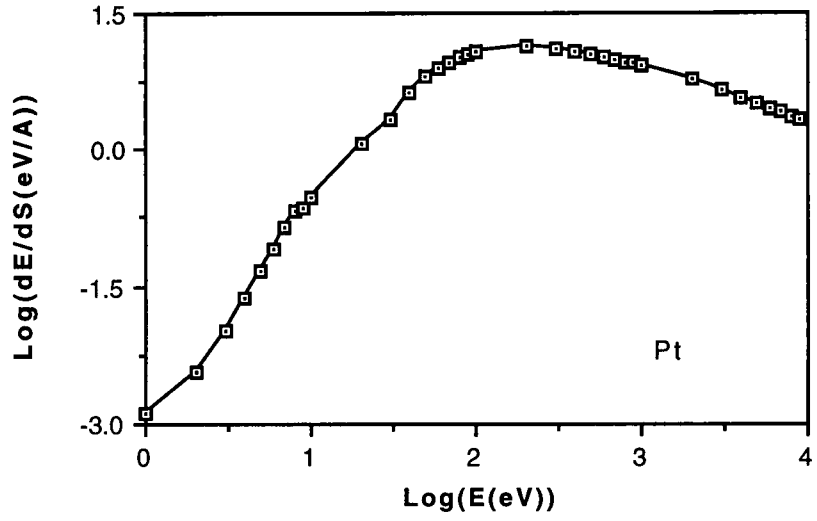


Figure 5.26 Stopping power for Pt (data from our experiment).

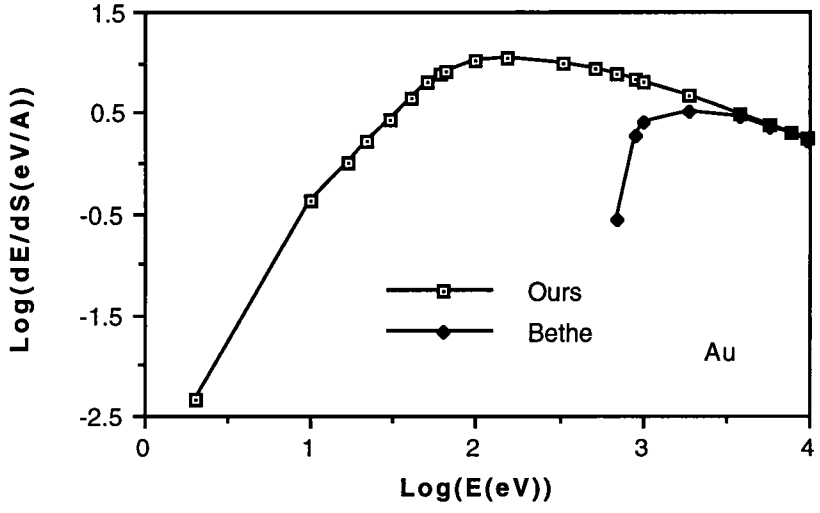


Figure 5.27 Stopping power for Au (data from our experiment).

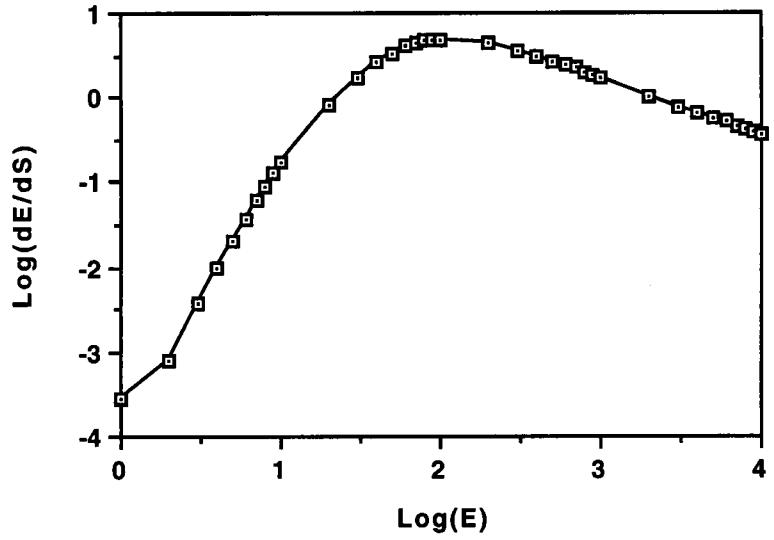


Figure 5.28 Stopping power for Superconductor: $Bi_{1.8}Pb_{0.3}Sr_2Ca_2Cu_3O_{10}$ (data from our experiment).

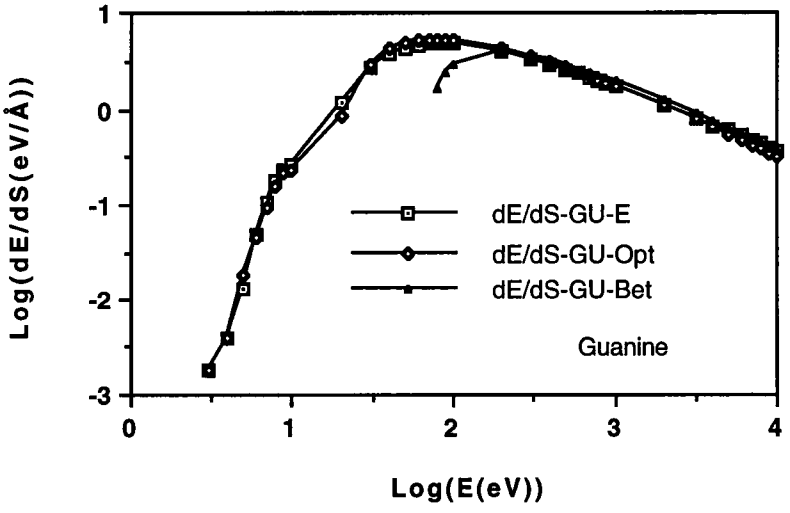


Figure 5.29 Stopping powers computed from this method for Guanine. E: from EELS data, Opt: from optical data (Ashley,1982); B: from standard Bethe equation

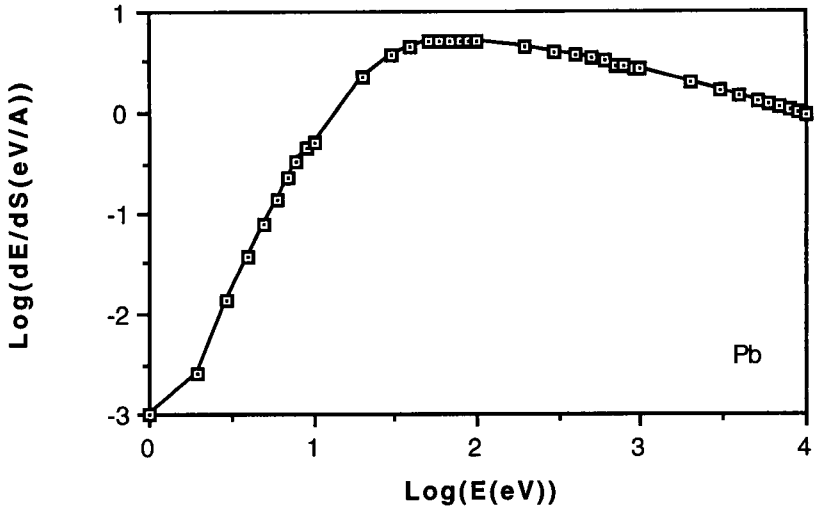


Figure 5.30 Stopping power for Pb (data from our experiment).

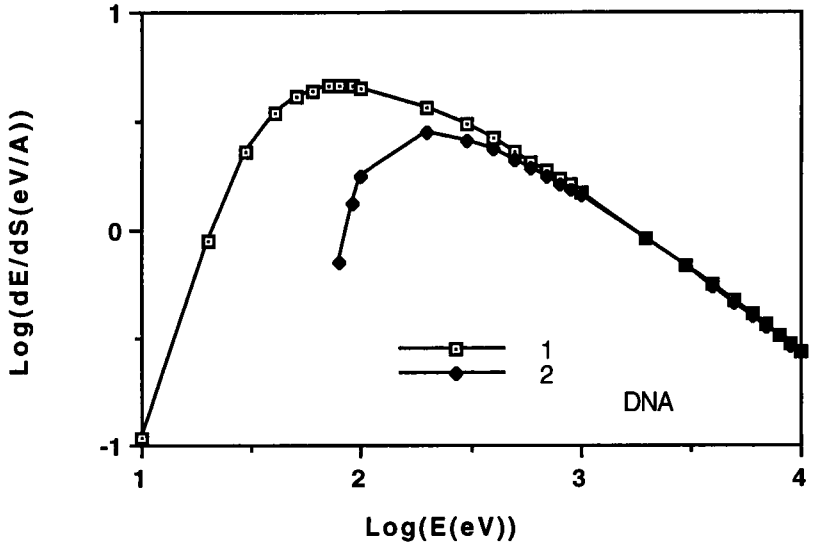


Figure 5.31 Stopping power for DNA. 1: calculated from dielectic function Ashley, 1982) ; 2: calculated from Bethe equation.

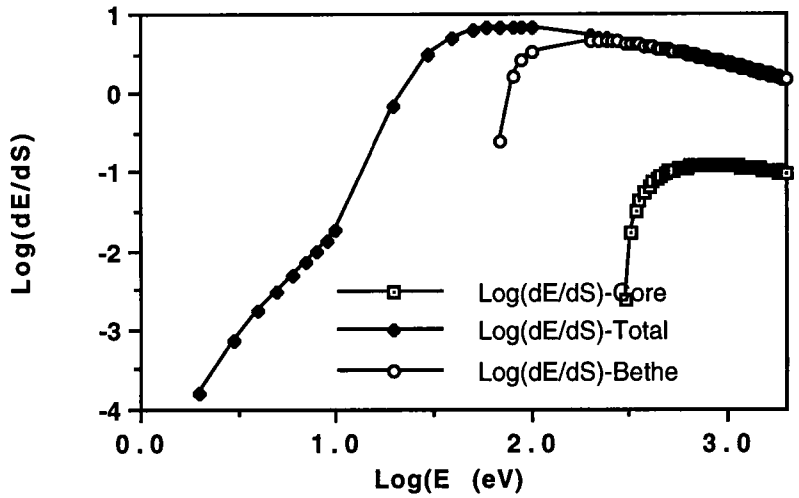


Figure 5.32 Experimentally determined stopping power for carbon including K shell contribution (data from our experiment) .

The method we discussed above is that from a few eV to 100 eV , $Im(-1/\varepsilon)$ used to be calculated from the inelastic single scattering distribution which is determined by an FFT deconvolution procedure using EELS , and above 100 eV, extrapolated to infinity by a function of E^{-r}.

However, the angular correction in the traditional deconvolution procedure is not completed , and the function E^{-r} is not accurate enough to represent all core energy losses .Hence we have proposed a new technique based on angular, and energy loss, three-dimension Poisson statistics , as we discussed in chapter 3 , in order to get more accurate single scattering distribution as well as the energy loss function below 100 eV. For the core energy loss the quantum wave functions are used to theoretically calculate the generalized oscillator strength (GOS) based on Hartree-Slater central self-consistent field model, which is essentially that described in Chapter 3. The properties of this oscillator

can then in turn be expressed in terms of the quantities N_{eff} and I_{eff}.

Figure 5.32 shows the total stopping power for carbon and the stopping power of carbon K shell calculated by the theoretical method, and a comparison with the standard Bethe stopping power data. Figure 5.34 shows the energy loss functions for C, Si and their compound SiC. Si has a sharp peak at the 16eV, C has a smooth peak at 24eV and SiC's peak is near 23eV. The energy loss function for SiC is between that for C and Si but is not a simple summation. Figure 5.35 are the effective electron number N_{eff}'s. The relationship of them is not a simple summation too, nor the stopping powers' as shown in Figure 5.36. It indicates that for a simple compound such as SiC, the electric property at very low energy loss area (less than several thousand eV) cannot mathematically computed the data for Si and C, but must be measured from experiments only.

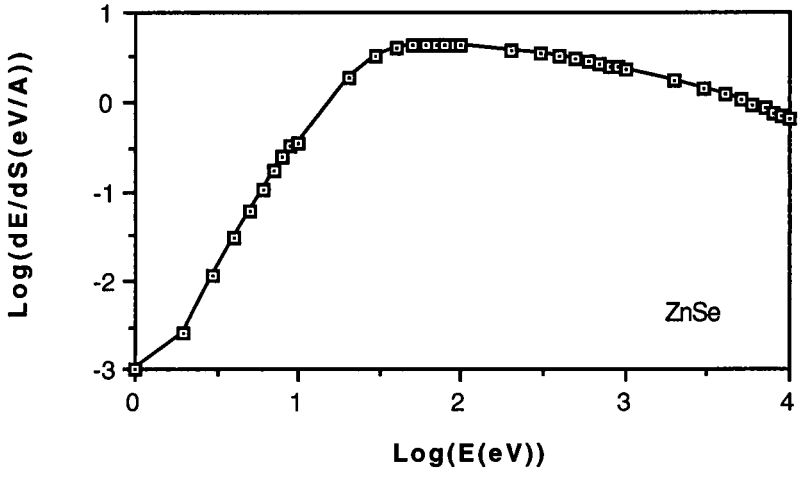


Figure 5.33 Stopping power for ZnSe (the dielectric function from Daniels et al., 1970)

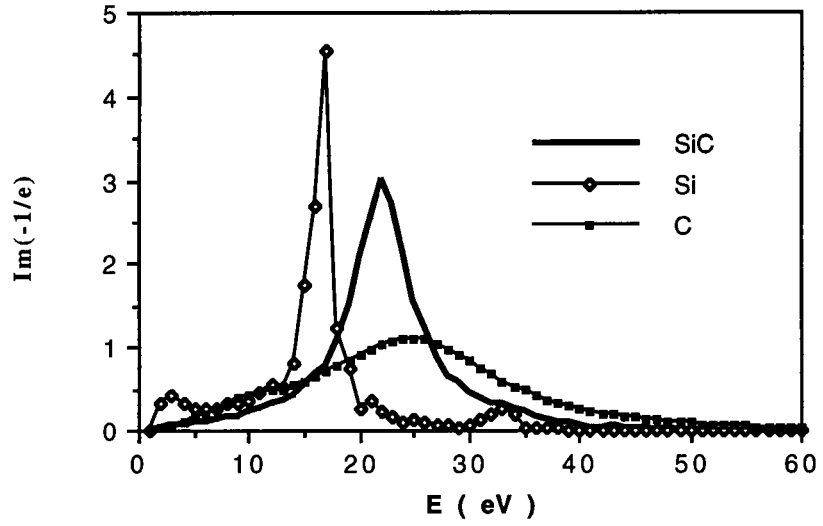


Figure.5.34 Comparison of electron energy loss functions for Si,C and their compound SiC (data from our experiments).

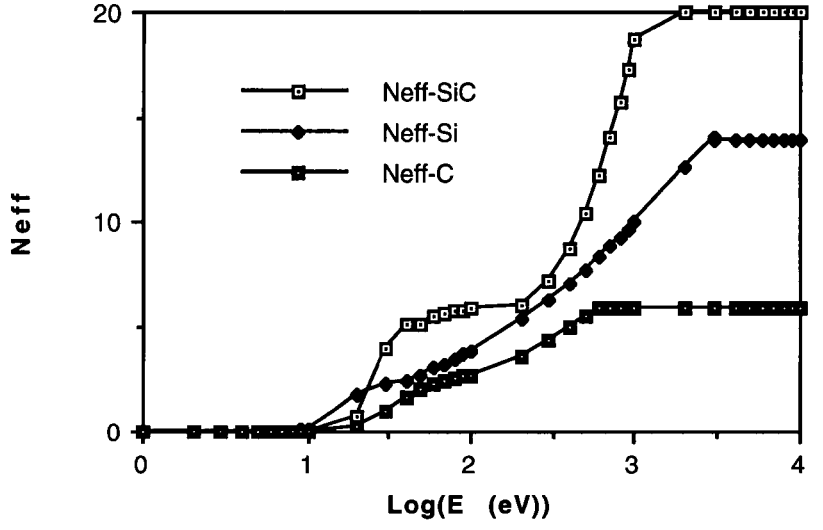


Figure 5.35 Comparison of the effective electron number N_{eff} for Si,C and their compound SiC (data from our experiments).

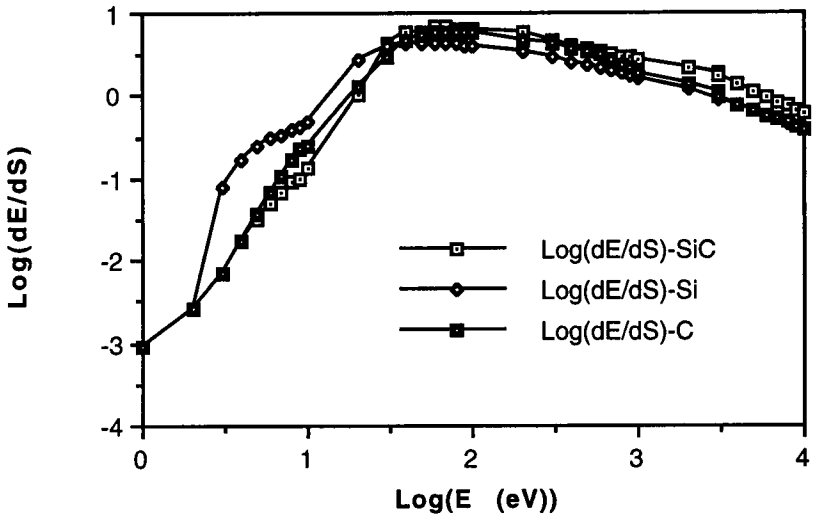


Figure 5.36 Comparison of the electron stopping powers for Si, C, and their compound SiC below 10 keV (data from our experiments).

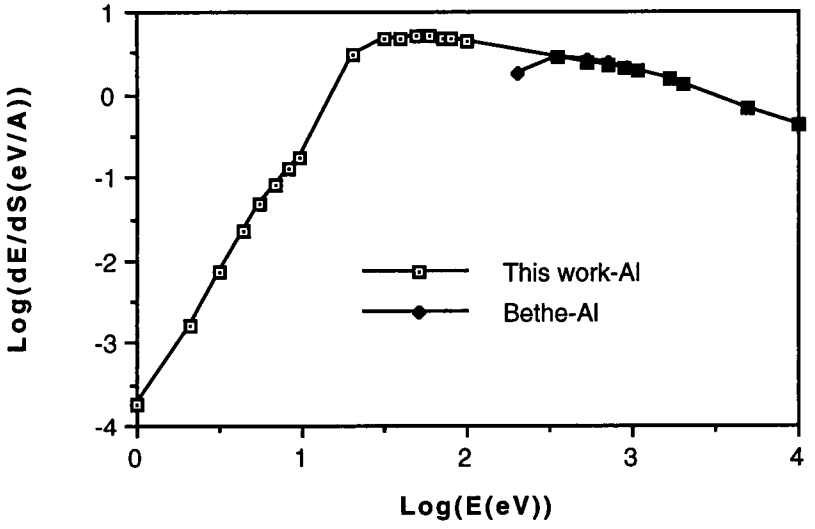


Figure 5.37 Comparison of the electron stopping powers for Al (data from our experiment).

CHAPTER 6

CALCULATIONS OF X-RAY IONIZATION CROSS SECTIONS

The ionization of atoms by electrons is a process of great importance in physics, because it is the primary mechanism for energy loss of electrons in matter and for electron microanalysis. When an energetic beam of electrons strikes a solid target then the fluorescent X-rays which are produced as the end product of these ionizations can be collected and analyzed by suitable detectors outside of the specimen to permit both the identification and quantification of the various elements making up the target. A quantitative description of the ionization process is essential to the successful conduct of microanalysis, and the most crucial feature in the description will be the magnitude and variation of the ionization cross section as a function of the various experimental parameters.

The theory of the details of inelastic collisions between fast charged particles and an atoms was developed by Bethe (1930) nearly sixty years ago. More recently Manson (1972, 1974) and McGuire (1971a,b, and 1974) have used the Bethe theory to calculate Generalized Oscillator Strengths (GOS) and hence cross sections for K and L shell excitations, while Leapman et al.(1980) , Rez(1984) , Ahn and Rez (1985), and Batchelor et al. (1988) have used wave functions based on numerical solutions of the Schrodinger equation to calculate both partial and total electron ionization cross sections for K , L and M shells for some elements. The comprehensive review on this subject by Powell (1976, 1984, 1985, and 1989) compares various theoretical, semi- or empirical formulations with experiments and it is clear from these studies that, at least for K-shell ionizations where the greatest body of experimental data is available, existing formulations and theories can

provide a good fit to measurements provided that the necessary parameters are chosen carefully and the model is restricted to the conditions for which it was derived. However, because the experimental work is difficult on an absolute scale, it is preferable to use theoretical method to get the necessary cross section information.

We have calculated K , L (L_1 and L_{23}) and M (M_1 ,M_{23} and M_{45}) shell ionization cross sections covering the entire periodic table and spanning the energy range from the critical ionization energy for a particular element up to 100 keV using Hartree-Slater central self-consistent field model. The calculation algorithm is essentially that described in Ref.of Manson (1972), Leapman et al (1980), and Rez (1984) but both exchange and correlation energy effects have been included in the computations to ensure that the computed cross-sections are valid at low overvoltage ratios, and relativistic corrections have also been included for accuracy at high incident energies. By performing a complete, systematic set of calculations as has been done here a self consistent table of cross-sections is obtained , which can then be more easily compared with experimental data from a variety of sources to check its accuracy both in the relative and absolute senses. In order to provide convenient access to this data some empirical formulae are derived,which provide good quality fits to the computed results.

6.1 INTRODUCTION

This chapter is concerned with cross section for the removal of inner shell electrons by electron impact. Inner shell cross sections are mainly used in three common methods of elemental microanalysises: electron-probe microanalysis (EPMA), Auger-electron spectroscopy (AES), and Electron energy loss spectroscopy (EELS).

Bethe (1930) has expressed the cross section, per atom, for ionization of the nl shell as:

$$\sigma_{nl} = \frac{\pi e^4}{E_{nl}} \frac{Z_{nl} b_{nl}}{E} \ln\left[\frac{c_{nl} E}{E_{nl}}\right] \qquad (6.1)$$

where E is the incident electron energy, E_{nl} is the binding energy of electrons in the nl shell, and Z_{nl} is the number of electrons in that shell. The terms b_{nl} and c_{nl} are referred to as the Bethe parameters and are expected to be approximately unity and in the range 1-4, respectively. When incident electron energy is greater than 50 keV the relativistic Bethe expression is:

$$\sigma_{nl} = \frac{\pi e^4}{\left(\frac{1}{2} m_0 \upsilon^2\right)} \frac{Z_{nl} b_{nl}}{E_{nl}} \left[\ln\left(\frac{c_{nl} m_0 \upsilon^2}{2E_{nl}}\right) - \ln(1-\beta^2) - \beta^2 \right] \qquad (6.2)$$

where β is the ratio of the electron velocity υ to the velocity of light .

In the review papers of Powell (1976; 1984a,b; 1991) whenever possible the experimental data or theoretical calculated data are fitted to obtained the Bethe parameters b_{nl} and c_{nl} . The Bethe Eq.6.1 and 6.2 provide a simple, convenient, and physically-based means for calculation of inner shell ionization cross section.

There are some other quantum-mechanical calculations of inner shell ionization cross sections (Powell, 1976). For example, Burhop (1940) computed K-shell cross sections for Ni, Ag, and Hg; and of L_1, L_2, and L_3 subshells for atomic Ag and Hg.

Burhop's formula has also been evaluated by Hink et al. (1969) for the K shell ionization cross section from Be, Al, and Ni. The cross section data of Burhop have been analyzed by Mott and Massey (1949), who obtained the Bethe parameters b_k~ 0.35, b_l~0.25 and c_k~c_l=2.42 if the contributions to σ_{nl} due to transitions to unoccupied discrete levels could be neglected. These data have been widely used for the calculation and the electron-probe microanalysis. However, a least-squares fit to the Burhop data, yielded substantially different values of b_{nl} and c_{nl} from those derived by Mott and Massey.

Arthurs and Moiseiwitsch (1958) have calculated an expression for K shell ionization using Moller's relativistic modification for Z < 30. Perlman (1960) extended their work to heavier atoms. Rudge and Schwartz (1966) have computed K shell and L_1 shell ionization cross sections for atomic hydrogen, He^+, and a fictitious hydrogenic ion with Z=128. McGuire (1971a, 1971b, 1974) has computed generalized oscillator strengths (Powell, 1976) for the various subshells of low-Z atoms from which he has derived the corresponding ionization cross sections, also calculated L_1, L_{23} and M_1-shell ionization cross sections for Z < 18. Manson (1972,1974) has calculated L_1 and L_{23}-shell ionization cross sections for Al using a model similar to McGuire's for incident energies of 2, 3, and 4 keV. Wallace, Berg, and Green (1973) have calculated generalized oscillator strengths for Ar and from which they derived cross sections for ionization of the L_1 and L_{23} subshells. Leapman, Rez, and Mayers (1980) have presented some calculations of cross sections for ionization of atomic K, L, and M shells up to some tens or hundreds of eV by fast electrons. Their calculation of the GOS follows closely that of Manson and McGuire, who used a Hartree-Slater central field model, and the method of calculation of the GOS matrix elements is the same with Manson's. Rez (1984) and Batchelor et al. (1988) has calculated the total cross-sections for ionization of K, L and M shells in

various atoms using first-order perturbation theory and Hartree-Slater wave functions. For K shells, the hydrogenic wave functions has been used. The calculation energy is up to 100 keV.

Another quantum based method is hydrogenic model. Egerton (1975, 1979, and 1986) has effectively used the hydrogenic approximation for partial ionization cross-sections for electron energy loss spectroscopy for K and L shells for low atomic number elements.

The most successful classical theory is that of Gryzinski (1965). Gryzinski's formula is very simple and general, so it is widely used in the Monte Carlo simulation for microanalysis. Gryzinski's formula can be expressed as:

$$\sigma_{nl} = 6.51\times10^{10}\frac{Z_{nl}}{E_{nl}^2}\cdot\frac{1}{U}\left(\frac{U-1}{U+1}\right)^{\frac{3}{2}}\left\{1+\frac{2}{3}\left(1-\frac{1}{2U}\right)\ln[2.7+(U-1)^{\frac{1}{2}}]\right\} \quad (6.3)$$

where σ_{nl} is in Barns (1Barn = 10^{-24} cm^2), E_{nl} is in eV, and $U=E/E_{nl}$.

6.2 CALCULATION PROCEDURE

The theory for calculation of inner shell ionization cross sections here is close to that of Manson (1972), Leapman et al. (1980), and Rez (1984) , and assumes the elements to be in atomic form and treated on the basis of a single electron wave function undergoing a transition to the continuum. The total cross sections for ionization of K, L, and M shells for all element atoms have been calculated using first-order perturbation theory (the first

Born approximation) and Hartree-Slater wave functions (except for H,for which the hydrogen wave function has been used). The theory has briefly been discussed in the Chapter 3. The initial state is a one-electron Herman-Skillman wave function, a solution of the radial Schrodinger equation with the self-consistent atomic potential including a spherically averaged exchange potential and a correlation potential. The final states are the results by solving the radial Schrodinger equation with the same central field for the continum positive energies. The continuum wave function $\Psi_{el'}(r)$ is normalized in energy scale such that $\Psi_{el'}(r) = \pi^{-1/2}\varepsilon^{-1/4} r^{-1} \sin[\varepsilon^{1/2}r - 1/2l'\pi + \delta'_{l'}(\varepsilon)]$ at infinity where $\delta'_{l'}(\varepsilon)$ is a function of ε (Manson, 1972) . (Exchange between the scattered electron and the atomic electron is not taken into account, however, this effect can be negligible except at very high energy losses and scattering angles (Leapman et al., 1980). The GOS then is obtained using Eq.3.17, and hence the Bethe differential cross section using Eq.3.16. To calculate the total electron impact ionization cross section the differential cross section has to be integrated over both E, the transferred energy, and **q**, the momentum transferred. The lowest energy integration limit is the binding energy of the K, L or M shells and the upper limit is the total kinetic energy of the incident electron. The **q** (momentum transfer) limits of integration are functions of energy transfer E and are determined by considerations of the conservation of energy and momentum discussed in the Chapter 3 (Eqs. 3.20, 3.21), and q_{min} and q_{max} are calculated from Eq.3.22. The integral intervals of E and **q** strongly influence the accuracy of the result. To minimize computer time while maximizing accuracy the program was designed to test the effect of various incremental changes ΔE and Δq in the numerical integration procedure and then to select the largest one which maintained the desired level of precision. Figure 6.1 shows how the apparent variation of the cross-section with overvoltage ratio, in this case for the aluminum K-shell, depends on the exact size of the integration steps. With coarse steps the data has the form shown as a dotted line, while with the optimally chosen step size the cross-section follows the

continuous line. The non-optimal data rises more rapidly than the optimized integration, and overshoots the correct peak value. Although the error is not severe at high overvoltage ratios it is significant for $U < 5$.

The computer code to implement these computations was written in Microsoft FORTRAN and run on 20Mhz IBM PS2/70 personal computers equipped with a high speed maths coprocessor chip (CYREX 80387). The computational time is typically 24 hours for just one shell (K, L, or M) of one element under these conditions. Using a smaller integration step than the optimal value will increase the time required for the computation by from 20 to 100% although the precision of the numerical integration is only improved by a few percent at most.

6.3 RESULTS AND DISCUSSIONS

6.3.1 General characteristics of the results

Some of the calculation data for K, L , and M shells are shown in Appendix C. The total data set computed, i.e. K, L_1, L_{23}, M_1, M_{23}, and M_{45} shells for 92 elements and for 30 to 50 U values per shell, comprises over 10,000 individual cross-section values. It is therefore not easy to provide a comprehensive overview of the results. However some general trends can be identified. Figure 6.2 shows graphically how the K-shell ionization cross section σ, given in units of barns, varies with the overvoltage ratio U for two light elements (carbon and silicon), a transition element (copper), and a heavy element (silver). These elements were chosen to illustrate the general features of the results across the periodic table . The behavior of all other elements for which computations were made follows the same trend. The profile of the cross-section variation is generically similar to

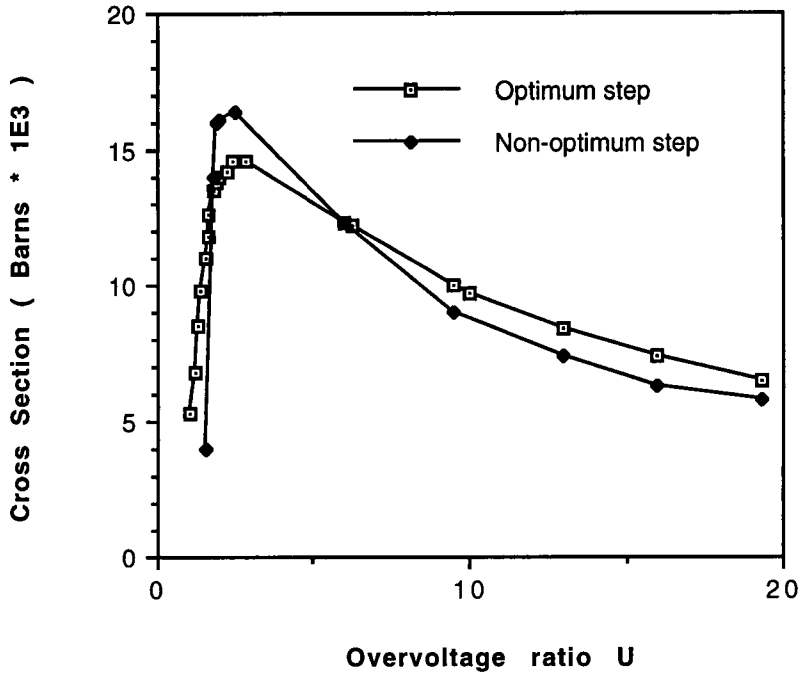


Figure 6.1 Comparison of the optimal and non-optimal steps data.

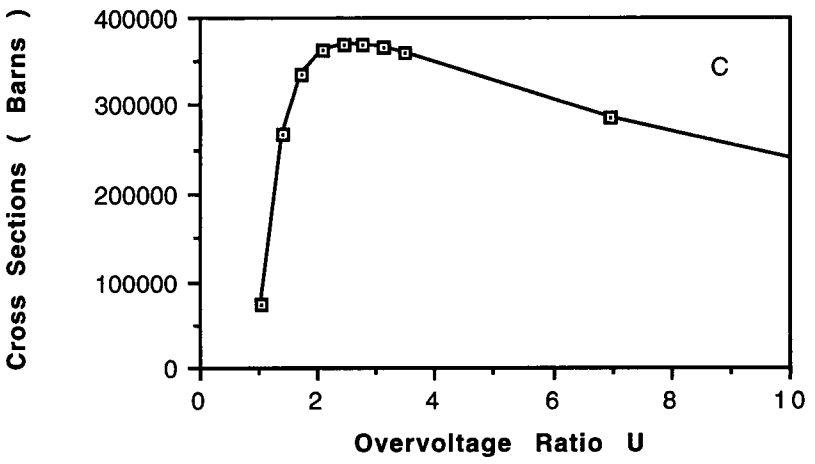


Figure 6.2a Calculated K shell cross section for carbon.

that expected from the classical Bethe expression of equation Eq.6.1, rising rapidly after the ionization onset at U=1, reaching a broad maximum and then falling smoothly away. For the standard Bethe form of the ionization cross section (Eq.6.1) the peak in the cross-section occurs for U ~ 2.72, independent of the element. For this more detailed computation that result is no longer true and, as shown in Figure 3, the overvoltage at which the peak cross-section occurs varies, being close to the expected value of U=2.7

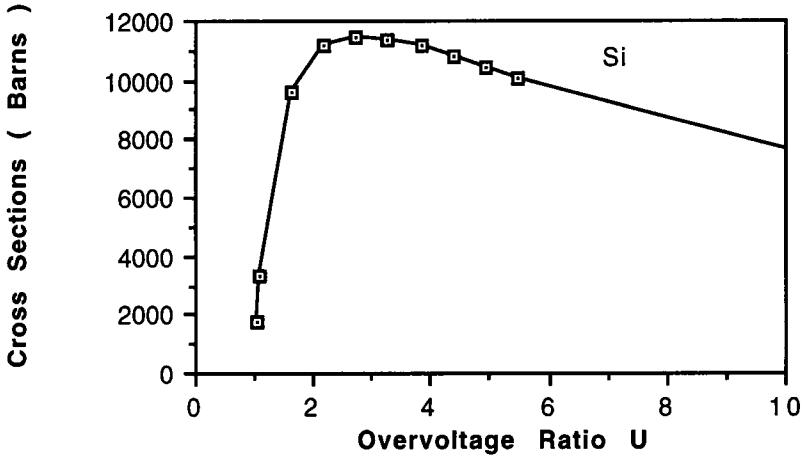


Figure 6.2b Calculated K shell cross section for silicon.

for low atomic number materials, but rising steadily to values in excess of U=4 for an atomic number of around 40. The peak is not visible in the plotted data for silver because the energy required exceeded the 100 keV upper limit set for these computations.Figure 6.4 shows the cross-section variation for the L_{23} shells of the same elements. Again the cross-section has a similar generic form, but the peak is now somewhat flatter and the

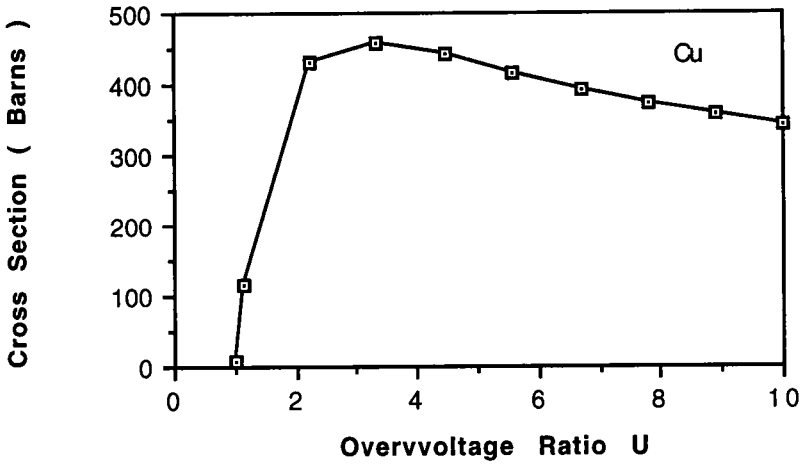


Figure 6.2c Calculated K shell cross section for copper.

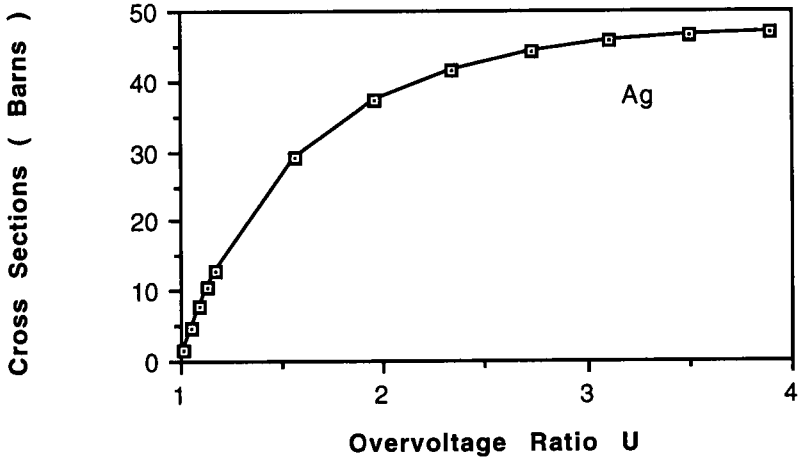


Figure 6.2d Calculated K shell cross section for silver.

subsequent reduction in the cross-section at high overvoltage is less pronounced. The peak itself occurs at an overvoltage of about 4 to 4.5, higher than the K-shellvalue, and in agreement with the limited experimental data available (Mayer and Vreking, 1980).

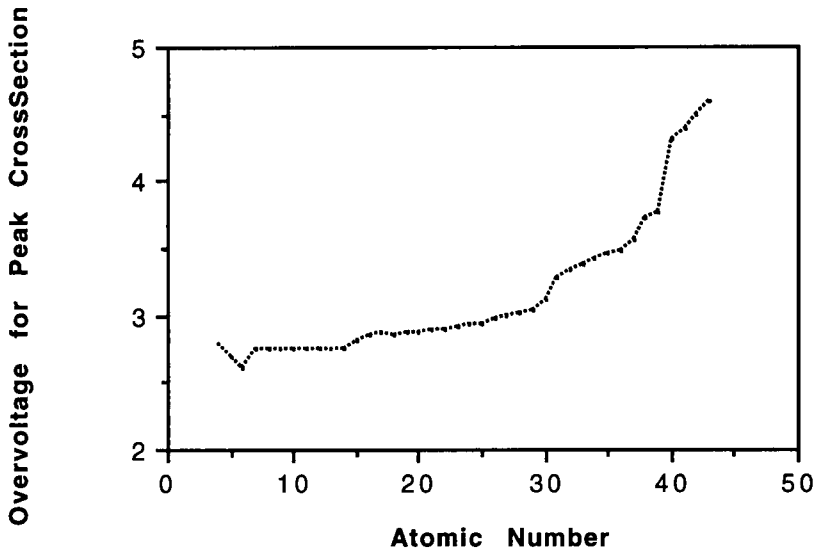


Figure 6.3 The overvoltage of cross section peak position.

Finally, Figure 6.5 shows M_{45} shell cross-sections for copper, silver and gold. In this case the data shows a very pronounced peak, occuring at around an overvoltage of around 5 to 6, then followed by a decay as U is increased.

6.3.2 Comparison with other models

Many other models of the inner shell ionization process are in current use, varying from rigorous first principles computations to empirical fits to existing data. Our computed data set has been compared to values predicted from other selected models. For the K-shell data we have employed:

(a) The Bethe expression of Eq.6.1 using the values for the constants b_{nl} and c_{nl} suggested by Powell (1972, 1976, 1985a,b; 1989; 1991) .

(b) The empirical expression derived by Casnati et al.(1982) as a fit to the best available experimental data in the low overvoltage regime and

(c) The 'classical' Gryzinski formulation (1965) of the ionization cross section, widely used for high electron energies (> 50keV).

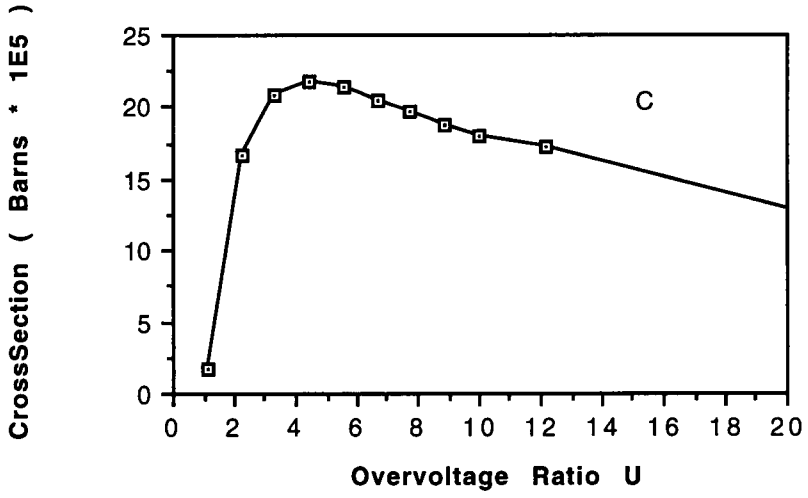


Figure 6.4a The calculated L_{23} cross sections for carbon.

While many other formulations are also in use those listed above cover a significant range of basic assumptions and expected regions of applicability and have been found in practice to be of value in quantitative work, and thus are suitable for testing the predictions of the computed data. Apart from the Bethe-Powell cross-section no attempt has been made to modify the constants in any of these models in order to improve their performance.

Figure 6.6 shows the comparison of these data for the aluminum K-shell. It is immediately clear that the various models generate a wide divergence of values, the maximum deviation being about $\pm$25%. As will be discussed later the reason why this is considered to be an acceptable state of affairs is that the spread in measured cross section data is much larger and as a result it is not possible to choose one model over another

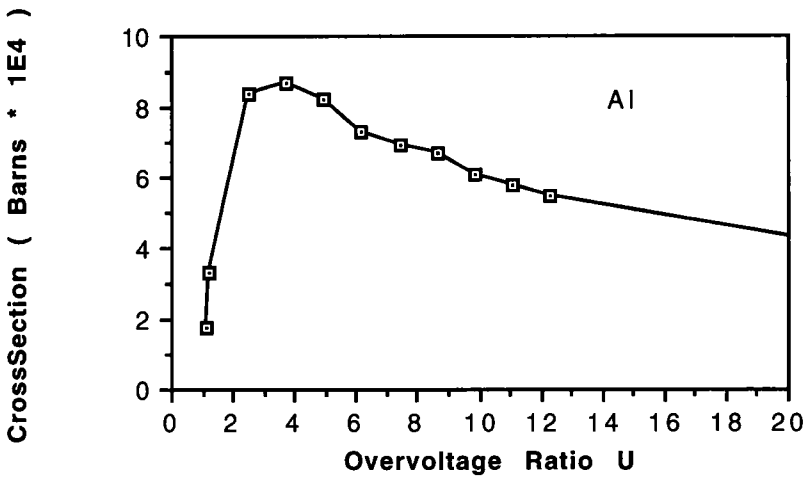


Figure 6.4b The calculated L_{23} cross sections for aluminum.

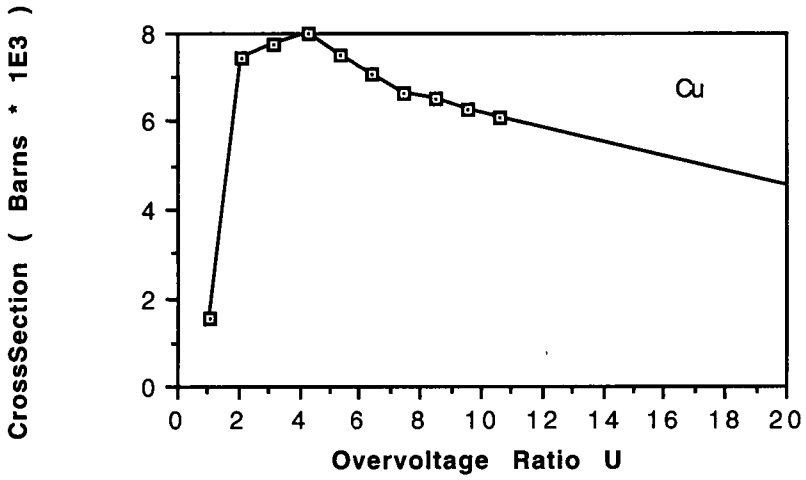


Figure 6.4c The calculated L_{23} cross sections for copper.

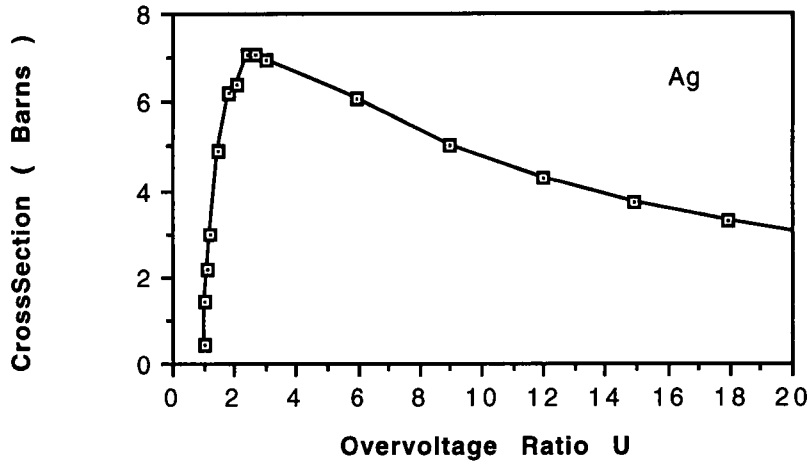


Figure 6.4d The calculated L23 cross sections for silver.

on the basis of its agreement with experiment. In this particular example the calculation described here is the highest of the four values at all energies; but for other elements both the relative order and the level of agreement also vary. It is also noteworthy that, for overvoltages in excess of about 4, the shape of each of the predictions is very similar implying that the different models have about a constant ratio to each other. In the low overvoltage region the discrepancies are more marked, as would be anticipated, since neither the Bethe nor the Gryzinski models are valid for U<3.

Figure 6.7 shows the corresponding comparison for the Al L_{23} line, the other models in this case being

(a) the hydrogenic SIGMAL model of Egerton (1975, 1986)

(b) the Gryzinski formula (1965) and

(c) the Bethe expression with the coefficients given by Powell (1985).

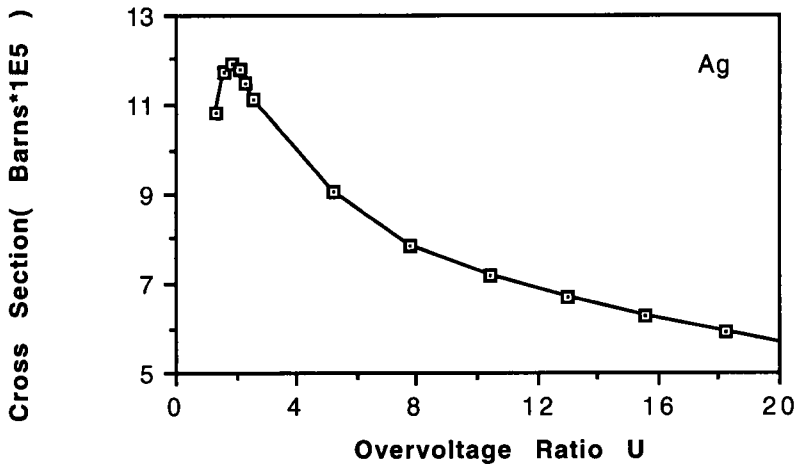


Figure 6.5a The calculated M45 cross sections for silver.

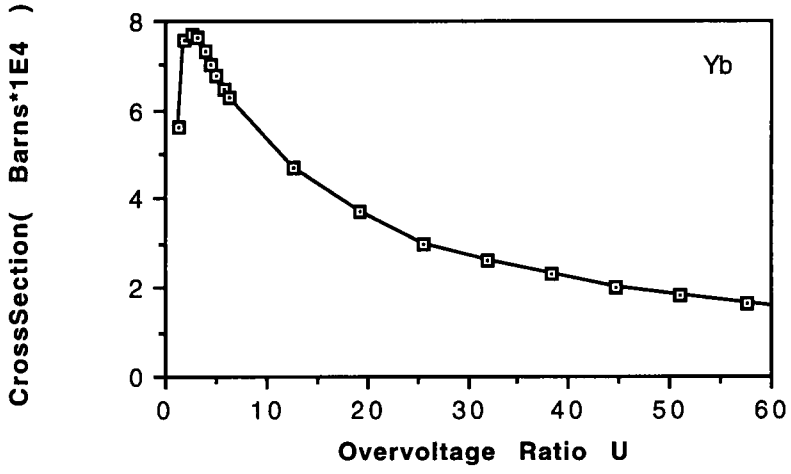


Figure 6.5b The calculated M45 cross sections for ytterbium.

In this example the variation between models at low overvoltages is even more marked reaching a peak of about 2 to 1, while a higher overvoltages the spread in the data smaller with all the models showing a similar trend.Again the relative ordering of the various computations varies from one element to another although the Brown model

usually predicts the highest cross-sectional value.

In the case of M-shells, Figure 6.8, this computation has been compared to

(a) the Gryzinski model (1965)

(b) the empirical fit of Schreiber and Wimms (1981) and

(c) the model of Lotz (1970).

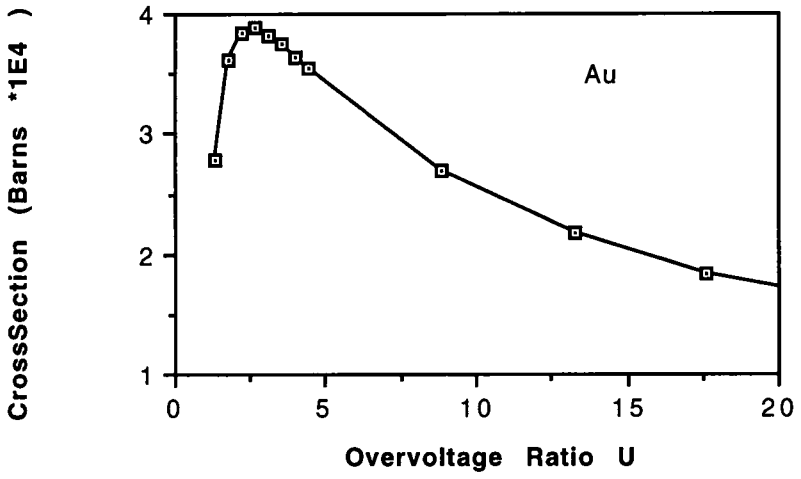


Fig.6.5c The calculated M45 cross sections for gold.

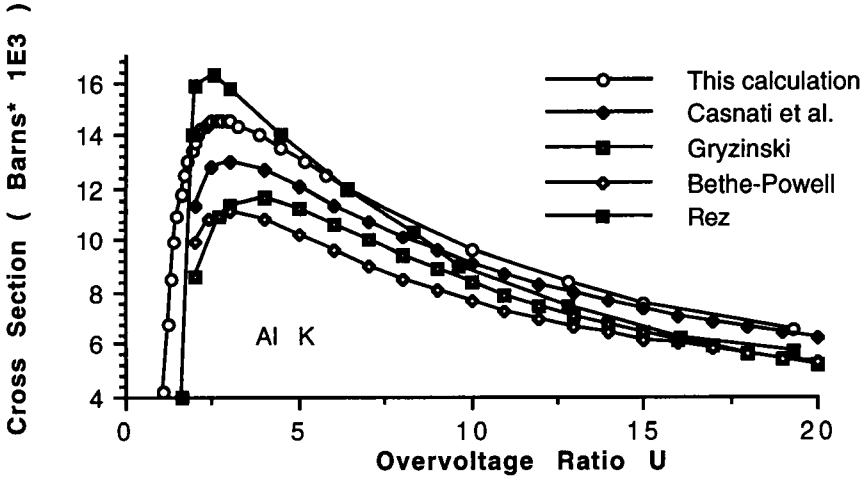


Figure 6.6 Comparison of our data with other calculated data for Al K shell.

The Schreiber and Wimms (1981) model is significantly higher (four times) than any of the other models for all of the elements computed. However the level of agreement between the other models is also quite poor until a high overvoltage is achieved. This reflects the reality that there is little or no quality experimental data with which to work.

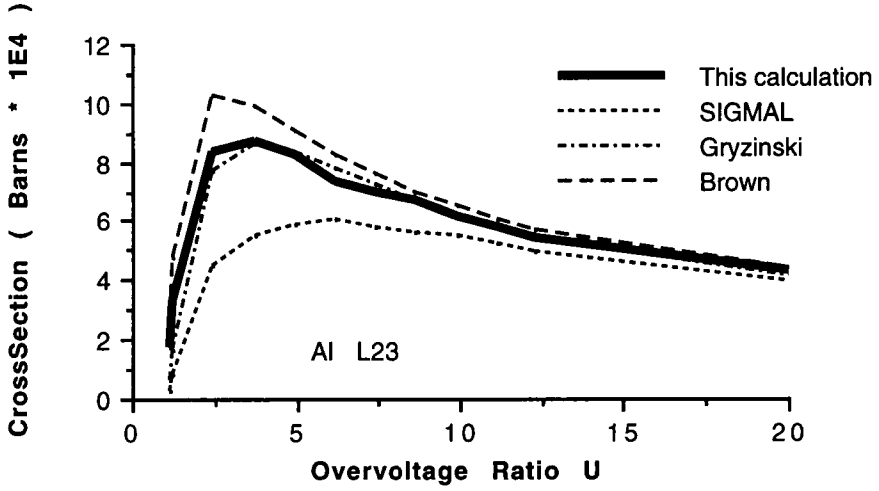


Figure 6.7 Comparison of our data with other calculated data for Al L_{23} shell.

6.3.3 Comparison with experiment

Theoretical data can only be validated by comparison with measured values. However care must be applied in making any such comparison. Figure 6.9 shows our computation for the K-shell of aluminum compared with the experimental data quoted by Powell (1976). The quality of the agreement is seen to be good with the absolute cross-section values being within $\pm$ 5% of the measured values over the whole overvoltage range. Unfortunately this may be an over optimistic result because different sets of experimental results show alarmingly wide variations. The case for which the most data is available is the K-shell of carbon and, as shown in Figure 6.10, the deviation between the lowest and

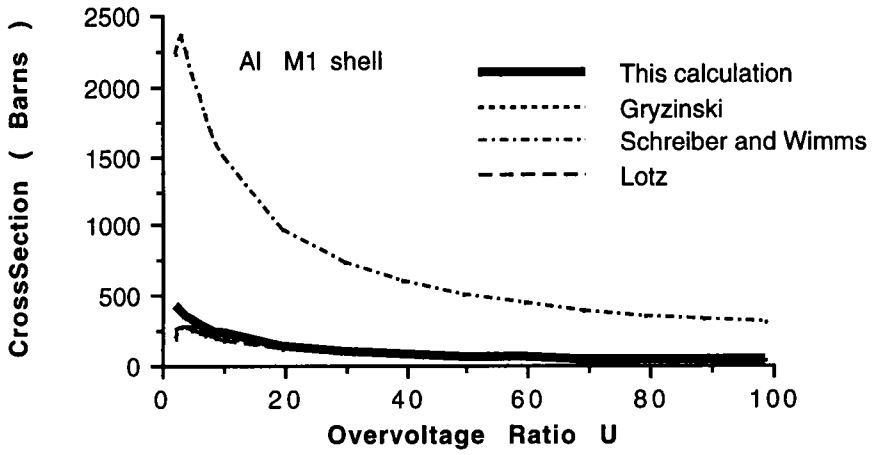


Figure 6.8 Comparison of our data with other calculated data for Al M_1 shell.

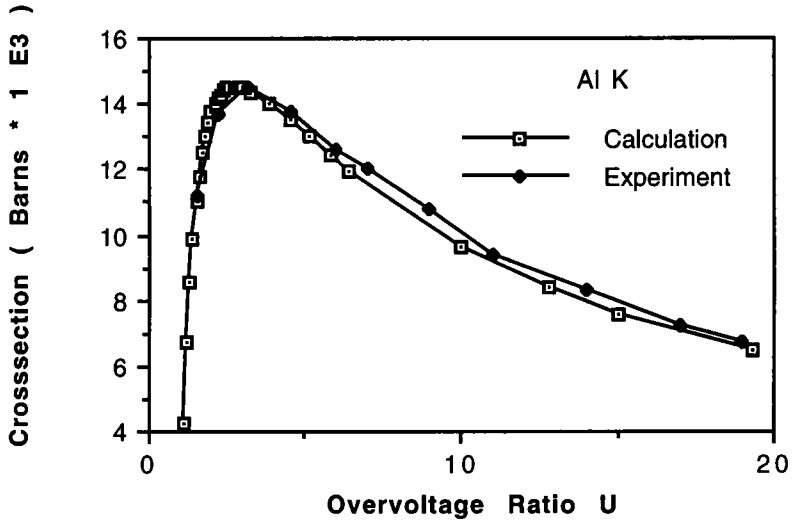


Figure 6.9 Comparison of our data with experimental data for Al K shell.

highest experimental data points at any given overvoltage can be as high as 40 %. With such a spread of values it is readily possible to find an experimental data set which agree well with almost any computation. Since the carbon values represent the best available

case it must be assumed that , for those elements and for the L- and M-shells where less data is available, a comparable lack of precision is inevitable and so no particular credence can be attached to any one set of experimental data.

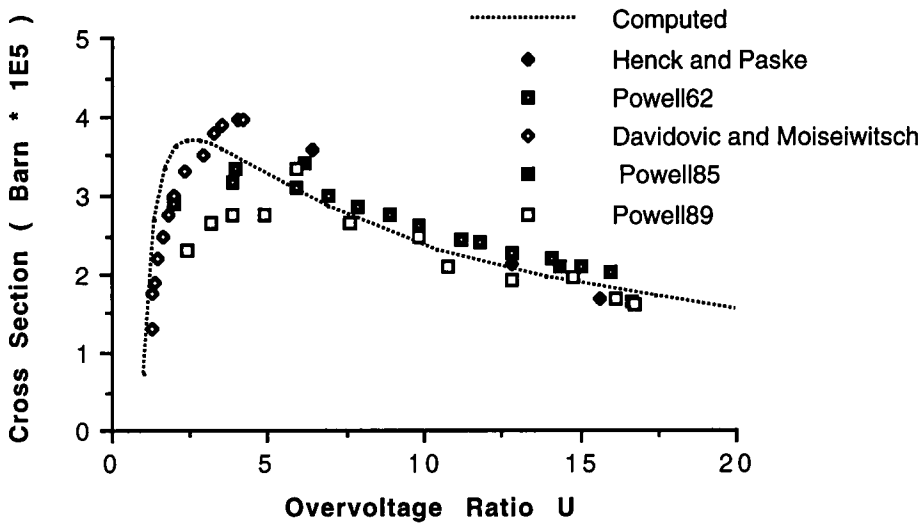


Figure 6.10 Comparison of our data with computed and measured data for C K shell.

As a consequence it is very difficult at the moment to use experimental data to test theoretical models. This is a most unsatisfactory situation that hampers further progress and we are currently attempting to eliminate this problem in some way. The root cause of the experimental difficulty is that the details of the electron interaction with the target element must be very carefully accounted for if a correct cross-section value is to be obtained, and even with the use of sophisticated Monte Carlo models this is hard to do for a solid specimen, The likely solutions would seem to be the use of gas target, or to borrow suitably corrected data from proton excited X-ray fluorescence where the charged particle interaction with the solid is much simpler and more predictable.

6.3.4 The Fano plot

If the Bethe expression of Eq.6.1 were satisfied then a plot of ($\sigma_{nl} E_{nl}^2 U$) against log U would be a straight line-the so-called Fano plot. The slope and offset of the line then represent the scaling parameters of the expression. Even in cases where the Bethe relation is not expected to apply a Fano plot is a useful tool, firstly because the degree of deviation from linearity provides a measure of how 'Bethe-like' the cross-section is, and secondly because all the data for one shell should fall on or close to the same line and hence any discrepancy is a sign that there might be a computational or systematic error. Figure 6.11 shows the Fano plot for a selection of K-shell data in the overvoltage range 1 to about 50 (where F(U) is $\log_e U$). It can be seen that for the ten elements selected the data all falls on a common line which is very closely linear up to F(U)< 4.5. Thus even in the near-threshold region our computed cross-sections have a ' Bethe-like' characteristic. Figures 6.12a and b show the corresponding Fano plots for L- and M-shells. The L-shell data is still linear and tightly confined about a single line, but the M-shell data shows both a deviation from linearity and a significant scatter of data points, especially at high overvoltages. The M-shell cross sections are therefore less Bethe-like, and the great variability in the cross section values when compared in this way suggest that at high overvoltages the data may be subject to some sources of error. This is understandable because the M-shell electrons are, as noted above, much less strongly bound than the corresponding K- and L- shell electrons. Consequently other effects such as collective excitations may become significant especially at high overvoltages and until better experimental data is available for the M-shells it may not be possible to fully understand and correct for this behavior.

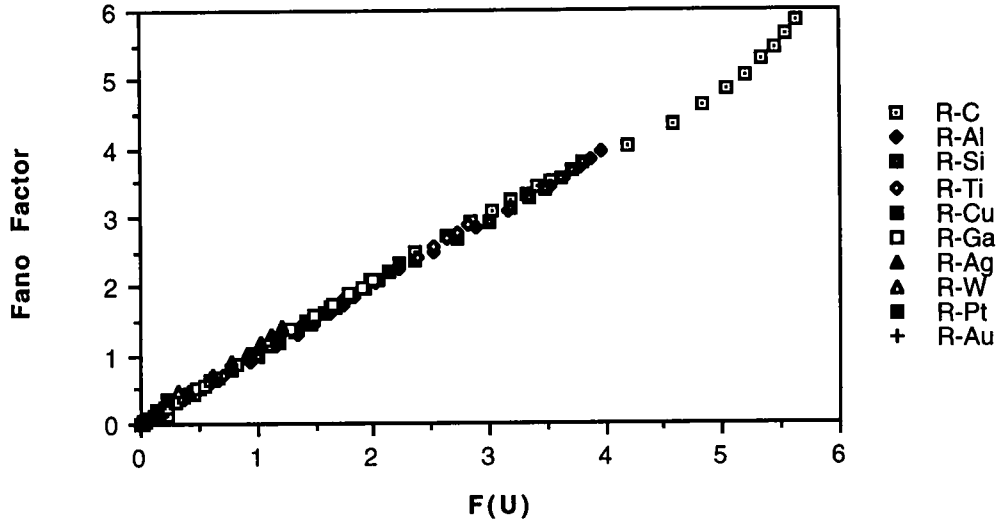


Figure 6.11 Fano plot of K shell data for selected elements.

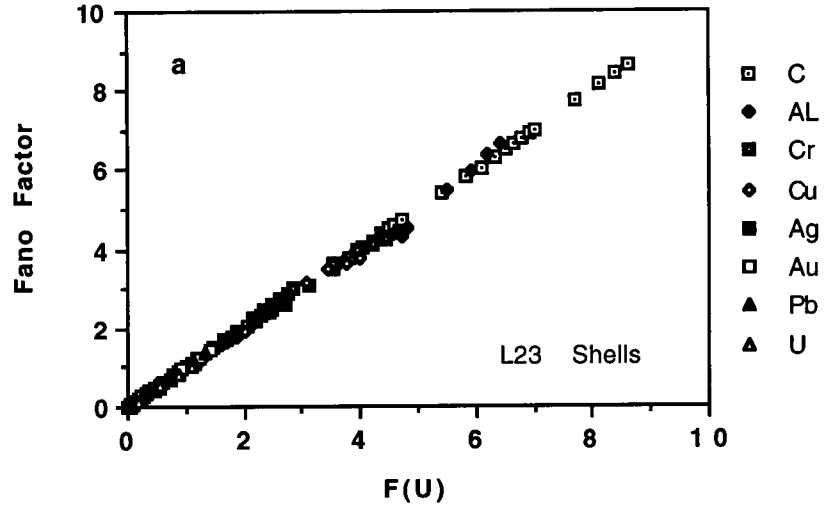


Figure 6.12a : Fano plot of L shell data for selected elements.

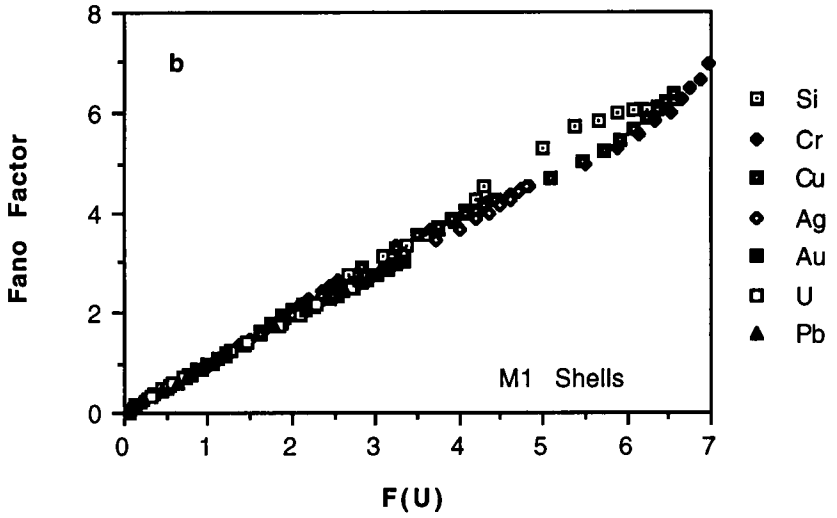


Figure 6.12b Fano plot of M shell data for selected elements.

However the fact that all three shells show an excellently linear Fano behavior in the overvoltage range 1 to 5, corresponding to the typical experimental overvoltage that would be used, means that a compact and convenient model of the data sets can be made by using a modified Bethe-like equation. This is not to imply that the original Bethe equation is correct in this overvoltage regime, but rather that the mathematical form of the Bethe equation is an accurate parametric representation of the data. For K-shells the equation has the form:

$$\sigma = 65100 \cdot n \cdot B \frac{\ln(U+U1)}{(U+U1)^{x} E_k^2} \qquad \text{(Barns)} \qquad (6.4)$$

where $U=E_0/E_k$, n is the number of K shell electrons and U1, X and B are fitted parameters. Figure 6.13 show these parameters vary as a function of atomic number. The use of Eq.6.4 predicts values which are within 3% of the directly values for the whole range of overvoltage values.

When incident electron energy is greater than 50 keV the relativistic empirical expression for K-shell is:

$$\sigma=65100\cdot n\cdot B\,\frac{Ln(U+U1)-Ln(1-\beta^2)-\beta^2}{U^{xxx}E_k^2} \quad \text{(Barns)} \quad (6.5)$$

where

$$U= T / E_k$$

$$T= 0.5\times 511\left(1-\left(\frac{511}{E_0+511}\right)^2\right)$$

$$\beta^2=1-\frac{1}{(1+E_0/511)^2}$$

Similarly for L-shells the fitting equation is written in the form:

$$\sigma=65100\cdot n\cdot B\cdot\left(1-\frac{x8}{E_0^{x9}}\right)\frac{Ln(U+U1)}{U^{x}E_{L_1}^2} \quad \text{(Barns)} \quad (6.6a)$$

$$\sigma=65100\cdot n\cdot B\cdot\left(1-\frac{x8}{E_0^{x9}}\right)\frac{Ln(U+U1)}{(U+U1)^{x}E_L^2} \quad \text{(Barns)} \quad (6.6b)$$

where Eq.6.6a is for the L_1 shell , and Eq.6.6b is for the L_{23} shell; n is the number of L_1 or L_{23} electrons, E_{L1}, E_L are the L_1, and L_{23} ionization threshold energy in keV respectively; E_0 is the incident beam energy in keV, and B, X, U1, X8 and X9 are parameters. The variation of these as a function of atomic number is shown in Figure 6.14.

When incident electron energy is greater than 50 keV the relativistic empirical expression for L-shell is:

$$\sigma=65100\cdot n\cdot B\left(1-\frac{x8}{E_0^{x9}}\right)\frac{Ln(U+U1)-Ln(1-\beta^2)-\beta^2}{U^{xxx}E_L^2} \quad \text{(Barns)} \quad (6.7)$$

where

$$T=0.5\times 511\left(1-\left(\frac{511}{E_0+511}\right)^2\right)$$

$$U=T/E_L$$

$$\beta^2=1-\frac{1}{(1+E_0/511)^2}$$

where E_L represents L shell ionization energies (L_1, or L_{23}).

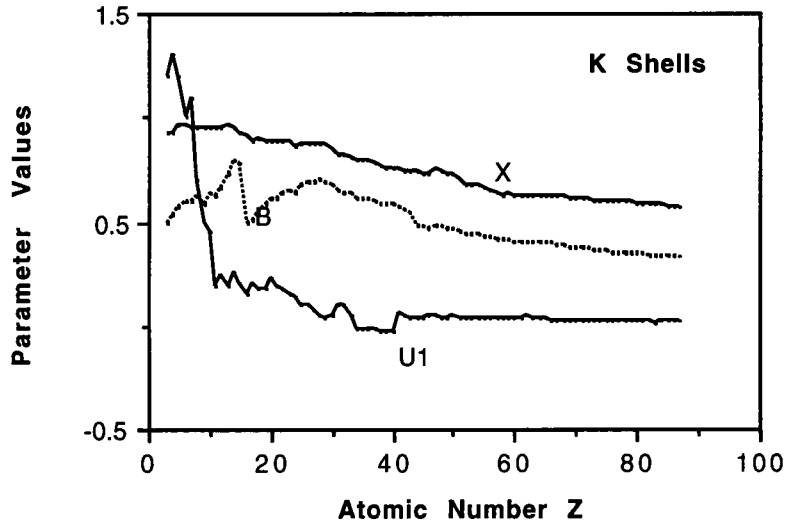


Figure 6.13 The parameters for empirical formula of K shells.

A similar analysis applies for the M-shell data . For M_1 shell the expression is:

$$\sigma=65100\cdot n\cdot B\cdot\left(1-\frac{x8}{E_0^{x9}}\right)\cdot\frac{Ln(U+UUU)}{U^{xxx}E_m^2} \quad \text{(Barns)} \quad (6.8)$$

The relativistic empirical expression for M_1 -shell is:

$$\sigma=65100\cdot n\cdot B\left(1-\frac{x8}{E_0^{x9}}\right)\frac{Ln(U+U1)-Ln(1-\beta^2)-\beta^2}{U^{xxx}E_m^2} \quad \text{(Barns)} \quad (6.9)$$

where

$$U= T / E_0$$

$$T= 0.5\times 511\left(1-\left(\frac{511}{E_0+511}\right)^2\right)$$

$$\beta^2=1-\frac{1}{(1+E_0/511)^2}$$

For M_{23} or M_{45} shell the expression is:

$$\sigma=65100\cdot n\cdot B\cdot\left(1-\frac{x8}{E_0^{x9}}\right)\cdot\frac{xx\cdot Ln(U+U1)}{U^{xxx}E_m^2} \quad \text{(Barns)} \quad (6.10)$$

The relativistic empirical expression for M_{23} or M_{45} -shell is:

$$\sigma=65100\cdot n\cdot B\left(1-\frac{x8}{E_0^{x9}}\right)\frac{xx\cdot Ln(U+U1)-Ln(1-\beta^2)-\beta^2}{U^{xxx}E_m^2} \quad \text{(Barns)} \quad (6.11)$$

where

$$U= T / E_0$$

$$T= 0.5\times 511\left(1-\left(\frac{511}{E_0+511}\right)^2\right)$$

$$\beta^2=1-\frac{1}{(1+E_0/511)^2}$$

n is the number of M_{23} or M_{45} shells, E_m is the ionization energy of M_{23} or M_{45} shells, xx, xxx, U1, B, x8 and x9 are parameters.

6.4 CONCLUSIONS

A complete set of K-, L-, and M- inner-shell X-ray ionizations has been computed from first principles using a detailed quantum mechanical method. Special attention has been given to the need to make the calculation accurate in the low overvoltage regime close

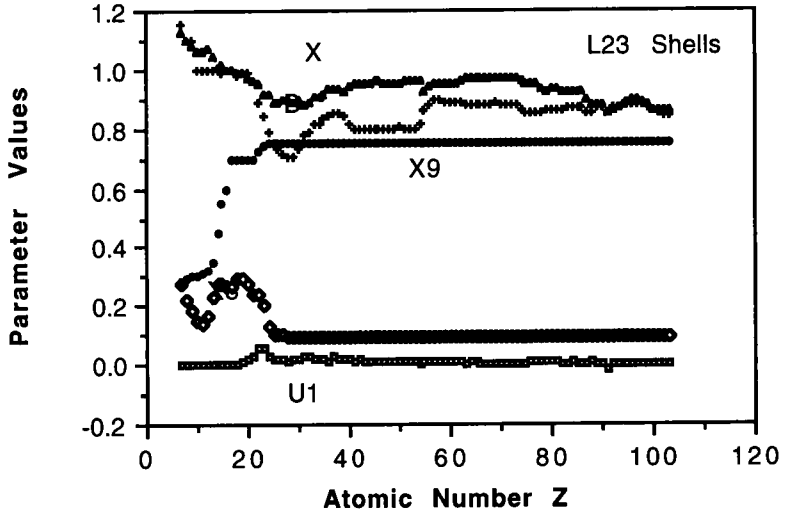


Figure 6.14 The parameters for empirical formula of L shells.

to the ionization threshold where previous models have failed. The majority of the data-set can be represented by a modified Bethe equation with fitted constants. Tests of the data show it to be both self-consistent and accurate when compared to existing models and experimental data over a wide range of elements and conditions. Work is now in progress

to produce more accurate experimental measurements so that these computations can be further validated and refined. We believe that this set of cross-section values, especially in the overvoltage range below U=4 represents better and more comprehensive set of values so far produced and should be of a benefit in microanalysis.

BIBLIOGRAPHY

BIBLIOGRAPHY

Ahn C C and Rez P(1985) Inner shell edge profiles in electron energy loss spectroscopy. Ultramicroscopy 17,105-116.

Amelio, G. F. (1970) Theory for the Energy Distribution of Secondary Electrons, J. of Vac.Sci. and Technol. 7,593-604.

Arthurs, A. M., and Moiseiwitsch, B. L. (1958) Proc. R. Soc. London A 247, 550.

Ashcroft, N.W. and Sturm, K. (1971) Interband Absorption and the Optical Properties of Polyvalent Metals. Phys. Rev.,B, 3, 1898-1910.

Ashley, J. C. and Ritchie, R. H.(1970)Double-Plasmon Excitation in a Free-Electron Gas. Phys.stat.sol.38,425-434.

Ashley, J. C., Tung, C. J., and Ritchie, R. H.(1975)IEEE Trans. Nucl. Sci. NS-22,2533.

Ashley, J. C., Tung, C. J., and Ritchie, R. H. and Anderson, V. E.(1976a)IEEE Trans. Nucl. Sci. NS-23,1833.

Ashley, J. C., Tung, C. J., and Ritchie, R. H.(1976b)Rome Air Development Center Report RADC-TR-76-350.

Ashley, J. C., Tung, C. J., and Ritchie, R. H.(1978)IEEE Trans. Nucl. Sci. NS-25,1566.

Ashley, J. C., Tung, C. J., and Ritchie, R. H.(1979) Electron inelastic mean free paths and energy losses in solids. I aluminum metal.Surf. Sci., 81, 409-426.

Ashley, J. C.(1980) IEEE Trans. Nucl. Sci. NS-27,1454.

Ashley, J. C. and Anderson, V. E.(1981) Interaction of low-energy electrons with silicon dioxide Journal of Electron Spectroscopy and Related Phenomena. 24,127-148.

Ashley, J. C.(1982) Rad. REs., 89, 25-31.

Ashley, J. C. (1988a) Interaction of low-energy electrons with condensed matter: stopping powers and inelastic mean free paths from opticaldata. J.Elect.Spect.

Ashley, J. C. (1988b) Interaction of low-energy electrons with the electron beam resist poly(butene-1-sulfone). J. App. Phys. 63,4620-4625.

Austin, L. and Starke, H. (1902) Ueber die Reflexion der Kathodenstrahlen und eine damit verbundene neue Erscheinung Secundarer Emission. Ann. Phys. (Leipzig) 9,271.

Baroody, E.M. (1950) A Theory of Secondary Electron Emission from Metals. Phys. Rev., 78, 780-787.

Batchelor, D. R., Rez, P., Fathers, D. J. , and Venables, J. A. (1988) Surf. Interface Anal. 13, 193.

Batson, P. E.(1978)Digital data acquisition of electron energy loss intensities. Proc. Specialist Workshop in Analytical Electron Microscopy. Ithaca, New York (Cornell University: Materials Science Center) Report 3082, 31-39, Ultramicroscopy 3, 367-371.

Batson, P. E. and Craven, A. J.(1979)Phys. Rev. Lett. 42,893.

Batson, P. E. and Silcox, J. (1983) Experimental energy-loss function, Im[-1/e(q,w)], for aluminum. Phys. Rev. B, 27,5224-5239.

Berger, M.J. and Seltzer, S.M. (1982) Stopping powers and ranges of electrons and positrons. NBSIR 82-2550.(Nat. Bur. of Standards, Washington DC).

Berger, M.J. and Seltzer, S.M. (1964)Tables of energy losses and ranges of electrons and positrons.Natl.Acad.Sci.Natl.Res.Council Publ.1133, pp205-268 (Washington D.C.,1964).

Berger, M.J.(1963) in Methods in Computational Physics, Vol. 1 (Eds. B. Adler, S . Fernbach, and M. Rotenberg), Academic Press : New York, P.135.

Bethe, H. and Ashkin , J.(1953) Passage of radiations through matter. In 'Experimental Nuclear Physics'(ed E Segre), Wiley, New York, 1, 166.

Bethe, H. (1930) Theoyy of passage of swift corpuscular rays through matter, Ann. Phys.5, 235.

Bethe, H.A. (1941) On the theory of secondary emission. Phys. Rev., 59, p.940.

Blackson, John, Luo, Suichu and Joy, David C.(1993)A new method for determining sample thickness A comparison to experimental results. Proc. 51th Annual Meeting of the Microscopy Society of America. P.582.

Bindi ,R., Lanteri, H. and Rostaing, P. (1980 a) Application of the Boltzmann eguation to Secondary electron emission from copper and gold. J. Phys. D: Appl. Phys., 13,461-70.

Bindi, R., Lanteri ,H., Rostaing, P. and Keller, P. (1980 b) Theoretical efficiency of back- scattered electrons in secondary electron emission from aluminium. J. Phys. D: Appl. Phys., 13 , 2351-2361.

Bindi, R., Lanteri, H. and Rostaing, P. (1980 c) A new approach and resolution method of the Boltzmann equation applied to secondary electron emission, by reflection from polycrystalline aluminium. J. Phys. 13, 267-280.

Bindi, R. (1978) Contribution a L'etude de L'emission electronique secondaire de cibles metalliques polycristallines, These d'Etat-Universite de Nice, France.

Bishop, H. E. (1965) Proc. Phys. Soc. 85, 855.

Blackson, John, Luo, Suichu and Joy, David C.(1993)A new method for determining sample thickness A comparison to experimental results. Proc. 51th Annual Meeting of the Microscopy Society of America. P.582.

Boersch,H., Geiger, J. an Hellwig,H.(1962)Steigerung der Auflosung bei der Electronen-Energieanalyse . Phys. Lett. 3, 64-66.

Bohr, H.(1948)Kgl. Danske Videnskab. Selskab, Mat.-Fys. Medd. 18, No.8.

Böngeler R, Golla U, Kässens M, Reimer L, Schendler B, Senkel R, Spranck M, 1993, Scanning, 15,1

Bronshtein, I.M., Fraiman, B.S. (1961) Inelastic Scattering of electrons and secondary electron emission from certain metals and semiconductors, Sov.Phys. Solid State, 3,1188-1196.

Bronshtein, I.M. and Denisov, S.S.(1967) Secondary electron emission of aluminum

and nickel for obliquely incident primary electrons. Sov. Phys. Solid State.9, 731-732.

Brown D B(1974)Cross sections for ionization of K and L shells by electron. Handbook of spectroscopy.Cleveland,CRC Press.

Browning, R.(1991)Appl.Phys.Lett. 58,2845.

Browning,R., Eimori, T., Traut, E.,P. , Chui , B.and Pease, R. F. W. (1991) J. Vac. Sci Technol. B9,3578.

Browning, R., Li, T. Z., Chui, B., Ye, Jun, Pease, R. F., Czyzewski , Z. and Joy, D.C. (1993)Empirical Forms for the Electron/Atom Elastic Scattering Cross Sections from 0.1-30keV. (unpublished).

Bruining H, and De Boer J M, (1938), Physica **V**, 17.

Burge, R. E. and Misell, D. L. (1968) Electron energy loss spectra for evaporated carbon films. Phil. Mag. 18, 251-259.

Burge, R. E. and Misell, D. L. (1969) Convolution effects in electron energy-loss spectra recorded by electron transmission. J. Phys. C 2, 1397-1404.

Burhop, E. H. S. (1940) Proc. Camb. Philos. Soc. 36,43.

Buseck, P. R., Cowley, J. M. and Eyring, L. (1992) High - Resolution Transmission Electron Microscopy and Associated Techniques. Eds., Buseck, P. R., Cowley, J. M. and Eyring, L. , New York Qxford Oxford University Press.

Cailler, M.and Ganachaud,J. P. (1972) Quelques aspects theoriques de L'emission electronique secondaire du cuivre produit par bombardement d'electrons de faible energie. J. Physique, 33, 903-13.

Casnati, E., Tartari, A., and Baraldi, C. (1982) J. Phys. B15, 155.

Castaining, R. and Henry, L. (1964)J. Microscopie 3, 133.

Castaining, R., Hili, Ali EL, and Henry, L. (1965)Computes Rendus. Hebd. Seanc. Acad. Sci., Paris, 261, 3399.

Castaining, R., Henoc, P., Henry, L. and Natta, M.(1967)Computes Rendus. Hebd. Seanc. Acad. Sci., Paris, 265, 1293.

Chung, M.S.and Everhart, T.E.(1974) Simple calculation of energy distribution of low-energy secondary electrons emitted from metals under electron bombardment. J.Appl. Phys.45, 707-709.

Chung, M.S. and Everhart, T.E. (1977) Role of plasmon decay in secondary electron emission in the nearly-free-electron metals: Application to aluminum, Phys. Rev. B,15, 4699-4715.

Colliex,C. and Trebbia, P. (1978) Electron energy loss spectroscopy in the electron microscope: present state of affairs. Proc. 9th Int. Congr. on Electron Microscopy 3(Toronto: Imperial) 268-279.

Colliex,C. (1984)Electron Energy Loss Spectroscopy in the Electron Microscope. In Advances in Optical and Electron Microscopy, ed. V.E. Cosslett and R. Barer, Academic Press, London, Vol. 9, pp.65-177.

Crozier, P. A. and Egerton, R. F.(1989)Mass-thickness determination by bethe-sum-rule normalization of the electron energy-loss spectrum.Ultramicroscopy 27, 9-18.

Cundy, S. L., Metherell, A. J. F. and Whelan, M. J.(1966)J. Sci. Instr. 43, 712.

Cundy, S. L. and Grundy, P.J.(1966)Phil. Mag. 14, 1233.

Cundy, S. L., Metherell, A. J. F., Whelan, M. J.,Unwin, P. N. T. and Nicholson, R. B. (1968)Proc. Roy. Soc. A307, 267.

Cundy, S. L., Howie, A. J. F. and Valdre, U.(1969)Phil. Mag. 20, 147.

Curgenven, L. and Duncumb, P., Tube Investments Research Laboratories Report (1971) 303.

Czaja W, (1966), J.A.P. **37**, 4236

Czyzewski, Z., MacCallum, D. O'Neill, Romig, A., and Joy, D. C. (1990)J. Appl. Phys. 68,3066. Lindhard,J.(1954) Kgl. Danske Videnskab. Selskab, Mat.-fys.

Medd. 28,No.8

Daniels, J., Festenberg, C. V., Reather, H. and Zeppenfeld, K. (1970) Optical constants of solids by electron spectroscopy. Springer Tracts in Modern Physics 54(Berlin: Springer) 77-135.

Dekker, A.J. (1958) Secondary Electron Emission. Solid State Phys., 6, p.251.

Devooght,J.,Dubus,A. and Dehaes,J.C.(1987) Improved age-diffusion model for low-energy electron transport in solids. I. Theory. Phys. Rev. B,36,5093-5109.

Ding, Z.-J. and Shimizu, R. (1988) Monte Carlo study of backscattering and secondary electron generation. Surf. Science. 197, 539-554.

Drescher, H., Reimer, L. and Seidel, H.(1970) Ruckstreukoeffizient und Sekundarelektronen Ausbeute Von 10-100keV, Z. Angew Phys.,29,331.

Dunlap, John. R., Luo, Suichu, Bunn, Rod D and Joy, David C.(1989) An electron spectroscopic study of ice. Proc. the 24th Annual Conference of the Microbeam Analysis Society , San Francisco Press, Inc.,P.127.

Dunlap, J. R., Luo, S., Joy, D. C., Chakoumakos, D. C., Zhu, S. and Sun, Y(1993) Electron energy Loss spectroscopy and stopping power calculation of the superconductor $Bi_{1.8}Pb_{0.3}Sr_2Ca_2Cu_3O_{10}$. Proc. 51th Annual Meeting of the Microscopy Society of America. P.1188.

Dwyer and Matthew (1985)Surface Science, 152, 884.

Egerton, R.F. (1974)Advances in Analysis of Microstructural Features by Electron Beam Techniques, P.67, The Metals Society, London.

Egerton, R.F. (1975) Phil. Mag. 31, 199.

Egerton, R.F. (1979) K-shell ionization cross-sections for use in microanalysis. Ultramicroscopy, 4, 169-179.

Egerton, R.F., Williams, B. G. and Sparrow, T. G. (1985) Fourier deconvolution of electron energy-loss spectra. Proc. R. Soc. Lond. A 398, 395-404.

Egerton, R.F.(1986) Electron Energy-Loss Spectroscopy in the Electron Microscope. Plenum Press. New York and London.

Egerton, R.F. and Cheng, S. C.(1987)Measurement of local thickness by electron energy loss spectroscopy. Ultramicroscopy 21, 231-244.

Egerton, R.F. and Wang, Z. L.(1990) Plural-Scattering deconvolution of electron energy-loss spectra recorded with an angle-limiting aperture. Ultramicroscopy 32,137-148.

Emerson, L. C., Williams, M. W., Tang, I'lan, Hamm, R. N., and Arakawa, E. T.(1975) Optical Properties of Guanine from 2 to 82 eV. Radiation Research 63, 235-244.

Fano, U.(1956)Differential Inelastic Scattering of Relativistic Charged Particles.Phys.Rev. 102, 385-387.

Fano, U.(1963) Ann. Rev. Nucl. Sci. 13, 1.

Ferrier, R. P. and Hills, R. T. P.(1974)Advances in Analysis of Microstructural Features by Electron Beam Techniques, P.41, The Metals Society, London.

Ganachaud, J.P. and Cailler, M. (1979) A Monte-Carlo culculation of the secondary electron emission of normal metals. Surface Science. 83, 498-518.

Green, M.(1963) Proc. Phys. Soc., 82, 204.

Gray (1958) Thesis

Gryzinski, M. (1965) Classical theory of atomic collisions. I : Theory of inelastic collisions, Phys. Rev. A.,138, 336.

Hebbard, D. F. and Wilson, P. R. (1955) Austral. J. Phys., 8, 90.

Heinrich, K. F. J. et al. eds (1976)" Use of Monte Carlo Calculations in Electron Probe Microanalysis and Scanning Electron Microscopy", NBS Special Publication 460.

Herman , F. and Skillman, S. (1963) Atomic Structure Calculations. Prentice-Hall, Inc. New Jersey.

Hibbert, G., Edington, J. W., Williams, D. B. and Doig, P.(1972) Phil. Mag. 26, 1491.

Hiller, J. and Baker, R. F.(1944) Microanalysis by means of electrons. J. Appl. Phys.

15,663-676.

Hink, W., Jessenberger, J., and Ziegler, A. (1969) Z. Phys., 266, 463.

Hirsch, P., Howie, A., Nicholson, R. B., Pashley, D. W. and Whelan, M. J.(1977) Electron microscopy of thin film. Robert E. Krieger Publishing CO., INC..

Ho,R., Zhao, L., Wang,Y. Y., Shao, Z. & Somlyo, A.P.(1993) Thickness measurements by EELS. Proc. 51st Annual Meeting of the Microscopy Society of America.P.434.

Hoeft H & Schwaab(1988)Investigations Towards Optimizing EDS Analysis by the Cliff-Lorimer Method in Scanning Trasmission Electron Microscopy. X-Ray Spectrometry,17,201-208.

Hohenberg, P. and Kohn,W. (1964) Phys. Rev, 136, B864.

ICRU (1984)Stopping powers for electrons and positrons. International Commission on Radiation Units and Measurements. ICRU Report 37 (1984).

Inokuti, M. (1971) Inelastic Collisions of Fast Charged Particles with Atoms and Molecules-- The Bethe Theory Revisited. Reviews of Modern Physics 43,297-347.

Isaacson, M. S. and Crewe, A. V. (1975) Electron Microspectroscopy. Annual Review of Biophysics and Bioengineering, 4, 165.

Jeanguillaume, C., Colliex, C., Ballongue, P. , and Tence', M. (1992) New STEM multisignal imaging modes, made accessible through the evaluation of detection effciencies. Ultramicroscopy 45,205-217.

Johnson, D. W. and Spence, J. C. H.(1974)Determination of the single-scattering probability distribution from plural-scattering data. J. Phys. D(Appl. Phys.)7, 771-780.

Jonker, J.L.H. (1951) The augular distribution of the secondary electrons of Nickel. Philips Res. Rep. 6 , 372-387.

Jonker, J.L.H. (1952) On the theory of secondary electron emission. Philips Res. Rep.

7, 1-20.

Joy, D.C. (1970) unpublished data.

Joy, D.C. and Mahe, D.M.(1977) The use of electron energy-loss spectrometry in materials science. Developments in Electron Microscopy and Analysis 1977. Inst. Phys. Conf. Ser. No.36, 357-360.

Joy, D. C. (1979) The basic principles of electron energy loss spectroscopy.InIntroduction to analytical electron microscopy, ed. J. J. Hren, J. I., Goldstein and D. C. Joy. Plenum Press, New York. pp.223-244.

Joy, D. C. and Mahe, D. M.(1980) Electron energy-loss spectroscopy. J. Phys. E., 13, 261-270.

Joy, D.C. (1984) Monte Carlo studies of high resolution imaging. In: Microbeam Analysis 1984 (ed. by A. Romig and J. Goldstein), San Francisco Press,pp.81-86.

Jo, D.C. (1985)Resolution in low voltage scanning electron microscopy, J.Microsc. 140, 283-292.

Joy, D.C. (1987) A Model for Calculating Secondary and Backscatter Electron Yields. J.of Microscopy, 147, 51-64.

Joy, D. C.(1988) An introduction to Monte Carlo simulations. In Proceedings of European Meeting on Electron Microscopy 1988(A J Craven, H Elder, Eds). Institute of Physics, London(1988) 23.

Joy, D. C. and Luo, S.(1989)An impirical stopping power relationship for low energy electrons. Scanning. 11, p.176.

Joy, D.C., Luo, Suichu and Zhang, Xiao (1990) Electron stopping powers and their experimental determination. Proc. XIIth International Congress for Electron Microscopy. P.8.

Joy, D.C.(1991)An introduction to Monte Carlo Similations. Scanning Microscopy. 5, 176.

Joy, D.C.(1993) A data-base on electron-solid interactions. Microbeam Analysis. Proc. 27th MAS Meeting. p.17.

Joy, D.C., Zhang,Y-S., Zhang, X., Hashimoto, T.,Bunn, R. D., Allard, L. and Nolan,T. A.(1993a)Practical aspects of electron holography. Ultramicroscopy 51 , p.1.

Joy, David C, Luo, Suichu, Blackson, John and Dunlap, Jonh R(1993b) Quantitative analysis of the electron energy loss spectrum. Microbeam Analysis. Proc. 27th MAS Meeting. p.282.

Joy, David C., Luo, Suichu, Dunlap, Jonh R , William, Richard W.,and Siqi Cao(1994) Stopping Power Determination For Compoumd By EELS. Proc. 27th Annual Meeting of the Microbeam Analysis Society , to be published.

Kahn, H.(1950) Nucleonics, (May), 27.

Kohn, W. and Sham L. J. (1965) Phys.Rev. 140 A, 1133.

Kanaya, K, Ono S, in "Electron Beam Interactions with Solids", ed D Kyser, (SEM Inc.: Chicago), (1984), 69-98.

Kanaya, K and Kawakatsu M, (1972), J. Phys. D. Appl. Phys. **5**, 1727.

Kanter M, (1961), Phys. Rev. **121**, 1677.

Kanter, H. (1961) Contribution of Backscattered Electrons to Secondary Electron Formation. Phys. Rev.,121, p.681.

Kihn, Y., Zanchi, G. and Sevely, J. (1991) Gas excitation cross-section measurements by EELS. Inst.Phys. Conf. Ser. 119,143-146.

Kolbenstvedt, H.(1967) J. Appl. Phys. 38, 4785.

Koshikawa T and Shimizu R, (1973), J. Phy. D. Appl. Phys. **6**, 1369.

Koshikawa, T. and Shimizu, R. (1974) A Monte Carlo calculation of low-energy secondary electron emission from metals. J.Phys. D: Appl.Phys.,7,1303-15.

Kotera, M., Murata, K. and Nagami, K.(1981), J. Appl. Phys. 52,997.

Koyama, R.Y. and Smith, N.V. (1970) Photoemission Properties of Simple Metals. Phys.

Rev. B2, 3049-3059.

Landau, L. (1944) Energy loss of fast particles by ionization. J. Phys. USSR 8, 201-205.

Lanteri,H.,Richard,C., Bindi, R. and Keller, P. (1975) Determination experimentale de L'efficacite des electrons retrodiffuses dans L'emission electronique secondare de Au et Al. Thin Solid Films,27, 301-310.

LaVerne J. A. and Mozumder, A. (1983)Rad. Res. 96, 219.

LaVerne J. A. and Mozumder, A. (1983)J. Phys. Chem. 89, 4219.

Leapman, R. D. and Cosslett, V. E.(1976) Extended fine-structure above X-ray edge in electron-energy loss spectra.J. Phys. D9, L29.

Leapman, R. D., Rez , P. and Mayers, D. F.(1980)K, L, and M shell generalized oscillator strengths and ionization cross sections for fast electron collisions. J. Chem. Phys. 72, 1232-1243.

Leapman, R. D., Fiori, C. E. and Swyt, C. R.(1984) Mass thickness determination by electron energy loss for quantitative X-ray microanalysis in biology. J. Micro., 133, 239-253.

Leapman, R. D. and Ornberg, R. L.(1988)Quantitative electron energy loss spectroscopy in biology. Ultramicroscopy 24, 251-268.

Leiss, J. E. , Penner, S. and Robinson , C. S. (1957) Phys. Rev. 107, 1544.

Lichte, H. Ultramicroscopy 20 (1986) 293.

Linders, P. W., Stols, A.L.H., van de Vorstenbosch, R.A., and Stadhouders, A. M. (1982)Mass determination of thin biological specimens for use in quantitative electron probe X-ray microanalysis. Scanning Electron Microscopy. IV,1603-1615.

Lindhard, J. (1954) Kgl. Danske Videnskab. Selskab, Mat-Fys. Mdee. 27, No. 15.

Lindner,T., Sauer, H., Engel, W., andbe, K.(1985)Near edge structure in EELS of MgO. Phys. Rev. B 33,22.

Lindgren, I., and A. Rosen, unpublished (1970) quoted from Mahan, 1983.

Livins,P., Aton, T. and Schnatterly, S.E.(1988)Inelastic electron scattering in amorphous silicon nitride and aluminum oxide with multiple-scattering corrections. Phys. Rev. B38,5511-5519.

Long, X., Liu, M., Ho, F., and Peng, X.(1990) Cross sections for K-shell ionization by electron impact. Atomic data and nuclear data tables 45, 353-366.

Love, G., Cox, M. G. and Scott, V. D.(1978)Aversatile atomic number correction for electron-probe microanalysis. J. Phys. D: Appl. Phys. 11, 7.

Loz, W.(1970)Electron-Impact Ionization Cross-Sections for Atoms up to Z=108. Z. Physik 232,101-107.

Luo, Suichu, Zhang, Yongsheng and Wu, Zichin (1987)Monte Carlo calculation of secondary electrons emitted from Au, Ag and Cu. J. Microscopy, 148, p.289.

Luo, Suichu and Joy, David C. (1988)Monte Carlo calculations of secondary electron emission. Scanning Microscopy, 2, 1901-1915.

Luo, Suichu and Joy, David C.(1990)Monte Carlo calculations of secondary electron emission. Scanning Microscopy, Supplement 4, 127-146.

Luo, Suichu , Zhang, Xiao and Joy, David C.(1991)Experimental determinations of electron stopping power at low energies. Radiation Effects and defects in solids. 117, p.235.

Luo, Suichu and Joy, David C.(1991)Calculations of X-ray ionization cross sections at low overvoltage ratios. Microbeam Analysis. p.67.

Luo, Suichu and Joy, David C.(1992)Calculations of electron ionization cross sections for K, L and M shells. The 14th Werner Brandt Workshop on Charged Particle Penetration Phenomena. P.264.

Luo, Suichu , Joy, David C., Dunlap, Jonh R and Wang, Xinlei (1992)Calculation and measurement of electron ionization cross sections for L and M shells. Proc. 50th

Annual Meeting of the Electron Microscopy Society of America Held jointly with the 27th Annual Meeting of the Microbeam Analysis Society and the 19th Annual Meeting of the Microscopical Society of Canada, ed,G.W.Bailey, J. Bentley and J. A. Small. p.1642.

Luo, Suichu, Dunlap, Jonh R and Joy, David C.(1993) Modulation electron energy loss spectroscopy and its application of quantitative analysis. Proc. 51th Annual Meeting of the Microscopy Society of America. P.454.

Luo, Suichu and Joy, David C. (1994a) An Empirical Rutherford Formula For Low Energy Electrons. Proc.27th Annual Meeting of the Microbeam Analysis Society, to be published.

Luo, Suichu and Joy, David C. (1994b) A New Method For Quantitative Analysis Of EELS. Proc. 27th Annual Meeting of the Microbeam Analysis Society , to be published.

Luo, Suichu, Dunlap, Jonh R , William, Richard W.,and Joy, David C.(1994c) Local Thickness Determination By Electron Energy Loss Spectroscopy. Proc. 52nd Annual Meeting of the Microscopy Society of America, to be published

Mahan, G. D. (1981) Many-Particle Physics. Plenum Press, New York.

Maher, D. M., Joy, D. C., Egerton, R. F. and Mochel, P.(1979) The functional form of energy differential cross sections for carbon using transmission electron energy-loss spectroscopy. J. Appl. Phys. 50, 5105-5109.

Manson, S. T.(1971)Minima in Atomic Continuum Generalized Oscillator Strengths. Phys. Rev. A, 3,1260-1267.

Manson, S. T.(1972)Inelastic Collisions of Fast Charged Particles with Atoms: Ionization of the Aluminum L shell. Phys. Rev. A, 6, 1013-1024.

McCracken, D. D.(1955) Sci. Amer. 192, 90.

McGuire, E. J. (1971a) J. Phys. (Paris) C4, 37.

McGuire, E. J. (1971b) Phys. Rev. A3, 267.

McGuire, E. J. (1974) private communication with Powell (1976).

Metropolis, N. and Ulam, S. (1949) J. Amer. Statistical Assoc., 44, 335.

Misell, D.L. and Jones , A.F.(1969)The determination of the single-scattering line profile from the observed spectrum. J. Phys. A 2,540-546.

Moncrieff D A, Barker P R (1976), Scanning 1, 195.

Mott, N. F.(1929) Proc. Roc. Soc. A124,425.

Mott, N. F. and Massey, H. S. W. (1949) The Theory of Atomic Collisions (Oxford University, London), second edition, 243-244.

NBSIR 82-2550(1982)Stopping powers and ranges of electrons and positrons. U.S. Department of commerce, National Bureau of Standards. Washington, D C.

Nieminen, R. M.(1988) Stopping power for low energy electrons. Scanning Microsc. 2, 1917.

Neuman, K. D. and Spence, J. C. H.(1987)The electron energy loss near edge tructure of MgO. In Proc. of EMSA, 1987, ed. G. W. Bailey, p.126. San Francisco Press.

Palinkas J & Schlenk B(1980)L-Subshell Ionizations for Au, Pb, and Bi by 60-600 keV Electron Impact. Z.Physik A. 297,29-33.

Painter, L. R. , Arakawa, E. T. , Williams, W. and Ashley, J. C. (1980) Optical properties of polyethylene : measurement and applications. Radiat., Res., 83, 1.

Perlman, H. S. (1960) Proc. Phys. Soc. London, 76, 623.

Philibert J and Weinryb, E.(1963)Proc. 3rd Conf on X-ray Optics and Microanalysis; also E.Weinryb and J Philibert, 1964, C.R.Acad.Sci., 256, 4535.

Pines, D.(1963)Elementary Excitations in Solids. New York, Benjamin.

Plummer,E. W., Tsuei, K.-D., Sprunger, P.T. and Watson, G. M.(1992) Collective Surface Excitations in Metals and Thin Films.The 14th Werner Brandt Workshop on Charged Particle Penetration Phenomena. P.140.

Powell C J (1962) Inelastic Scattering of Electrons in Solids. Electron Beam Interactions With Solids. SEM, Inc., AMF O'Hare(Chicago),IL 60666,U.S.A. pp.19-31.

Powell, C. J. (1972) Scanning Microscopy SEM, Inc., AMF O'Hare, (Chicago), IL, 60666, U.S.A. pp.19-31.

Powell, C. J.(1976)Cross sections for ionization of inner-shell electrons by electrons.Rev. Rev. Mod. Phys. 48, 33-47.

Powell, C. J.(1982)in Electron Beam Interactions with Solids, eds.Kyser, D., Shimizu, R. and Newbury, D. E., SEM Inc.: Chicago.

Powell, C. J.(1984a) Inelastic mean free paths and attennuation lengths of low-energy electrons in solids. SEM, IV, 1649-1664.

Powell, C. J. (1984b) Inelastic scattering of electrons in solids. In : Electron Beam Interactions with Solids for Microscopy, Microanalysis and Microlithography, Eds. D. F. Kyser, H. Niedrig, D. E. Newbury and R. Shimizu (SEM, AMF O'Hare, IL, 1984), 19-31.

Powell, C. J.(1985a)The Energy Dependence of Electron Attenuation Lengths Surf Interface Anal., 7, 256-262.

Powell, C. J.(1985b)Innershell Ionization Cross Sections in Electron Impact Ionization. Ed. by T D Mark and G H Dunn. Springer- Verlag Wien New York, 1985. pp.199-231.

Powell, C. J.(1989)Cross sections for inelastic electron scattering in solids. Ultramicroscopy, 28, 24-31.

Powell, C. J.(1991) Inner-shell Ionization cross sections. Unpublished.

Raether, H. (1980) Excitation of Plasmons and Interband Transitions by Electrons. Springer Tracts in Modern Physics, 88.

Rao-Sahib T. S. and Wittry D. B.(1974) X-ray continuum from thick elemental targets for 10-50 keV electrons. J. Appl. Phys. 45, 5060.

Reimer L, Tolkamp C, (1980), Scanning 3, 35

Reimer, L. and Drescher, H. (1977) Secondary electron emission of 10-100 keV electrons from transparent films of Al and Au. J.Phys.D: Appl.Phys.,10, 805-815.

Reimer, L. and Stelter, D., B.(19886) FORTRAN 77 Monte Carlo program for minicomputers using Mott cross sections. Scanning 8,265.

Reimer, L. and Lodding, B.(1984)

Reusch S , Genz H , Low W & Richter A(1986)A Method to Determine L-Subshell Ionization Cross Sections for Medium and Heavy Elements.Z. Phys. D ,3 , 379-389.

Rez, P.(1984)Electron Ionization Cross-Sections for K, L and M Shells. X-ray Spectrometry 13,55-59.

Rez, P., Chiu, W., Weiss, J. K. and Brink, J.(1992) The thickness determination of organic crystals under low dose conditions using electron energy loss spectroscopy. Microscopy Research and technique , 21, 166-170.

Riley, M. E., MacCallum , C. J.and Biggs, F. (1975) Theoretical electron-atom elastic scattering cross sections. Atomic Data and Nucl Tables 15,443.

Ritsko, J. J., Shnatterly, S. E. and Gibbons, P. C.(1974) Simple calculation of LII, III absorption-spectra of NA, AL and Si. Phys. Rev. Lett. 32, 671.

Ritchie, R.,H.(1957) Plasma Losses by Fast Electrons in Thin Films. Phys. Rev. 106, 874-881.

Ritchie, R.,H.(1959)Interaction of charged particles with a degenerate Fermi-Dirac gas. Phys. Rev. 114, 644.

Ritchie,R. H., Garber, F. W., Nakai , M. Y., and Birkhoff, R. D.(1969)Low energy electron mean free paths in solids. Advan. Radiation Biol. 3,1-27.

Ritchie, R. H. and Howie , A.(1977) Electron excitation and the optical potential in electron microscopy. Phil.Mag. ,36,463-481.

Ritchie, R. H. and Brandt , W .(1978a) Projectile charge dependence of stopping powers. Phys. Rev. A17, 2102.

Ritchie, R. H.,Hamm, R. N., Turner, J. E., and Wright, H. A.(1969b) Proc. 6th Symposium on Microdosimetyr, Brussels, Belgium(eds. Booz, J. and Ebert, H. G.) Harwood Academic Publishers (New York), 1, 345.

Roptin, D.(1975) Etude experimentale de L'emission electronique secondare de L' aluminium et de L'argent. Thesis, University of Nantes, Nantes.

Rosler, M. and Brauer, W. (1981 a) Theory of Secondary Electron Emission. I. General Theory for Nearly-Free-Electron Metals. Phys. stat.sol.(b)104,161-75.

Rosler, M. and Brauer, W. (1981 b) Theory of Secondary Electron emission. II. Application to Aluminum. Phys. stat. sol. (b) 104, 575-587.

Rosler,M. and Brauer,W.(1988) Theory of Electron Emission from Solids by Proton and Electron Bombardment. Phys.stat.sol.(b) 148 ,213-226.

Rothwell , T. E. (1987) Techniques for Determining Secondary Electron Yield of Integrated Circuit Materials. Thesis, North Carolina State University.

Rudge, M. R. H and Schwartz, S. B.(1966) Proc. Phys. Soc. London, 88, 563.

Salow, H. (1940) Sekundarelektronen-emission. Phys. Z., 41, p.434.

Samoto, N. and Shimizu,R. (1983) Theoretical study of the ultimate resolution in electron beam lithography by Monte Carlo simulation, including secondary electron generation: Energy dissipation profile in polymethylmethacrylate. J. Appl. Phys., 54, 3855-3859.

Scheinfein, M. R., Drucker, J. K. and Weiss, J. K. (1993) The origins of high-resolution secondary-electron microscopy. Proc.51th Annual Meeting of the Microscopy Society of America. P.766.

Schreiber T P & Wims A M(1981)A Quantitative X-Ray Microanalysis thin film method using K-, L-, and M- lines. Ultramicroscopy, 6, 323-334.

Schou, J .(1980) Transport theory for kinetic emission of secondary electrons from solids. Phys.Rev.B,22,2141-74.

Schou, J. (1988) Secondary electron emission from solids by electron and proton bombardment. Scanning Microscopy, 2, 607-632.

Schreiber, T. P. and Wimms, A. M. (1981). Ultramicroscopy, 6, 323-334.

Scofield J H(1978)K- and L-shell ionization of atoms by relativistic electrons.Phys. Rev. A18,963-970.

Seah, M.P. and Dench, W.A.(1979) Quantitative Electron Spectroscopy of Surfaces: A Standard Data Base for Electron Inelastic Mean Free Paths in Solids. Surf. Interface Anal. 1, 2-11.

Seiler,H. (1983) Secondary electron emission in SEM. J. Appl. Phys.,54, pR1-R17.

Shimizu., R. (1974) J.A.P. 45, 2107.

Shimizu., R. and Ichimura, S.(1981)Quantitative Analysis by Auger Electron Spectroscopy. Toyota Foundation Research Report No.I-oo6, Toyota Foundation, Tokyo.

Shuman, U. and Somlyo, A. P.(1987)Electron energy loss analysis of near-trace-element concentrations of calcium. Ultramicroscopy 21, 23-32.

Sidei, T. , Higasimura, T., and Kinosita, K.(1957) Men. Fac. Engng. Kyoto Univ. 19, 220.

Siegbahn, K., Nordling, C., Fahlman, A., Nordberg, R., Hamrin, K., Hedman, J., Johanson, G., Bergmark, T.,Karlsson, S., Lindgren, I., Lindgren, B. (1967) Nova Acta R Soc Sci Uppsata. IV, 20.

Skiff, W. M., Carpenter, R. W., Lin, S.H. and Higgs, A.(1988)K, L, M, N, O and P ionization cross sections for electron energy loss spectroscopy. Ultramicroscopy 25, 47-60.

Spalding, D. R., Villagrana, R. E. and Chadwick, G. A.(1969)Phil. Mag. 20, 471.

Spence,J.C.H.(1985) The structrural sensitivity of ELNES. Ultramicroscopy 18,165.

Spence,J.C.H.(1992) in: High-Resolution Transmission Electron Microscopy and Associated Techniques, ed P. Buseck, J. Cowley and L. Eyring. New York Oxford, Oxford University Press.

Sugiyama, H. (1976) Energy loss and range of electrons below 10 keV. Japanese J. of Appl. Phys. 15, 1779.

Teo, B. K. and Joy, D. C. eds.(1981)EXAFS spectroscopy, techniques and applications. Plenum, New York.

Thomas, S. and Pattinson, E.B. (1970), Range of electrons and contribution of backscattered electrons in secondary production in aluminum. J. Phys. D. 3, 349-357.

Tougaard, S. (1986) Low Energy Inelastic Electron Scattering Properties Of Noble And Transition Metals. Solid State Communications 61, 547-549.

Tung,C.J., Ritchie,R.H., Ashley, J. C. and Anderson, V. E.(1976a) Inelastic interactions of swift electrons in solids. Thesis, unpublished.

Tung, C.J., Ashley, J. C. , Anderson, V. E. and Ritchie,R.H.(1976b) Inverse mean free path, stopping power, csda range and straggling in silicon and silicon dioxide for electrons of energy < 10 keV. Rome Air Development Center, Report RADC-TR-76-125.

Tung,C.J. and Ritchie,R.H.(1977) Electron slowing-down spectra in aluminum metal. Phys. Rev.B,16,4302-4313.

Tung,C.J., Ashley, J.C. and Ritchie,R.H.(1979)Electron inelastic mean free path and energy losses in solids.II Electron Gas Statistical Model. Surface Science 81 , 427-439.

Tonomura, A., Electron Holography, in: Progress in Optics 13 (Elsevier, Amsterdam, 1986), p.183.

Vrakking, J. J. and Meyer, F. (1974) Electron-impact-ionization cross sections of inner shells measured by Auger-electron spectroscopy. Phys. Rev. A9, 1932-1937.

Wallace, S. J., Berg, R. A., and Green, A. E. S. (1973) Phys. Rev., A7, 1616.

Wang, Y.-Y (1990)Multiple scattering correction by a direct convolution method for electron energy loss spectrum. Ultramicroscopy 33,151-157.

Watenabe, H. and Uyeda,R.(1962) J. Phys. Soc., Japan 17, 569.

Whelan, M. J. (1976) On the energy loss spectrum of fast electrons after plural inelastic scattering. J. Phys. C: Solid State Phys. 9, L 195-197.

Williams,L.E., Callcott,T.A., Ashley,J.C. and Anderson,V.E. (1989)Interactions of electrons with PMMA. J. Electro. Rad. Phen.

Wittry, D. B.(1966) Proc. 4th Conf. on X-ray Optics and Microanalysis, ed R Castaing et al , (Hermann:Paris), p168.

Wittry, D. B., Ferrier, R. P., and Cosslett, V. E.(1969)J. Phys. D2, 1767.

Wolff, P.A. (1954) Theory of Secondary Electron Cascade in Metals. Phys. Rev. 95, 56-66.

Yougaard, S.(1987)Low energy inelastic electron scattering properties of noble and transition metals. Solid State Communications, 61,547-549.

Yuan, J., Brown, L. M. and Liang, W. Y.(1988)Electron energy-loss spectroscopy of the high-temperature superconductor $Ba_2Y\ Cu_3O_{7-x}$. J. Phys. C:Solid State Phys. 21,517-526.

Zhao, L., Wang, Y. Y., Ho, R., Shao, Z., Somlyo, A. V. and Somlyo, A.P.(1993) Thickness determination of biological thin sections by multiple-least-squares fitting of the carbon K-edge in the electron energy-loss spectrum. Ultramicroscopy 25, 47-60.

Zanchi, G., Kihn, Y. and Sevely, J. (1990) On the simulation of EEL Spectra corresponding to solid and gaseous samples. Proceedings of XIIth International

Congress for Electron Microscopy . 18-19.

Zeiss, G. D., Williams, J. M., MacDonald, J.,C.,F. and Dowson, D. J. (1975) Rad.Res., 63,64-82.

APPENDICES

APPENDIX A: ANGULAR DISTRIBUTION OF TWO SUCCESSIVE SCATTERING EVENTS

Assume an electron is initially traveling along the direction **OB** as shown in Figure A1, after a collision its moving direction is **OA**, and the angle between **OB** and **OA** is θ_1. Assume there is a successive scattering event after the first collision and **OC** is the final moving direction. In the second collision the scattering angle is θ_2. The scattering angle of the two successive collisions is θ, and from Figure A1 we see that

$$|\theta_1-\theta_1| < \theta < \theta_1+\theta_1 .$$

If we take

$$|OA| = 1, \text{ then } |OB| = 1/\cos\theta_1;$$
$$|OC| = 1/\cos\theta_2 ;$$
$$|AC| = \tan\theta_2 ;$$

and

$$|BC| = \sqrt{(\tan\theta_1-\tan\theta_2\cos\varphi)^2+ \tan\theta_2^2\sin^2\varphi} .$$

From Figure A1 we have the expression for the scattering angle θ :

$$\cos\theta = \frac{|OB|^2 + |OC|^2-|BC|^2}{2\,|OB|\cdot|OC|} \qquad (A1)$$

Substitute the values of $|OB|$, $|OC|$ and $|BC|$ into Eq.A1 , we get the result for the scattering angle θ:

$$\cos\theta = \cos\theta_1\cos\theta_2 + \sin\theta_1\sin\theta_2\cos\varphi \qquad (A2)$$

Using Eq.A2 for a given scattering angle θ' we can calculate the corresponding azimuthal angle φ', and for $\theta'+\Delta\theta'$ we can calculate $\varphi'+\Delta\varphi'$. Because the probability of a

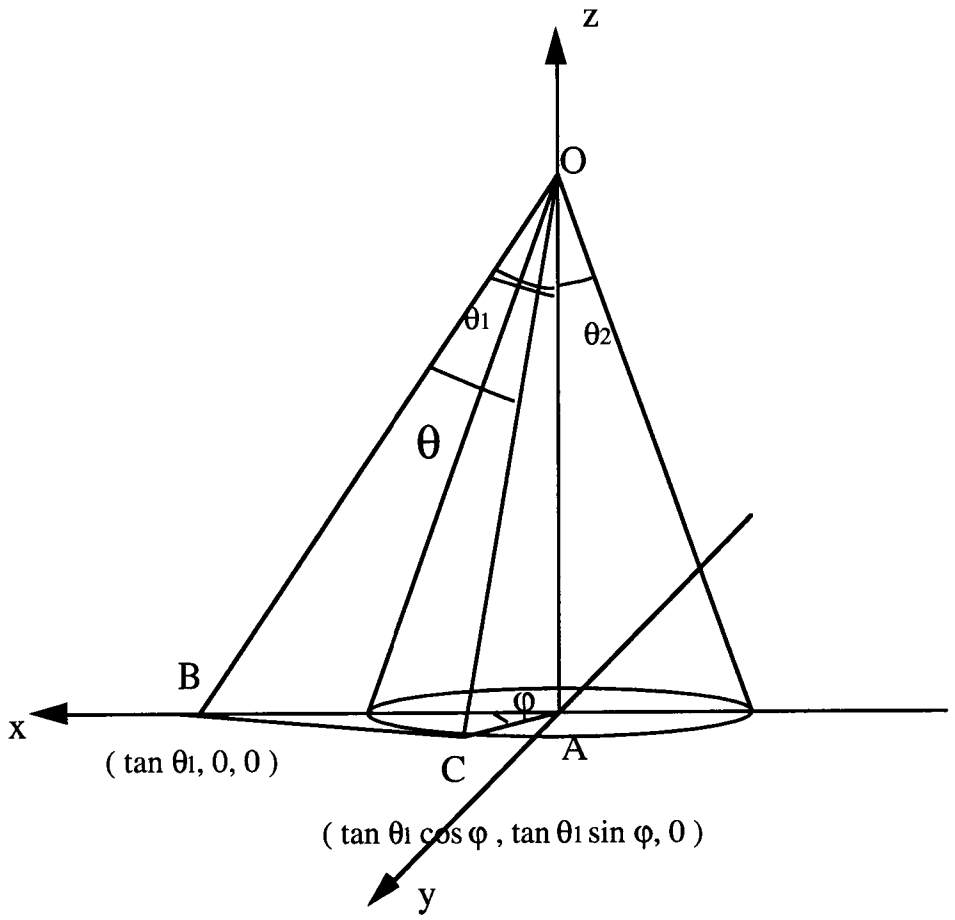


Figure A1 Schematic representation of angular distribution of two successive scattering events.

collision event with an azimuthal angle $\varphi' < \varphi < \varphi'+\Delta\varphi'$ is $\Delta\varphi'/\pi$, so the probability of a collision event with the scattering angle $\theta' < \theta < \theta'+\Delta\theta'$ is $\Delta\varphi'/\pi$.

APPENDIX B: COMPUTER PROGRAM

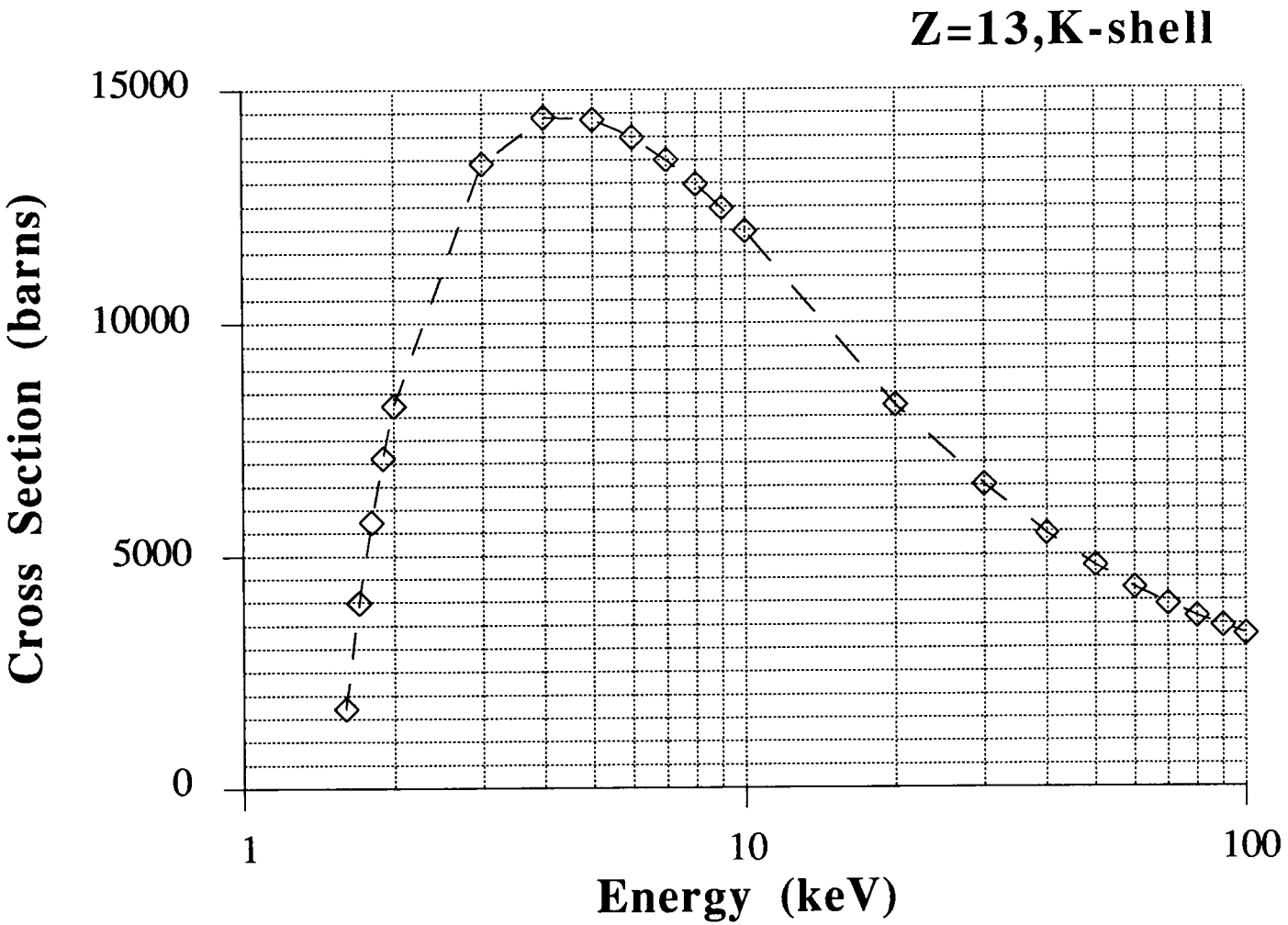
```
C*****************************************************
C*                                                   *
C*     PROGRAM - STOPPING POWER CALCULATION          *
C*                    April,1994                     *
C*                                                   *
C*****************************************************
C
      DIMENSION D(2048),YI(35100),YN(35100)
      CHARACTER*8 EL,ELL,TAB
      TAB=CHAR(9)
      WRITE(*,*)
      WRITE(*,*)'WELCOME TO THE STOPPING POWER PROGRAM'
      WRITE(*,*)
C
C     Z  -- Atomic number;
C     A  --  Atomic weight;
C     P  -- Density
C     E  -- Electron energy (eV);
C     N  -- Number of effective electrons;
C     I   -- Effective ionization energy;
C     B  -- Bethe formula;
C     B1 -- Log10(dE/dS-Bethe).
C
C*****************************************************
C          DATA INPUT PART OF THE PROGRAM           *
C*****************************************************
      WRITE(*,*) "GIVE THE NAME OF THE DATA FILE  OF DIELECTRIC "
      WRITE(*,*) "FUNCTION TO BE USED IN THE CALCULATION"
      READ(*,*) EL
      WRITE(*,*)
990   OPEN(5, FILE=EL)
      READ(5,*) Z,A,P,N
      READ(5,*) (D(I), I=1,N)
      CLOSE(5)
      WRITE(*,*) "PLEASE INPUT FOLLOWING PARAMETERS:"
      WRITE(*,*)
      WRITE(*,*)"MEAN EXCITATION POTENTIAL J=?"
      READ(*,*)XJ
      WRITE(*,*)
      WRITE(*,*) "J2= 6.34*J   (IN INTEGER) ?"
      READ(*,*) J2
      WRITE(*,*)
      WRITE(*,*) "R10 = ?"
      READ(*,*) R10
      WRITE(*,*)
C*************************************************
C*     THE CALCULATION PART OF THE PROGRAM      *
C*************************************************
C
C
      WRITE(*,*)'  THE DIELECTRIC FUNCTION Im(-1/ε)  BEING USED:'
      WRITE(*,*)
```

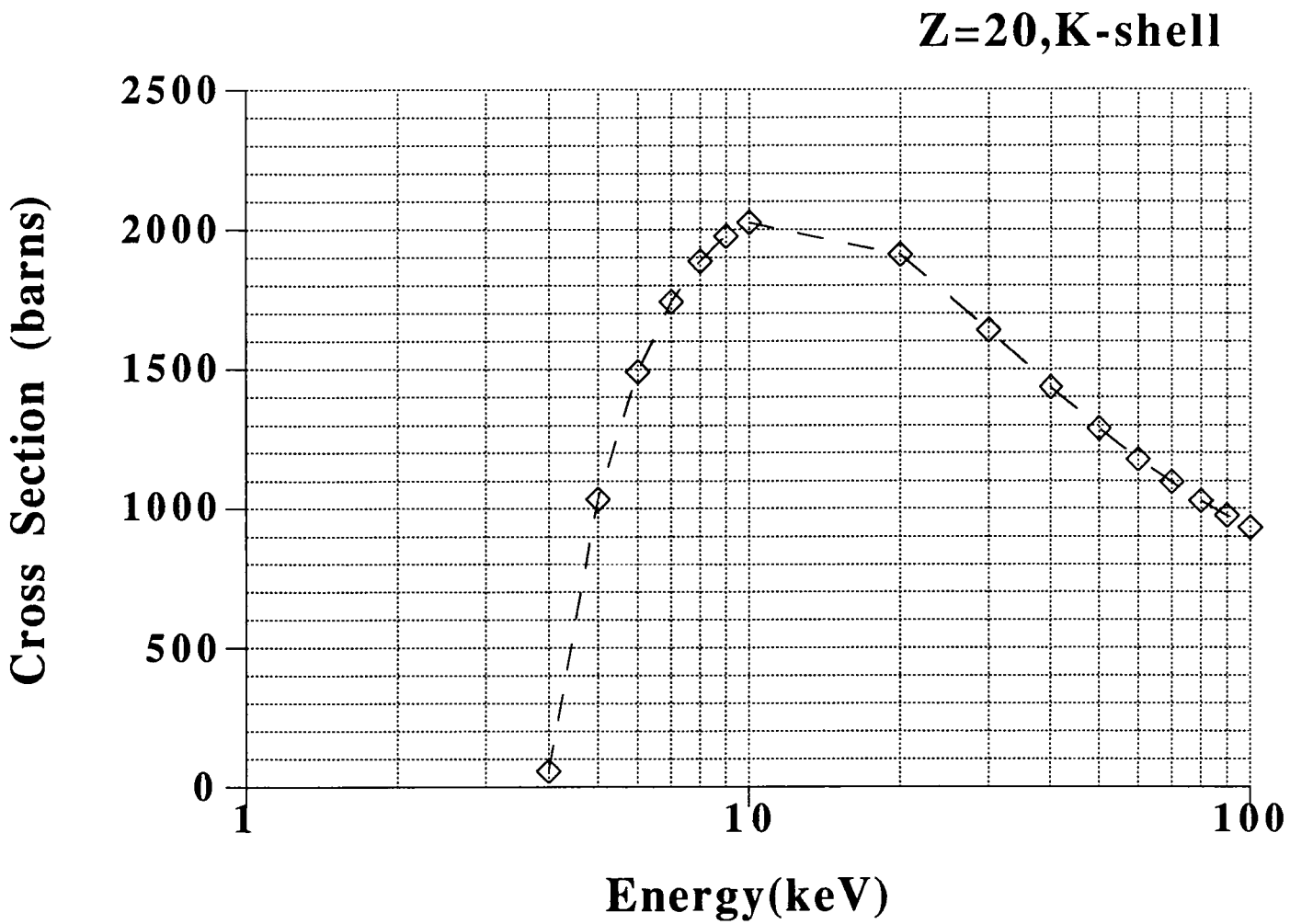
```
      DO  51  I = 1, N,6
      WRITE(*,41)I, D(I), I+1, D(I+1), I+2, D(I+2), I+3,
     6   D(I+3), I+4, D(I+4), I+5, D(I+5)
41    FORMAT(1X, 6('D(',I2,')= ', F7.4,2X))
51    CONTINUE
      Y = 0
      Y1 = 0
      B1=0
      RI = 3.14159265 * 3.72 * 3.72 * 60.23* P
      RI = 2 * A / RI
      Y5 = 785 * P / A
      EPC = 1.
      WRITE(*,*)
      WRITE(*,*)
      WRITE(*,*) "PLEASE GIVE A NAME OF THE DATA FILE"
      WRITE(*,*) "THAT TO BE USED TO STORE THE CALCULATED RESULTS"
      READ(*,*)ELL
      OPEN(6, FILE=ELL, STATUS='NEW')
      WRITE(*,70) "E","Log(E)","dE/dS","Log(dE/dS)","N","I"
      WRITE(*,*)
70    FORMAT (A5,A9,A8,A11,A8,A8)
      DO  72  J = 1, N
      E = EPC * J
      X1 = D(J)
      Y = Y + EPC * E * X1 * ALOG(E/27.2)
      Y1 = Y1 + 0.0007647 * EPC * E * X1 * A / P
      RK = RI * Y / Y1
      RK1 = 27.2 * EXP(RK)
      YN(J) = Y1
      YI(J) = RK1
      E1 = 0.5 * (E + RK1)
      J4 = IFIX(E1)
      IF (J4 .EQ. 0) J4 = 1
      RK = YI(J4)
      Y6 = YN(J4)
      Y3 = Y5 * Y6 * ALOG(1.166 * E / RK) / E
      B=Y5*Z/E
      B=B*ALOG(1.166*E/XJ)
      IF(B.GT.0)B1=LOG10(B)
      YJ = LOG10(FLOAT(J))
      Y2 = LOG10(Y3)
      IF (J.LE.10)WRITE(6,*)J,TAB, YJ, TAB,Y3,TAB, Y2,TAB,
     6   B,TAB,B1, TAB,Y6, TAB,RK
      IF (J.LE.10)WRITE(*,11) J, YJ, Y3, Y2, Y6, RK
11    FORMAT(I5,F8.4,F9.4,1X,7(F9.4,1X))
      DO 73  I = 20, N, 10
      IF (J .EQ. I) WRITE(6,*)J,TAB, YJ, TAB,Y3,TAB, Y2, TAB,
     6   B,TAB,B1, TAB,Y6, TAB,RK
      IF(J.EQ.I)WRITE(*,11) J, YJ, Y3, Y2, Y6, RK
73    CONTINUE
      IF (J .EQ. N) OA = X1
72    CONTINUE
      PAUSE
```

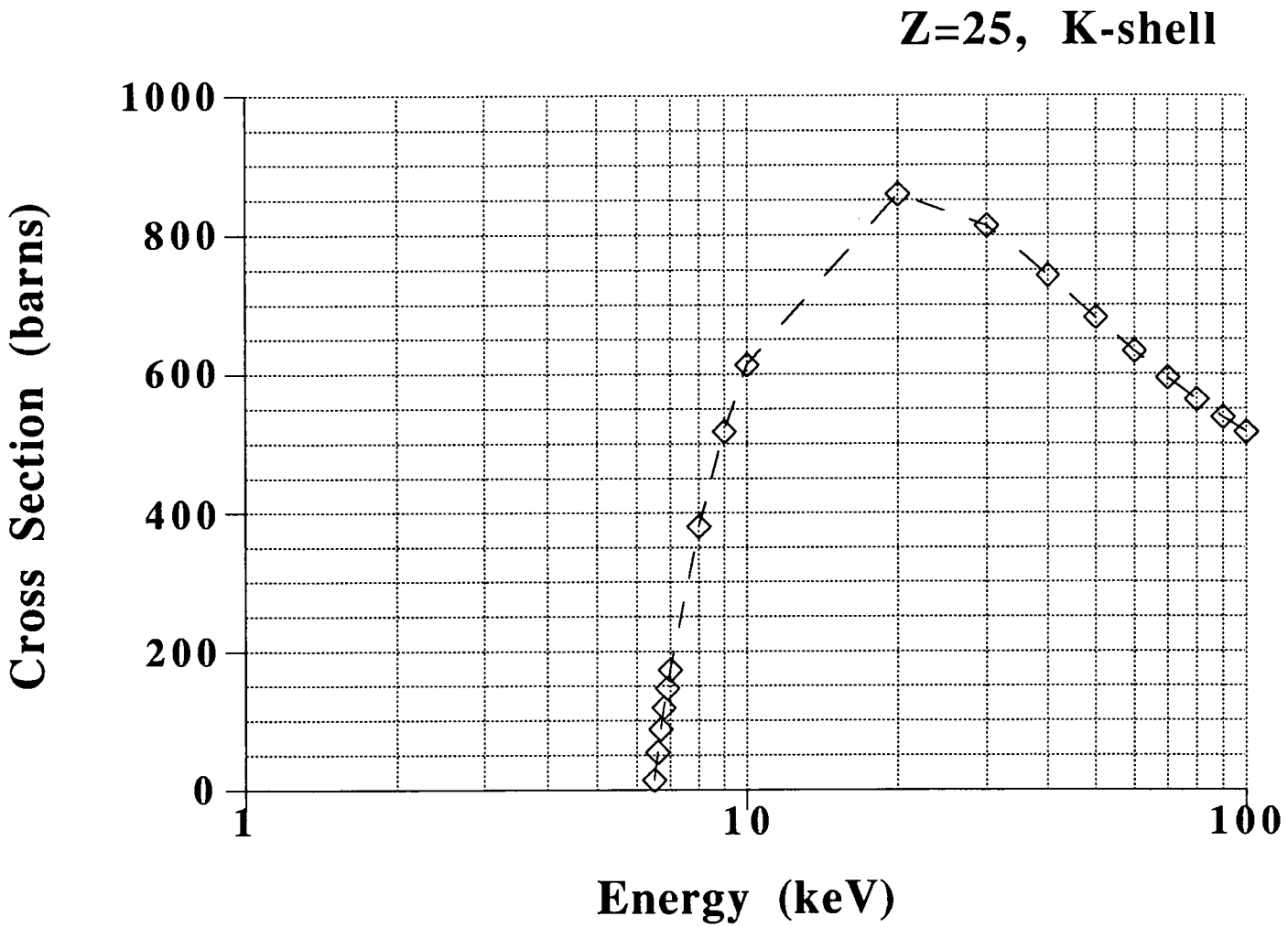
```
      R = R10
      E = N
      DNN = N + EPC * (J2 - N + 1)
      DN = D(N) * (E / DNN) ** R
      EPC = 1.0
      B1=0.0
      DO  74   J = N, DNN,1
      E = J * 1.0
      OO = OA * (N / E) ** R - DN
      Y = Y + E * EPC * OO * ALOG(E / 27.2)
      Y1 = Y1 + 0.0007647 * A * EPC * E * OO / P
      RK = RI * Y / Y1
      RK1 = 27.2 * EXP(RK)
      YN(J) = Y1
      YI(J) = RK1
      E1= 0.5 *  (E + RK1)
      J4 = IFIX(E1)
      RK = YI(J4)
      Y6 = YN(J4)
      Y3 = Y5 * Y6 * ALOG(1.166 * E / RK)/ E
      B=Y5*Z/E
      B=B*ALOG(1.166*E/XJ)
      IF(B.GT.0.0)B1=LOG10(B)
      YJ = LOG10(FLOAT(J))
      Y2 = LOG10(Y3)
      IF (J .EQ. DNN) THEN
      WRITE(*,*)'J = ', J,' Neff(J) =',Y1,' Ieff(J) =',RK1
      WRITE(*,*)'R10= ', R10,'  J2=',J2
      WRITE(*,*)
      WRITE(*,*)'DO YOU SATISFY THE RESULTS ?'
      WRITE(*,*)'IF YOU DO NOT, ENTER 2'
      READ(*,*)II
      IF(II.EQ.2) THEN
      GOTO 990
      ELSE
      GOTO 2222
      ENDIF
2222  ELSE
      GOTO 1111
      ENDIF
1111  DO 436 I = 30,90,10
      IF (J .EQ. I)  WRITE(6,*)J,TAB, YJ, TAB,Y3,TAB, Y2, TAB,
   6   B,TAB,B1, TAB,Y6, TAB,RK
14    FORMAT(I5,F8.4,F9.4,1X,7(F9.4,1X))
      IF(J.EQ.I) WRITE(*,14) J, YJ, Y3, Y2, Y6, RK
436   CONTINUE
      DO 77  I = 100, 900, 100
      IF (J .EQ. I) WRITE(6,*)J,TAB, YJ, TAB,Y3,TAB, Y2, TAB,
   6   B,TAB,B1,TAB,Y6, TAB,RK
      IF(J.EQ.I) WRITE(*,14) J, YJ, Y3, Y2, Y6, RK
77     CONTINUE
      DO 75  I = 1000, 10000, 1000
```

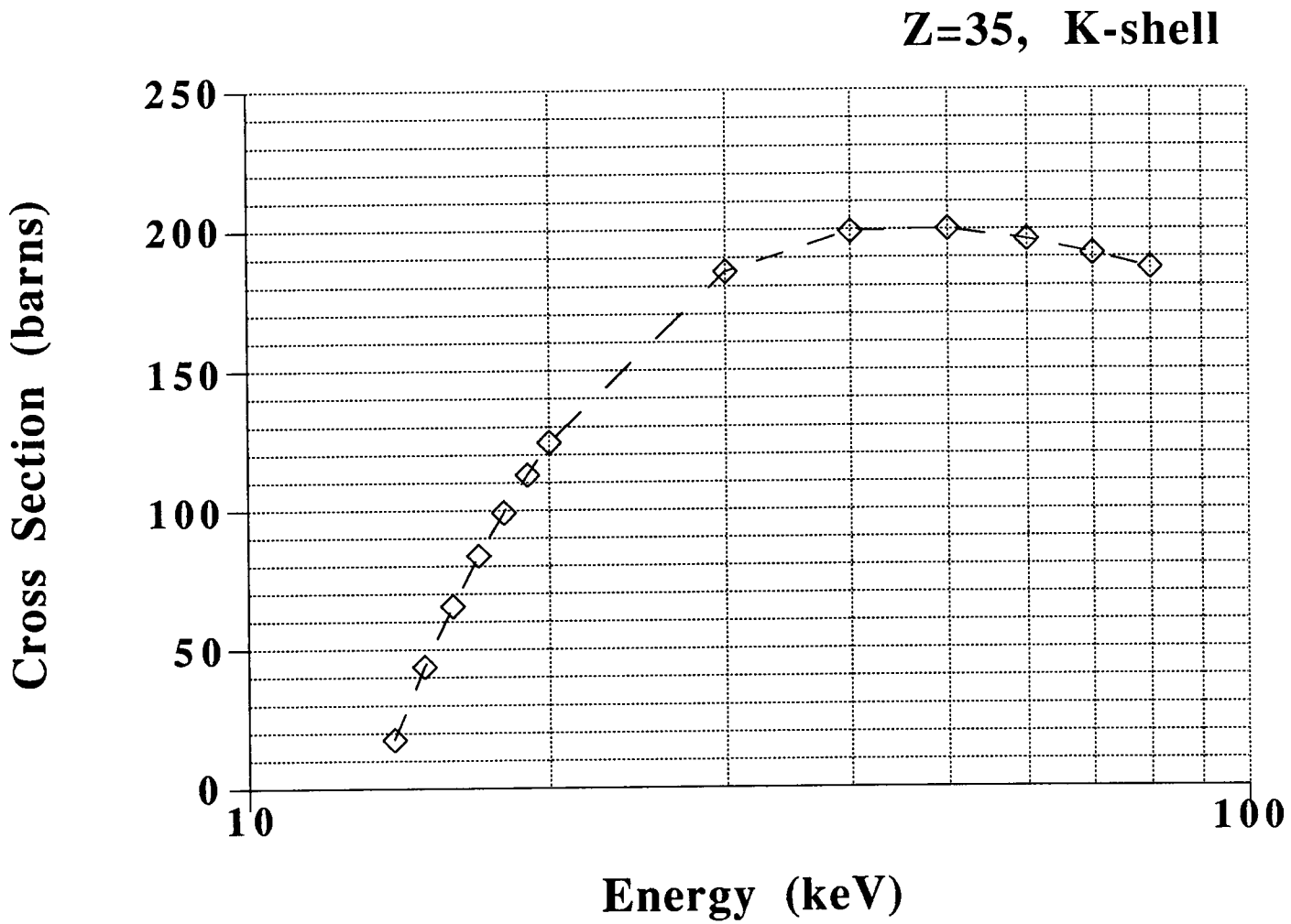
```
      IF (J .EQ. I) WRITE(6,*)J,TAB, YJ, TAB,Y3,TAB, Y2, TAB,
     6  B,TAB,B1,TAB,Y6, TAB,RK
      IF(J.EQ.I) WRITE(*,14) J, YJ, Y3, Y2, Y6, RK
75    CONTINUE
74    CONTINUE
      B1=0.0
      IF(DNN.GT.10001)GOTO  99
      DO  97  J=30,100,10
      IF(J2.GT.J)GOTO 97
      E=FLOAT(J)
      YJ=LOG10(E)
      B=Y5*Z/E
      B=B*ALOG(1.166*E/XJ)
      IF(B.GT.0.0)B1=LOG10(B)
       WRITE(6,*)J,TAB,YJ,TAB,B,TAB,B1,TAB,B,TAB,B1,
     6  TAB,Z,TAB,XJ
97    CONTINUE
      DO 98  J=200,1000,100
       IF(J2.GT.J)GOTO 98
       E=FLOAT(J)
       YJ=LOG10(E)
       B=Y5*Z/E
       B=B*ALOG(1.166*E/XJ)
       IF(B.GT.0.0)B1=LOG10(B)
       WRITE(6,*)J,TAB,YJ,TAB,B,TAB,B1,TAB,B,TAB,B1,
     6  TAB,Z,TAB,XJ
98    CONTINUE
      DO  96  J=2000,10000,1000
      IF(J2.GT.J)GOTO 96
      E=FLOAT(J)
      YJ=LOG10(E)
      B=Y5*Z/E
      B=B*ALOG(1.166*E/XJ)
      IF (B.GT.0.0)B1=LOG10(B)
      WRITE(6,*)J,TAB,YJ,TAB,B,TAB,B1,TAB, B,TAB,B1,
     6  TAB, Z,TAB,XJ
96    CONTINUE
99    WRITE(*,*)
      WRITE(*,*)
      ENDFILE(6)
      CLOSE(6)
2500  WRITE(*,*)'YOU ARE GOING TO EXIT NOW'
      PAUSE
      STOP
      END
```

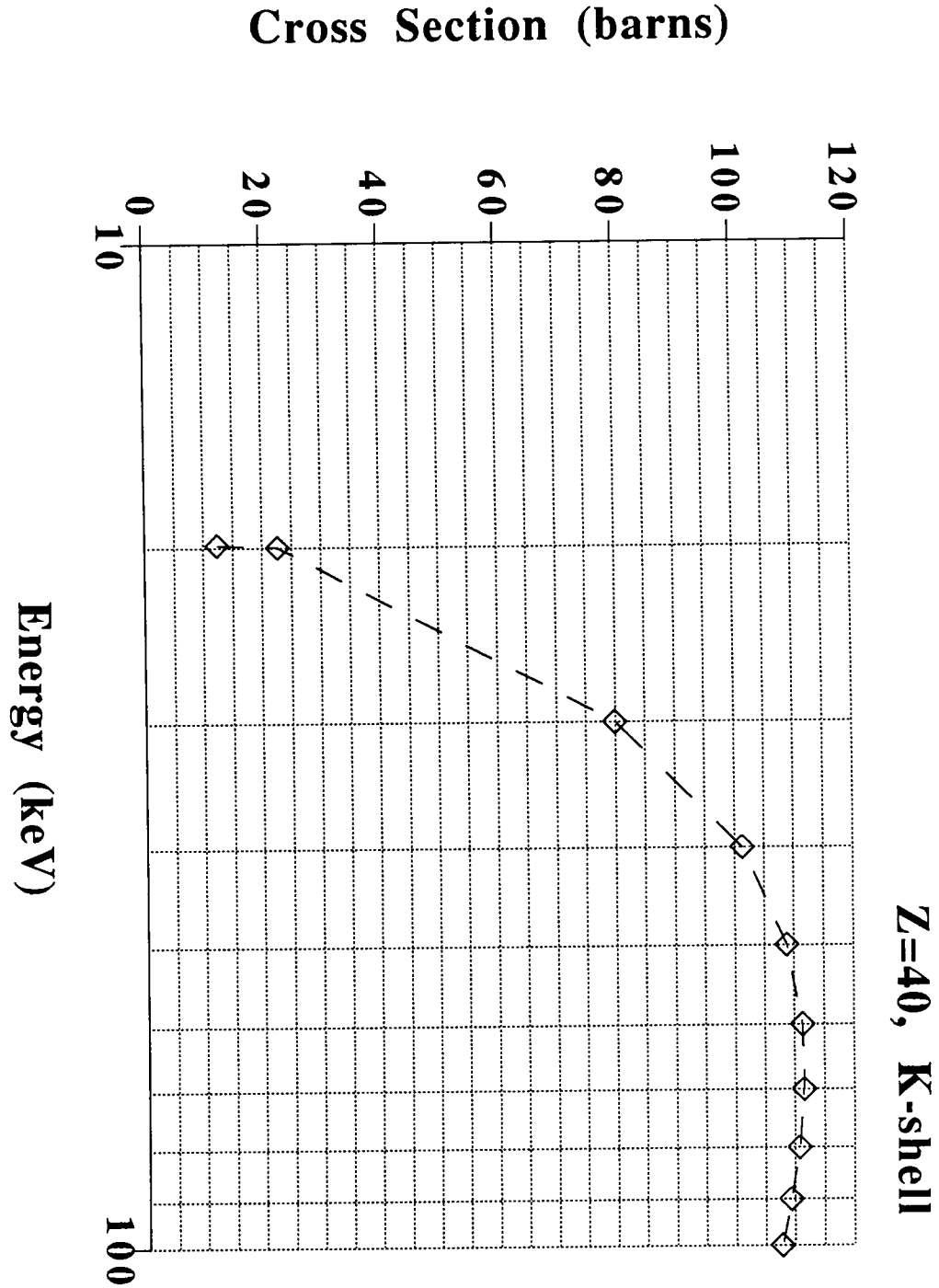
APPENDIX C: CALCULATED DATA OF X-RAY IONIZATION CROSS SECTIONS FOR K, L, AND M SHELLS

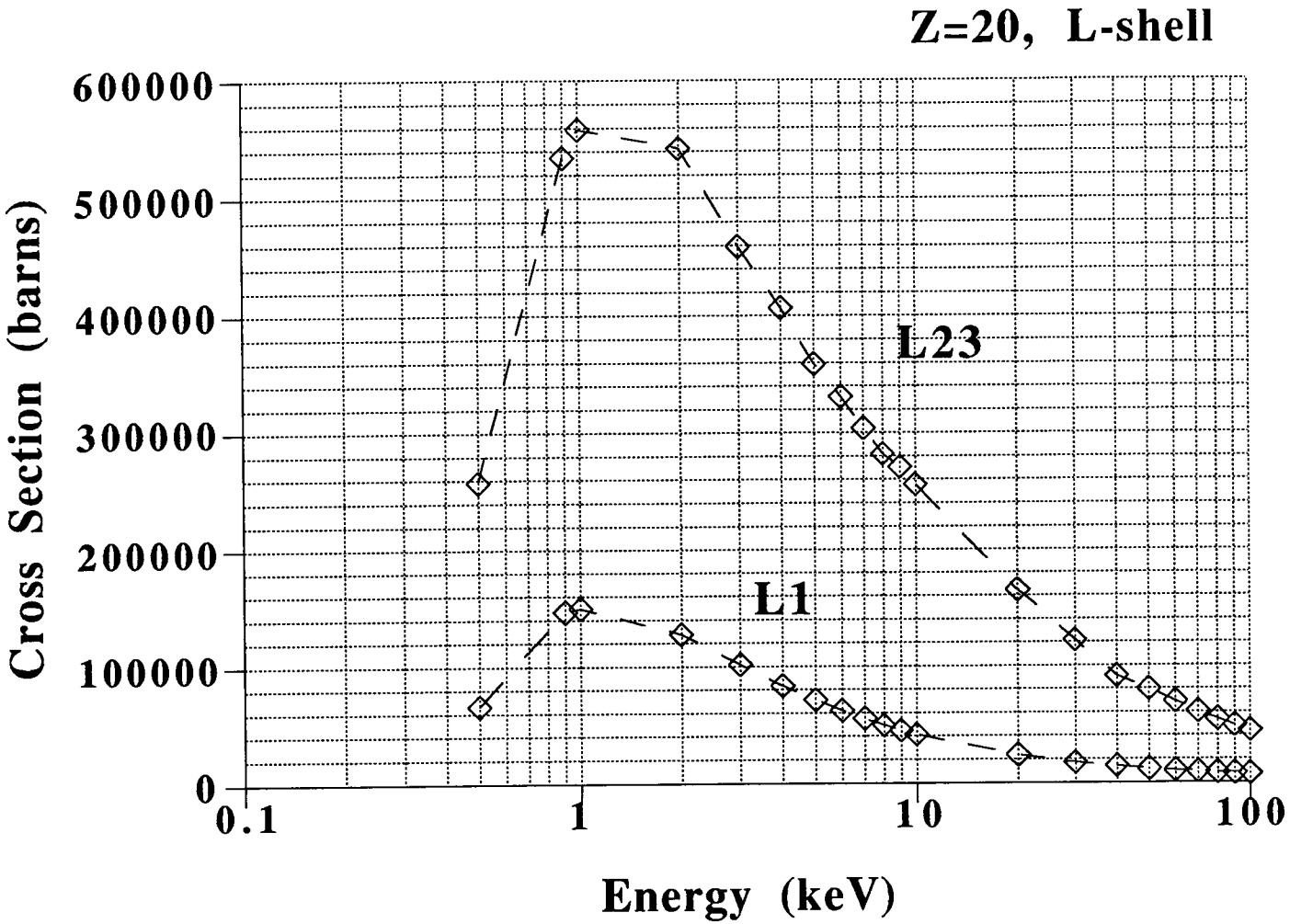

Z=13,K-shell
15000
10000
5000
0
Cross Section (barns)
1
10
100
Energy (keV)

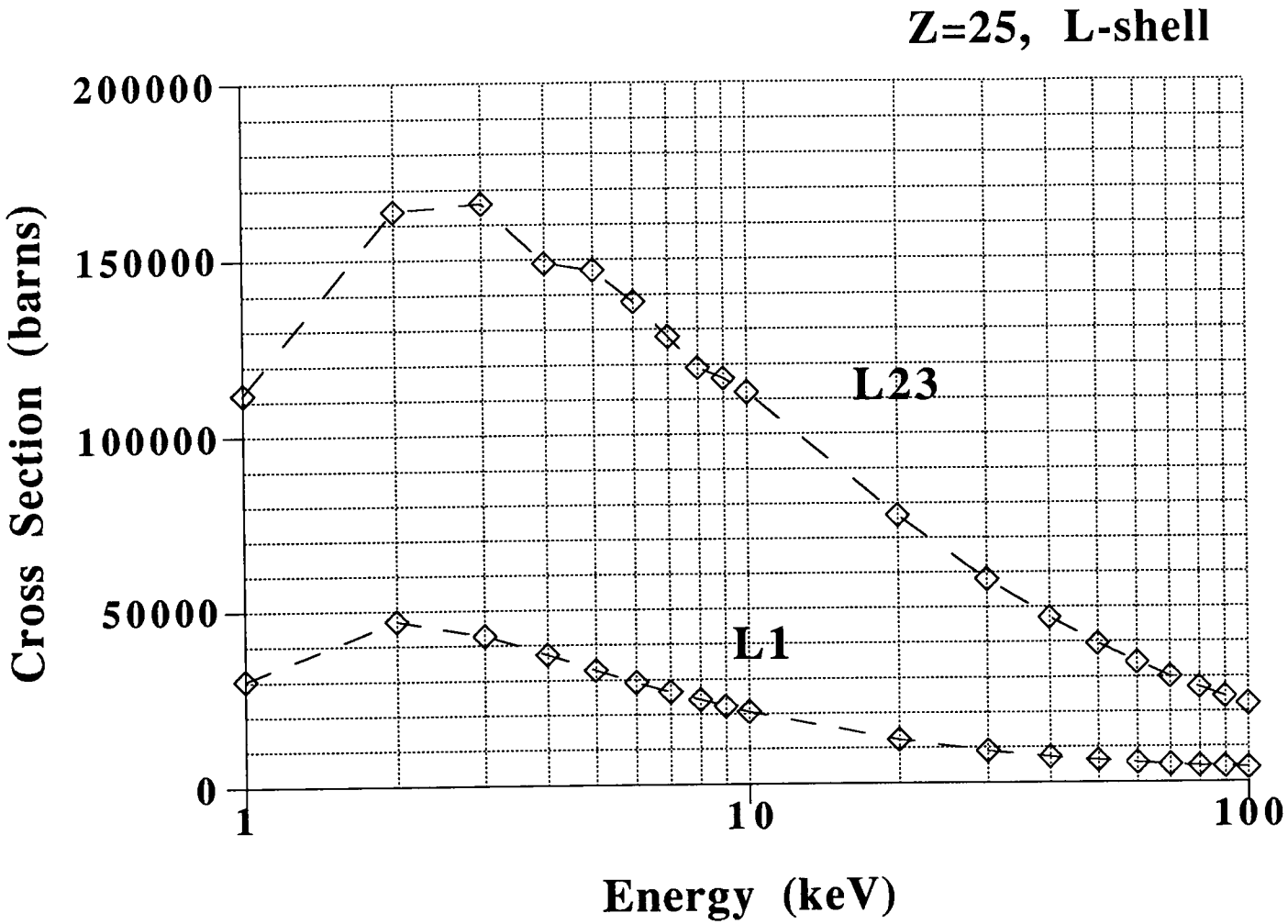

Z=20,K-shell
Cross Section (barns)
2500
2000
1500
1000
500
0
1
10
100
Energy(keV)

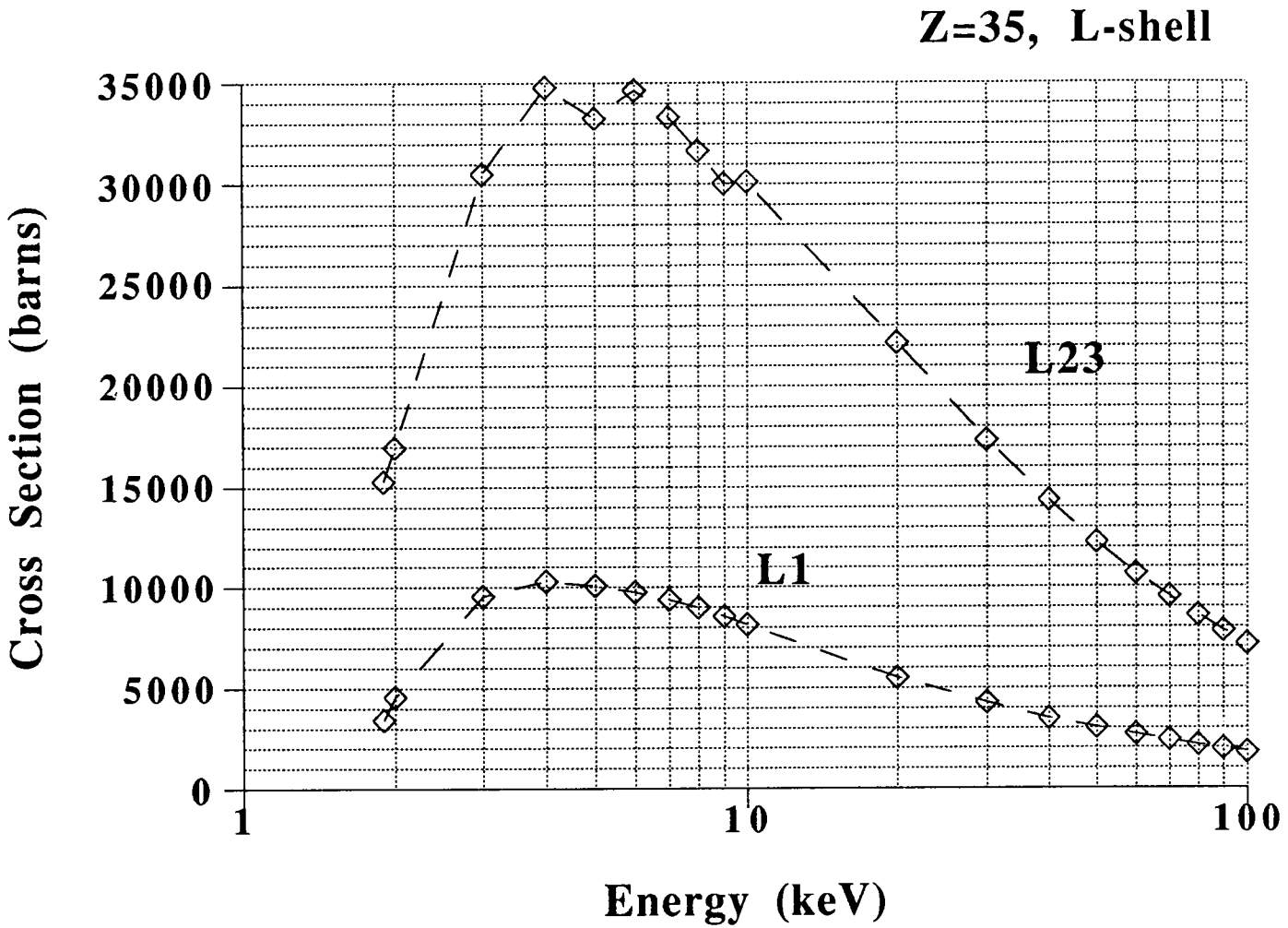

Z=25, K-shell
Cross Section (barns)
1000
800
600
400
200
0
1
10
100
Energy (keV)

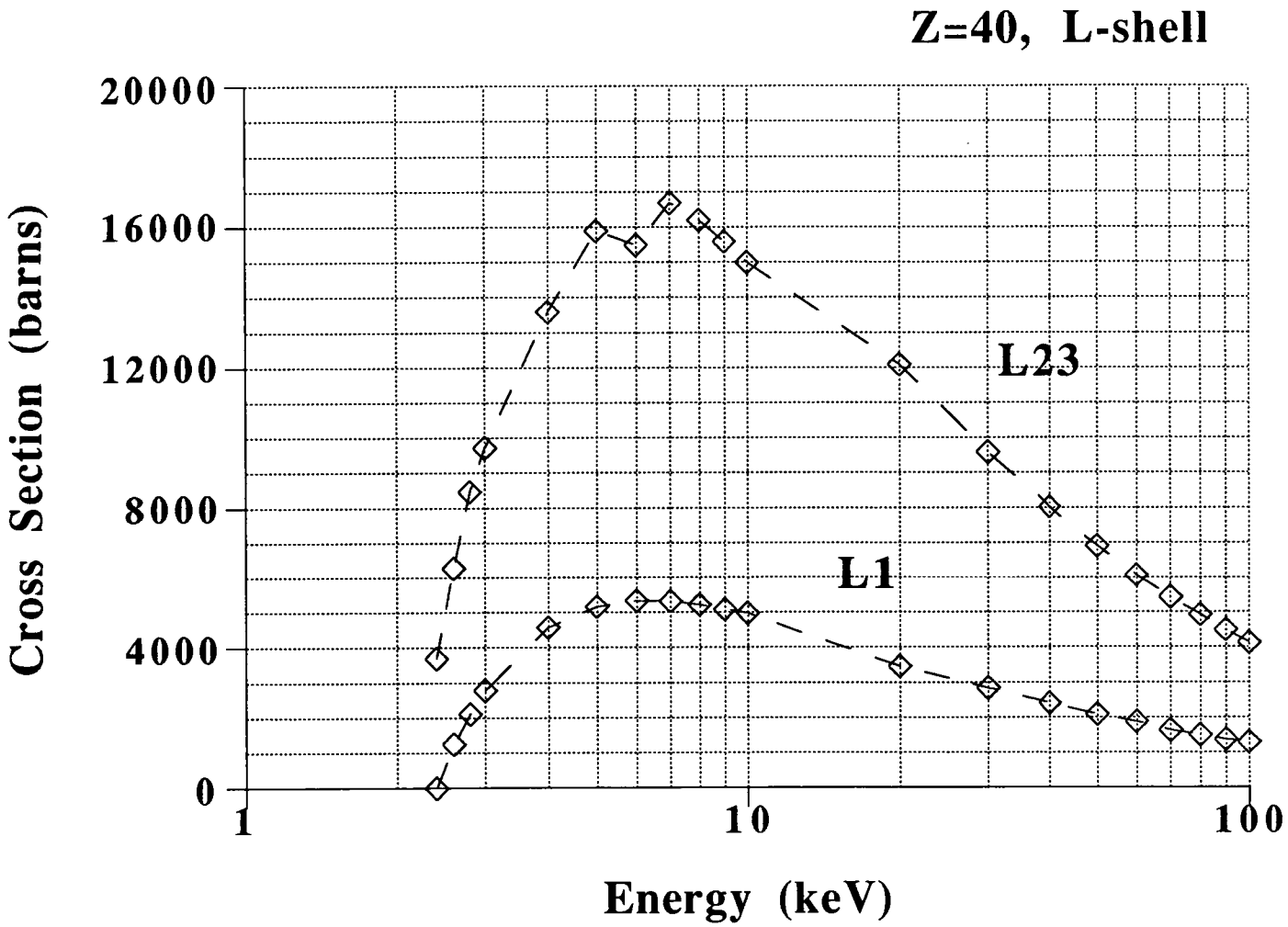

Z=35, K-shell
Cross Section (barns)
250
200
150
100
50
0
10
100
Energy (keV)

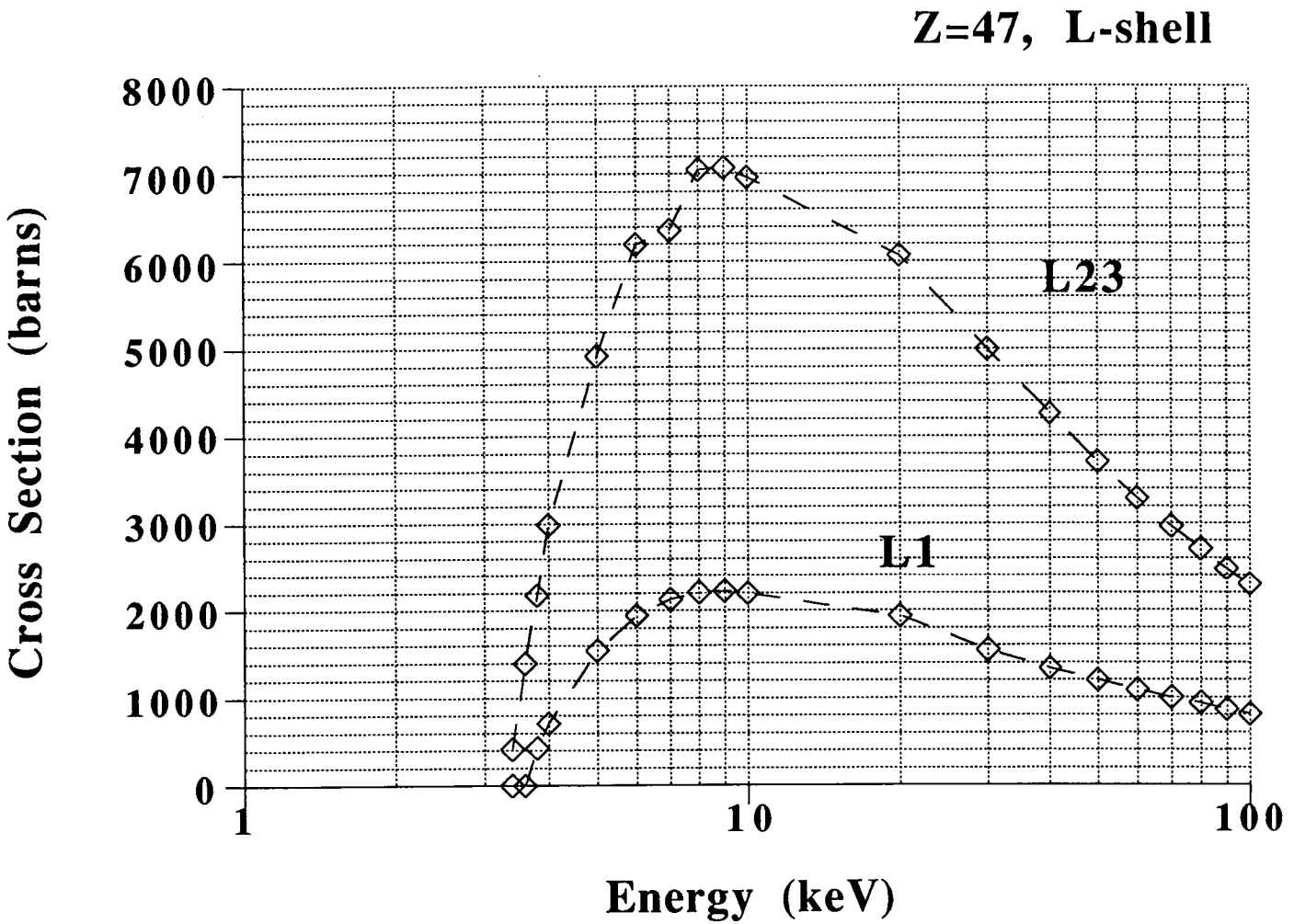

Cross Section (barns)
0
20
40
60
80
100
120
Energy (keV)
10
100
Z=40, K-shell

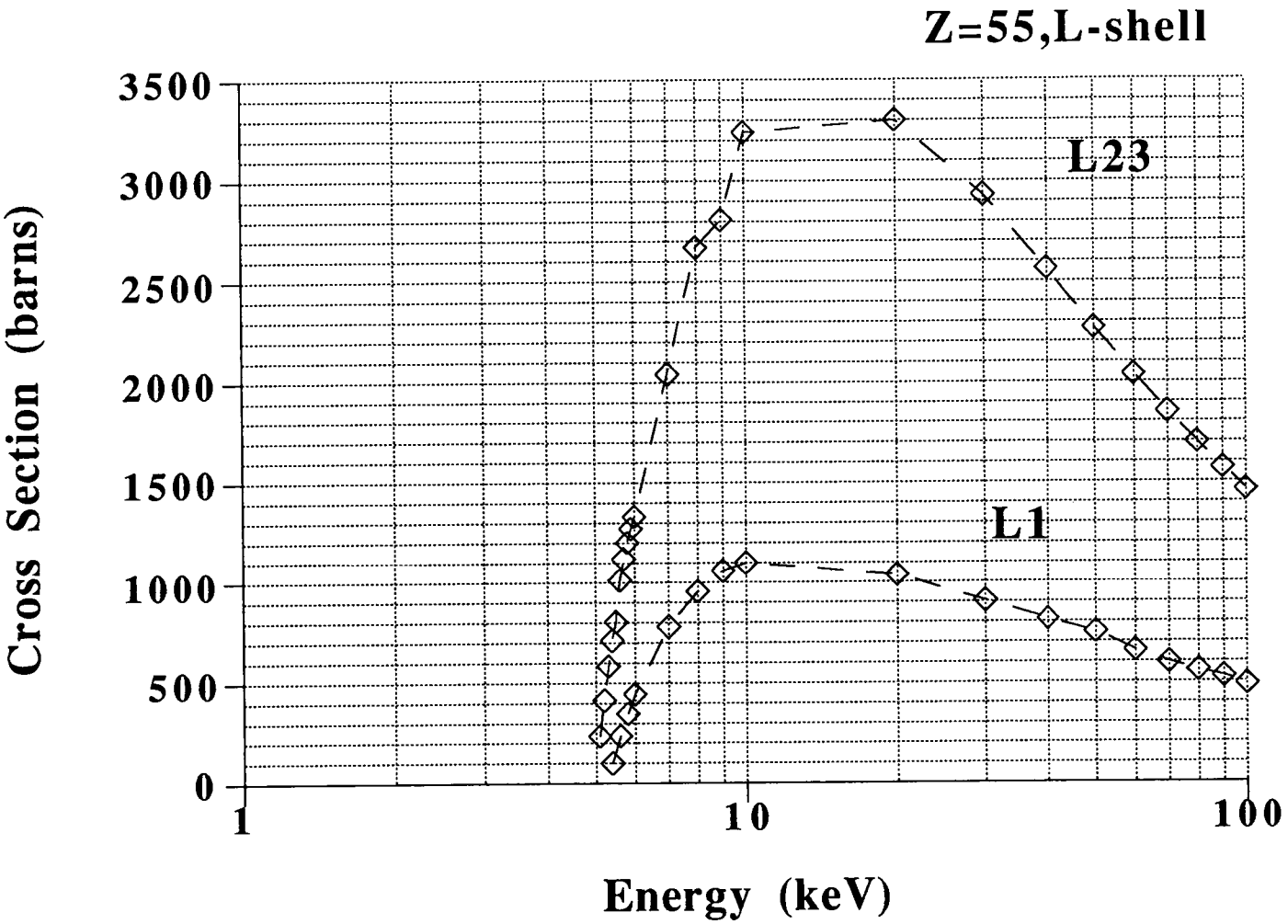

Z=20, L-shell
600000
500000
400000
300000
200000
100000
0
Cross Section (barns)
L23
L1
0.1
1
10
100
Energy (keV)

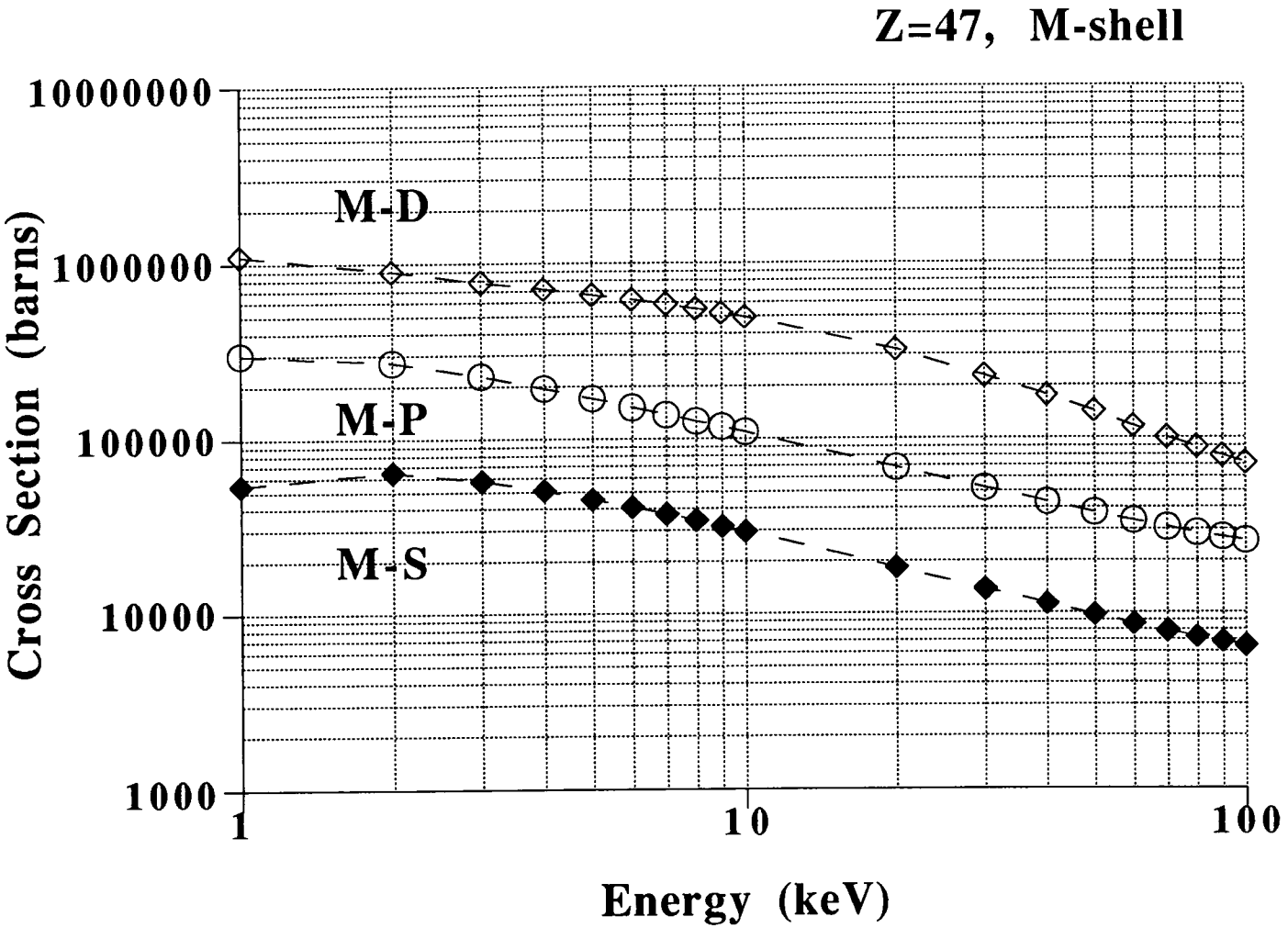

Z=25, L-shell
200000
150000
100000
50000
0
Cross Section (barns)
L23
L1
1
10
100
Energy (keV)

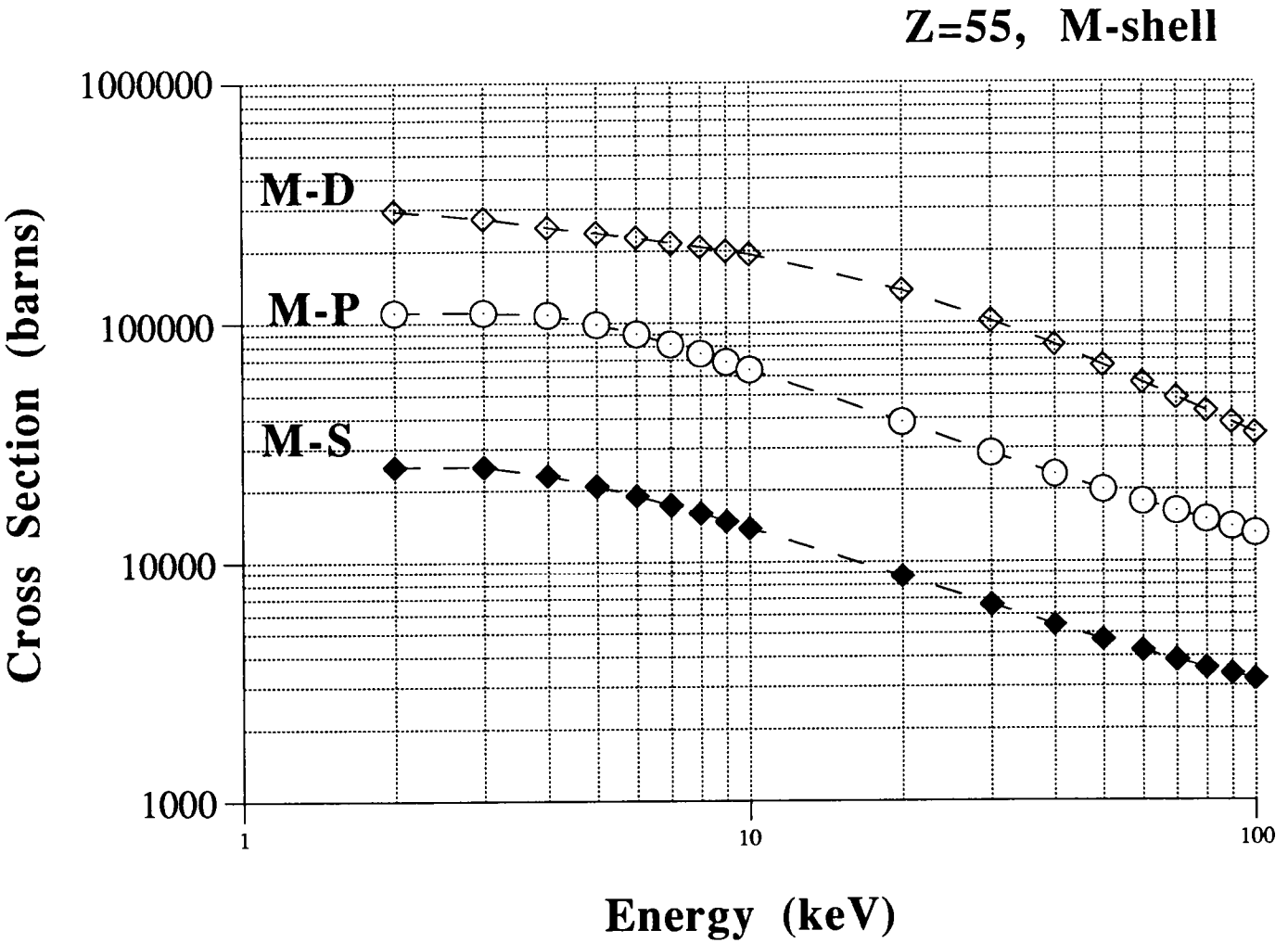

Z=35, L-shell
35000
30000
25000
20000
15000
10000
5000
0
Cross Section (barns)
L23
L1
1
10
100
Energy (keV)

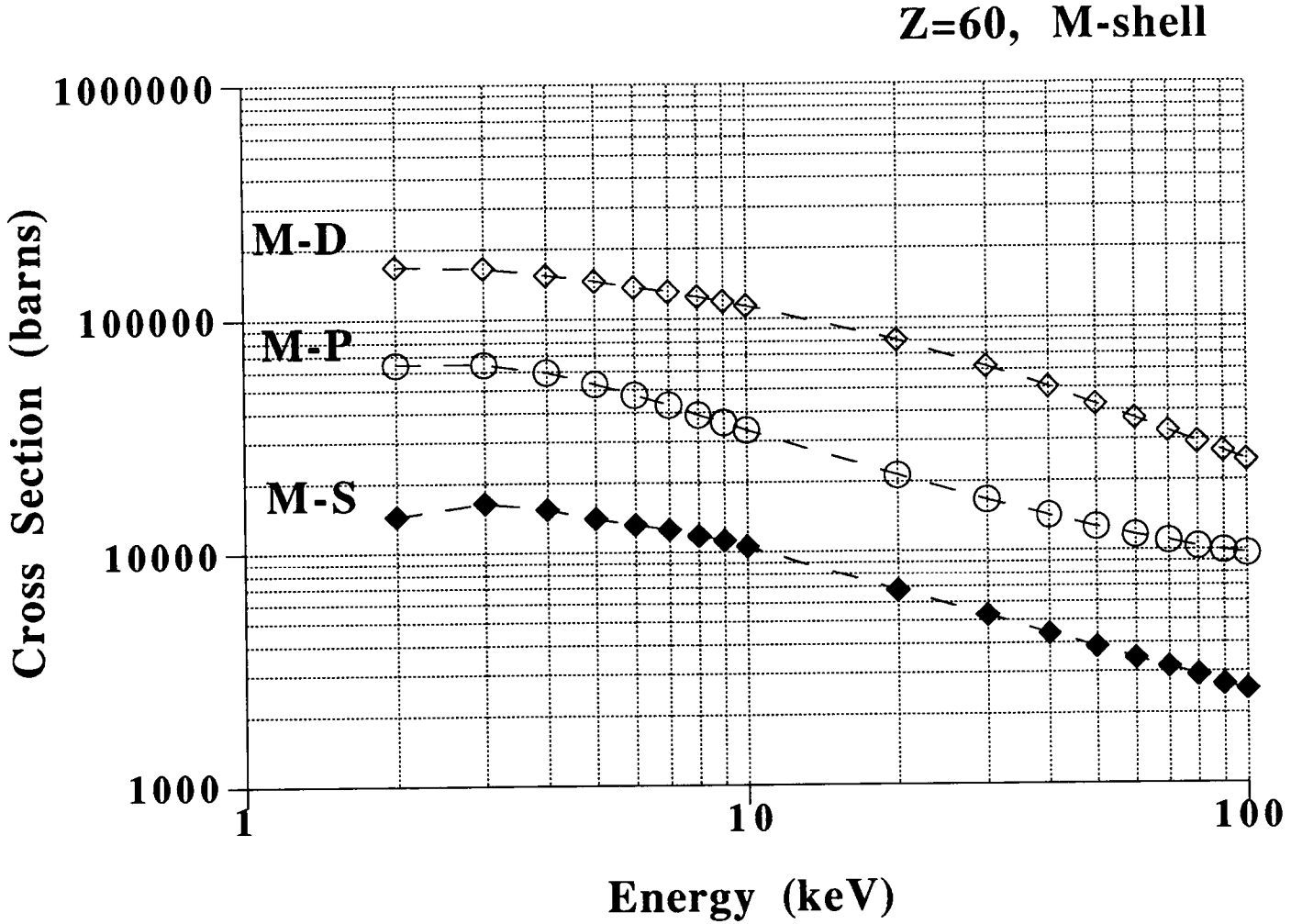

Z=40, L-shell
20000
16000
12000
8000
4000
0
Cross Section (barns)
L23
L1
1
10
100
Energy (keV)

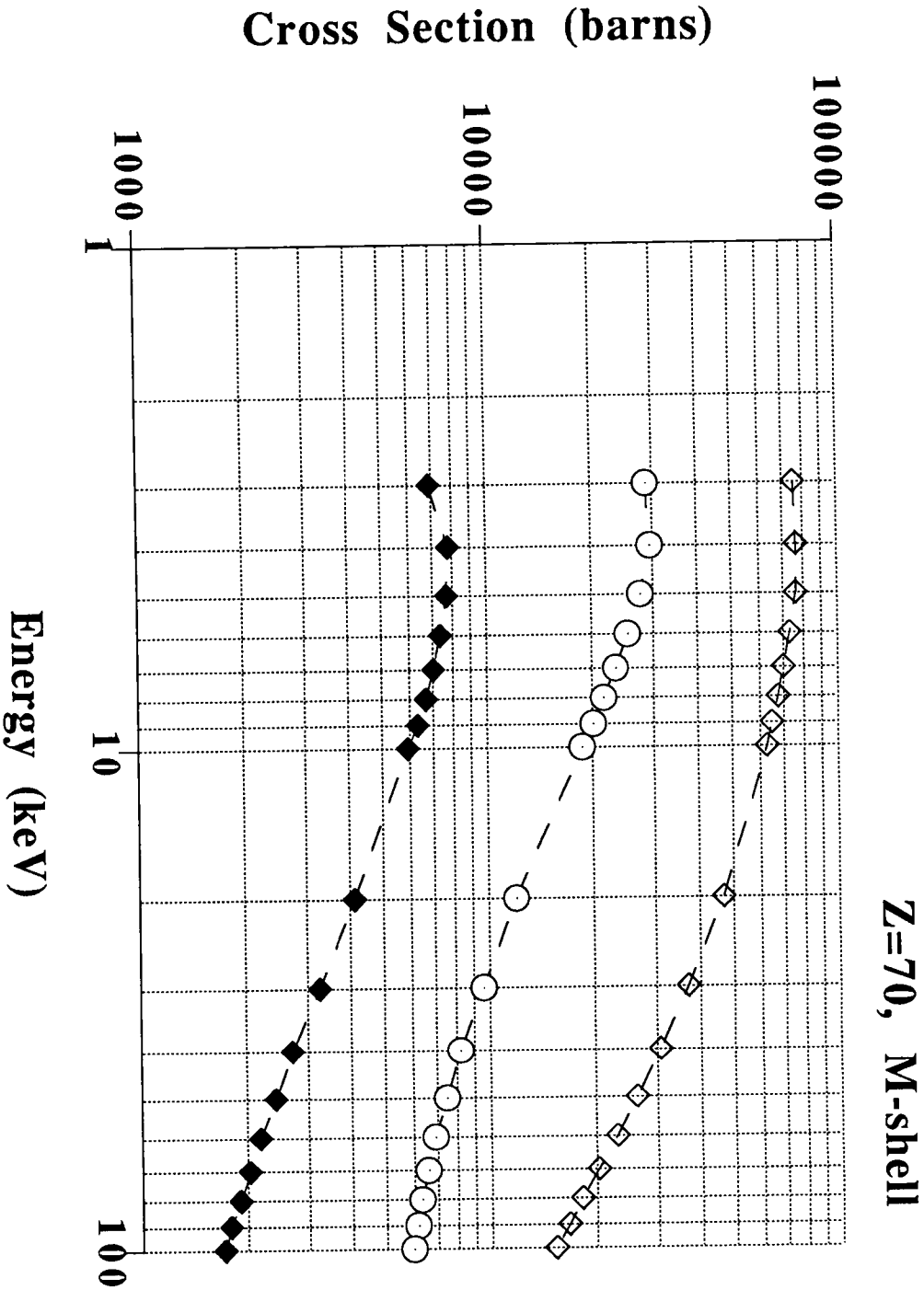

Z=47, L-shell
Cross Section (barns)
8000
7000
6000
5000
4000
3000
2000
1000
0
1
10
100
Energy (keV)
L23
L1

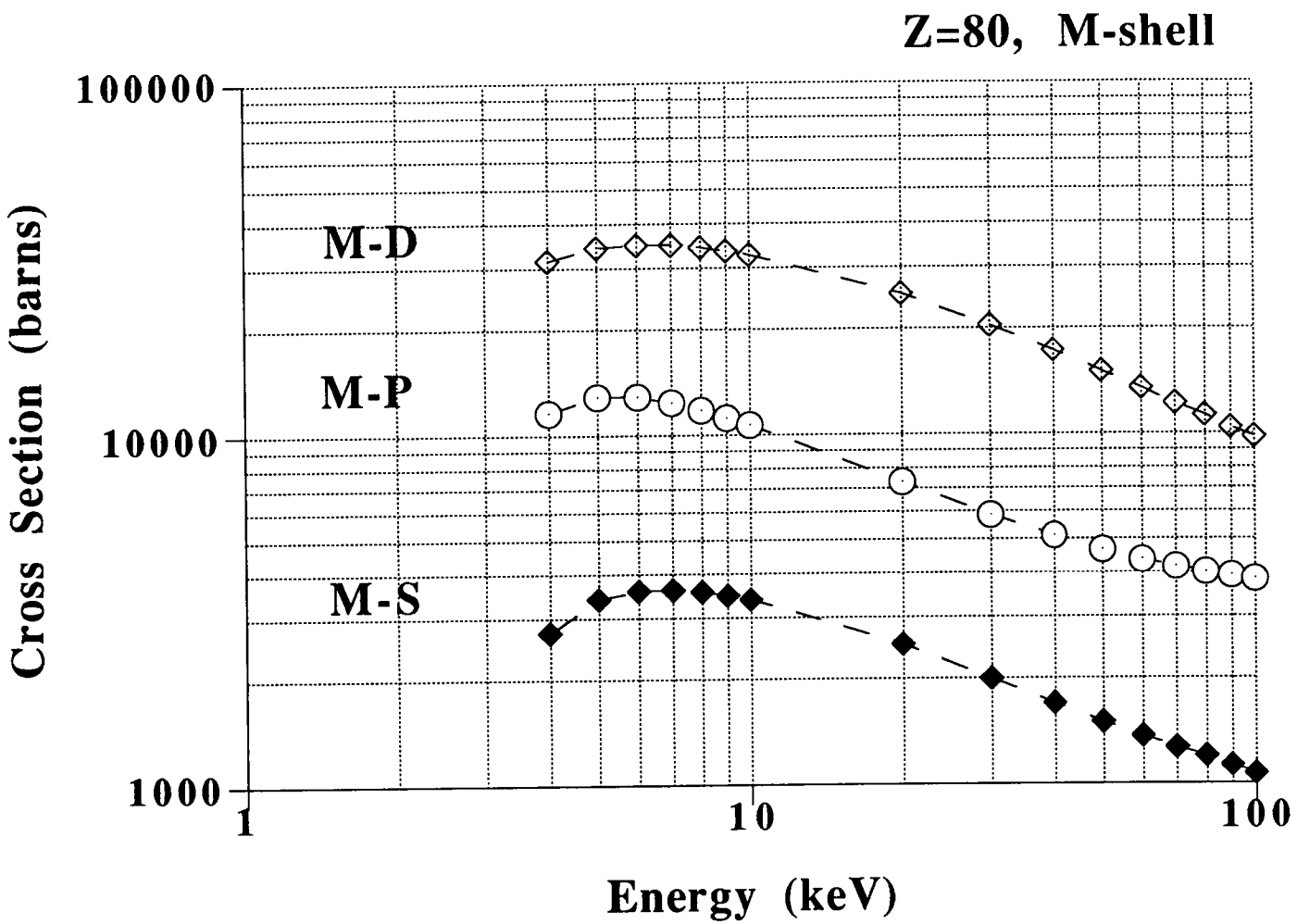

Z=55,L-shell
L23
L1
Cross Section (barns)
3500
3000
2500
2000
1500
1000
500
0
1
10
100
Energy (keV)

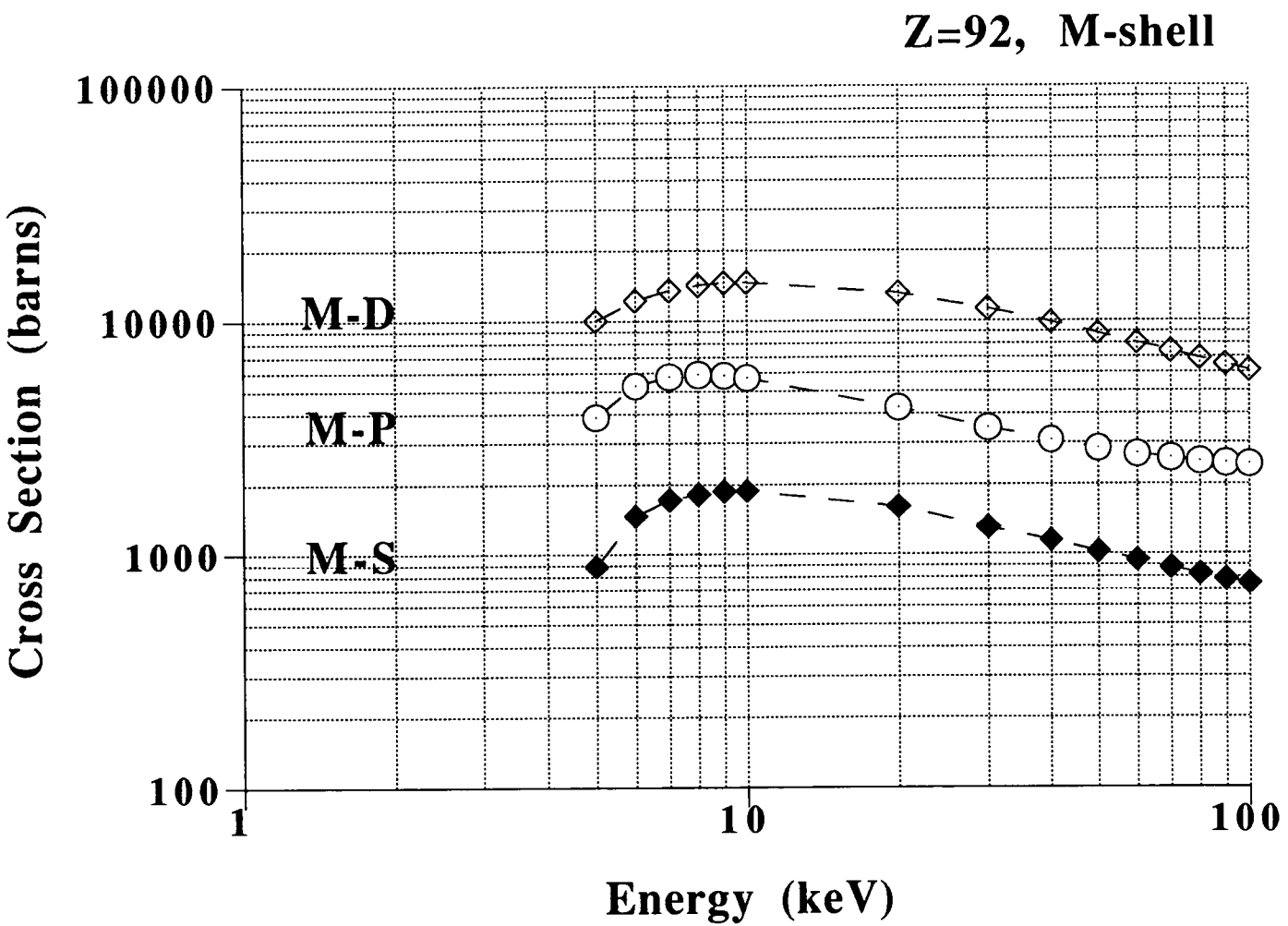

Z=47, M-shell
10000000
1000000
100000
10000
1000
Cross Section (barns)
M-D
M-P
M-S
1
10
100
Energy (keV)


Z=55, M-shell
1000000
100000
10000
1000
M-D
M-P
M-S
Cross Section (barns)
1
10
100
Energy (keV)


Z=60, M-shell
1000000
100000
10000
1000
Cross Section (barns)
M-D
M-P
M-S
1
10
100
Energy (keV)


Cross Section (barns)
1000
10000
100000
1
10
100
Energy (keV)
Z=70, M-shell


Z=80, M-shell
100000
10000
1000
Cross Section (barns)
M-D
M-P
M-S
1
10
100
Energy (keV)


Z=92, M-shell
100000
10000
1000
100
Cross Section (barns)
M-D
M-P
M-S
1
10
100
Energy (keV)

VITA

Suichu Luo was born in Sichuan, China on December 2, 1945. She graduated from Beijing University, Radioelectronics Department in 1970. A Master's degree of Solid State Physics was awarded in 1983 from Beijing Normal University. After being a instructor of Physics in Beijing Broadcasting Institute for five years and a half, she came to the EM Facility, University of Tennessee, as a research associate in Dr. D.C. Joy's group. She continued her education in January 1991. A Doctor of Philosophy in Physics was awarded in May 1994.